The role of APC in cellular and tissue organisation in intestinal tumorigenesis

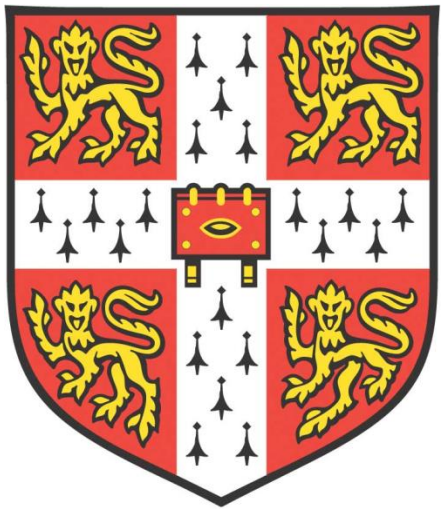

Helena Rannikmäe

Sidney Sussex College

Department of Biochemistry

University of Cambridge

This dissertation is submitted for the degree of Doctor of Philosophy

September 2019

Preface

This dissertation is the result of my own work and includes nothing which is the outcome of work done in collaboration except as specified in the text. It is not substantially the same as any that I have submitted, or, is being concurrently submitted for a degree or diploma or other qualification at the University of Cambridge or any other University or similar institution except as declared in the Preface and specified in the text. I further state that no substantial part of my dissertation has already been submitted, or, is being concurrently submitted for any such degree, diploma or other qualification at the University of Cambridge or any other University or similar institution except as declared in the Preface and specified in the text.

This dissertation does not exceed the word limit of 60 000 words and meets the requirements set by the relevant Degree Committee.

Helena Rannikmäe
September 2019

Summary

The tumour suppressor adenomatous polyposis coli (APC) is a multifunctional protein regulating a diverse array of effector pathways essential for cellular homeostasis. In most sporadic colon cancers, truncating mutations in APC lead to the loss of the Wnt pathway and microtubule regulatory domains. Studies have established key roles of mutant APC in malignant growth via deregulation of Wnt pathway activity. However, the consequence of the loss of the microtubule regulatory domains of APC in intestinal tumorigenesis has not been determined. In addition, it is widely believed that intestinal tumorigenesis is initiated from a stem cell, with limited studies addressing the potential for adenomas originating from non-stem cells. I hypothesise that the stem cell supporting Paneth cells act as an intrinsic organising centre for the intestinal epithelia, thereby providing a barrier for tumorigenesis.

I utilise intestinal tissue and generate various genetically modified 3-dimensional organoid models to study the role of APC in malignant transformation of the intestinal epithelia. I show that APC inactivation leads to alterations in tissue morphology. Intriguingly, my results reveal a novel phenotype upon loss of APC resulting in compromised intracellular organisation that is linked to the deregulation of microtubules. Sufficiency experiments suggest that the different effector roles of APC in the intestinal epithelia are domain-specific. The generation of a novel Paneth cell specific promoter allowed me to demonstrate that the loss of APC specifically in Paneth cells does not compromise intestinal epithelial tissue morphology, a key characteristic of intestinal tumorigenesis.

The results presented in here demonstrate that solely the loss of APC in a Paneth cell is not sufficient to initiate intestinal tumorigenesis, suggesting that further insults could be necessary for this non-stem cell to acquire the potential to initiate tumorigenesis. My findings indicate that APC has distinct domain-specific roles in the intestinal epithelia and reveal its novel role in regulating intracellular organisation. I conclude that there are additional consequences for APC mutational inactivation in intestinal tumorigenesis beyond deregulation of the Wnt pathway activity.

Presentations and publication relating to this thesis

Conference presentations

- Platform presentation: Gordon Research Conference, Wnt signalling, Vermont, USA, August 2019
- Poster presentation: Gordon Research Seminar, Wnt signalling, Vermont, USA, August 2019
- Poster presentation: EMBO Symposium, Organoids: Modelling Organ Development and Disease in 3D Culture, Heidelberg, Germany, September 2018
- Platform presentation: AstraZeneca PhD Symposium, Cambridge, UK, September 2018
- Poster presentation: Conference Young Scientists in Estonia and Abroad, Tallinn, Estonia, January 2018

Conference attendance and travel was possible due to the generous funding from **AstraZeneca** travel fund, **Cambridge Philosophical Society** travel grant (x2), **Sidney Sussex College** Graduate fund (x2) and the **Parry Dutton** Student fund.

Publication

Manuela Urbischek, **Helena Rannikmae**, Thomas Foets, Katharina Ravn, Marko Hyvönen & Marc de la Roche. Organoid culture media formulated with growth factors of defined cellular activity. Scientific Reports 2019; 9 (6193)

Acknowledgments

First and foremost, I would like to thank my main supervisor Dr. Marc de la Roche for giving me the opportunity to undertake this research. I am very grateful for the teaching, extensive support and guidance you have provided me throughout the four years. Your enthusiasm and passion for science is something I hope I will be able to replicate in my future; from day one you welcomed dialogue, open discussion of ideas and encouraged me to think outside the box, allowing me to develop as a scientist. Thank you!

I am also very grateful to my second supervisor Dr. Simon Barry for his support and for the valuable discussions about the project. I highly valued and learnt from your scientific reasoning and approach.

I would like to thank Prof. Gerard Evan and Dr. Trevor Littlewood for the valuable guidance and insights. I am grateful for having been able to attend your lab meetings and learn from the way you conduct high-level science and apply critical thinking. Trevor, thank you for giving me the well-appreciated advice whenever I needed it.

I would like to give my sincere thanks to Dr. Samantha Peel for all the microscope (and bureaucratic) help. Your genuine passion for high quality work was inspiring and your good chat made sitting by the microscope fun.

My PhD studies would not have been the same without the MAD lab. Thomas, thank you for your friendship, help, advice and company, in and out of the lab. I hugely appreciate the chats we had over the years and this PhD would not have been the same without you. Manuela, thank you for being a fellow organised member of the lab and for the fun talks. I would also like to thank all the students we had during my time in the lab who made the atmosphere so entertaining, especially Heidi, Vicci, Bartek, Alice, Iris and Alissa.

I had the pleasure of working side by side to the Evan and McCaughan laboratories alongside excellent scientists with genuine passion and commitment to meaningful, solid science. Luca, Tania, Roderick, Lindsey, Cathy, Nicole, Lucia, Frank —thank you for all the discussions, help and advice throughout the years. I would also like to give my appreciation to Deborah and

Michaela for keeping the lab up and running and to Teresa, Mekdes and Sylvia next door for scientific help and good lunch company.

I would like to thank my PhD funder AstraZeneca for allowing me to undertake this PhD research and for giving me the opportunity to use their facilities for experiments. I am also grateful for the various facilities and expertise available within the Department of Biochemistry that have allowed me to carry out my daily experiments with ease.

I am grateful to Dr. Maike de la Roche and Dr. Hung-Chang Chen for help with FACS, Yinhai Wang for carrying out computational modelling, Dr. Inderpreet Kaur Sur for help with mice and Dr. Yuu Kimata for assistance with the microscope.

To my friends—old and new—I would like to give a huge thank you for the listening ear and distraction when I needed it. Each and every one of you has made my PhD time enjoyable and memorable: Aga, Cassie, Sushmitha, Carly, Chiara, Karola, Jessica, Sofia, Elen, Kristel, Phil, Ben.

Stuart, thank you for your uplifting advice and genuine interest, it has been fun being in this PhD path with you.

Johan, thank you for your unlimited support in the past months. Your encouragement and well-needed distraction came when I most required it.

My PhD studies could not have been possible without the eternal support from my family, and I dedicate this thesis to them. Collectively, they have been an unshakable support system. I have been lucky enough to have the best sisters one could ask for. Hanna, the many trips we did, mountains we conquered—you have kept me motivated and enthusiastic throughout the years. Krissu, you have been my mentor, somebody who I look up to and whose advice I appreciate dearly. Jack, your positive view of life is something I try to follow, and I am forever grateful for your unconditional support throughout my education. Finally, Miia, a person I adore and admire more than anything, my biggest fan and rock. You have set an extremely high bar for success in life and work, and I can only attempt to meet that.

Table of contents

List of Figures

List of Tables

List of common abbreviations

µm	micrometre
4-OHT	4-hydroxytamoxifen
βDC	β-catenin destruction complex
γ-TURC	γ-tubulin ring complex
APC	Adenomatous polyposis coli
AB polarity	Apical-basolateral polarity
Asef	APC-stimulated guanine nucleotide exchange factor
ATOH1	Atonal homologue 1
BMP	Bone morphogenic protein
CK1α	Casein Kinase 1 α
CIN	Chromosomal instability
CRC	Colorectal cancer
Dox	Doxycycline
Dsh	Dishevelled
EDTA	Ethylenediaminetetraacetic acid
EGF	Epidermal growth factor
ER	Endoplasmic reticulum
FAP	Familial adenomatous polyposis
F-actin	Filamentous actin
GSK3β	Glycogen Synthase Kinase 3 β
h	hour
IQGAP1	IQ Motif Containing GTPase Activating Protein 1
Lgr5	Leucine-rich-repeat-containing G-protein-coupled receptor 5
LOH	Loss of heterozygosity
Min	Multiple intestinal neoplasia
MCR	Mutation cluster region
ml	Millilitre
MTOC	Microtubule-organising centre
nm	Nanometre
nM	Nanomolar

PBS	Phosphate-buffered saline
RCF	Relative centrifugal force
TA cell	Transit amplifying cell
tdTom	tandem dimer Tomato

Chapter 1:

Introduction

1.1 Intestinal epithelia

The intestinal tract, composed of the small intestine and colon, hosts the second largest epithelial tissue in the human body (after the skin). The intestinal epithelium is a single-layered columnar epithelium that has two main functions: uptake of metabolites and protection against environmental attacks like foreign bacteria [1]. The basic units of the intestinal epithelium are adjacent invaginations, termed crypts of Lieberkühn, each of which serves as a semi-autonomous cell factory to replenish the intestinal (colon and small intestine) epithelium. The villi are structures present in the small intestine that contain differentiated, post-mitotic cells geared towards absorbing nutrients and lining the epithelia with protective mucus. The colon epithelium lacks villi and consists of a flat epithelial monolayer interspersed with crypts [2]. At the base of the crypt lie the self-renewing and continuously dividing stem cells that give rise to progenitor cells (termed transit-amplifying cells). The transit-amplifying cells proliferate rapidly and mature into one of the cell types present in the intestinal epithelium (Figure 1.1). As the cells mature, they move out of the crypt towards the villus where they are eventually shed by apoptosis [2].

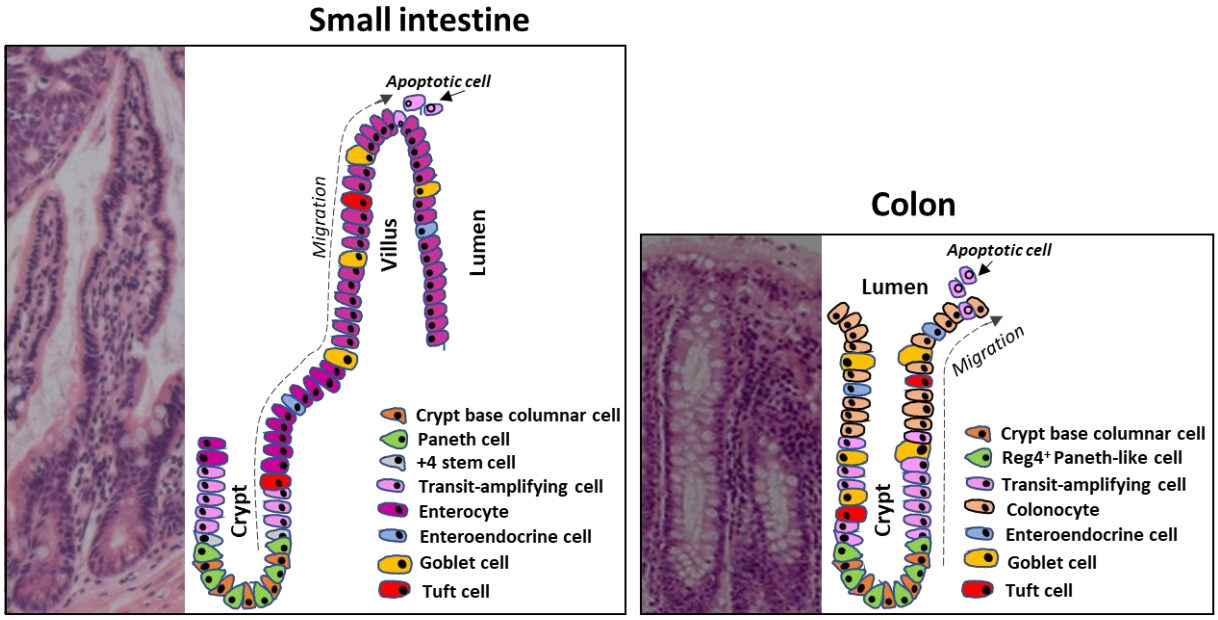

Figure 1. 1: The structure of the small intestine and colon. Left panel on both images: haematoxylin and eosin stain of the small intestine (SI) and colon. Right panel: representation of the cell types present in the SI and colon.

1.1.1 The intestinal epithelial cells

At least two, physically distinct stem cell populations, have been identified in the intestinal epithelium: stem cells and reserve stem cells. The intestinal stem cell has been identified as the rapidly cycling crypt base columnar (CBC) cell that lies deep in the crypt and expresses a proto-typical stem cell marker Lgr5 (leucine-rich-repeat-containing G-protein-coupled receptor 5), a Wnt target gene [3]. Lineage tracing studies demonstrate Lgr5-expressing CBCs that exhibit long-term self-renewal and the production of all the intestinal epithelial cell lineages, indicating it is the stem cell compartment. An additional stem cell compartment has been reported that resides at the +4 position in the crypt and represents a reserve for the stem cell pool [4,5]. These so called label-retaining cells, a defined property of quiescent or slowly cycling stem-cells, are precursors to the secretory cell lineage, express Lgr5 and can be recalled to the stem-cell state [5].

As the stem cells divide at the bottom of the crypt, one of the daughter cells may translocate, stochastically, away from the influence of growth factors that promote "stemness" [6]. Displacement from the stem cell niche is believed to induce a differentiation programme to the highly proliferative transit-amplifying (TA) cells. The TA cells divide rapidly and differentiate into mucus secreting goblet cells, hormone secreting enteroendocrine cells, nutrient absorbing enterocytes, M cells and tuft cells, while moving upwards from the crypt compartment towards the villus [1]. A sixth cell type, the Paneth cell escapes this upward flow and instead migrates downward to settle at the bottom of the crypt, intermingled between the stem cells (Figure 1.1) [6]. While it has been previously thought that the differentiated cells are terminally differentiated, it is now understood that the cell fate status is dynamic and reversible with several studies showing plasticity of the mature intestinal cells to de-differentiate into stem-like cells [1,7–9].

The mechanism underpinning the translocation of cells from the base of crypts to the tip of villi is controversial. One accepted model, that epithelial cell migration is passive and driven by the forces originating from dividing stem cells [10] has recently been challenged by the finding that cells in the intestine migrate collectively, using actin-based basal protrusions for active migration [11]. Alternatively, migration along the crypt-villus axis may be a combination of both passive and active mechanisms.

1.1.1.1 Paneth cells

One of the primary goals of my thesis work is to determine whether Paneth cell regulation of the stem cell niche acts as a barrier to intestinal tumorigenesis. Paneth cells are long-lived cells, approximately 6-8 weeks as opposed to other intestinal epithelial cells that persist for up to 5 days [12]. Paneth cells have a characteristic pyramidal shape with a basal nucleus and apical cytoplasm that is filled with large secretory vesicles (Figure 1.2). These apically-localised vesicles contain antimicrobial peptides and proteins such as lysozyme and cryptdins/defensins for secretion into the lumen of the crypt, allowing protection against invading pathogens [13]. Gene expressions studies have shown that Paneth cells express a number of growth factors, including epidermal growth factor (EGF), Wnt ligand and Notch ligand that are presented to stem cells as signals to maintain multipotency [14]. Stem cells thereby compete for the growth-factor rich Paneth cell surface [15]. Alternatively, Paneth cells have recently been shown to attenuate Wnt pathway activity in stem cells in ageing, through expression of Notum, an extracellular Wnt ligand inhibitor [16]. In addition, Paneth cells have been shown to be more rigid in shape compared to stem cells and anchor the crypt base to provide its shape [17]. Taken together, Paneth cells functionally and physically support the environment that controls stem cell activity and maintenance, defined as the stem cell niche [13]. The colon lacks Paneth cells; however, a deep crypt secretory cell type, marked by regenerating family member 4 (REG4), has been identified and is thought to serve as a surrogate Paneth cell in the colon, intermingling and supporting $Lgr5^+$ colon epithelial stem cells at the crypt base [18].

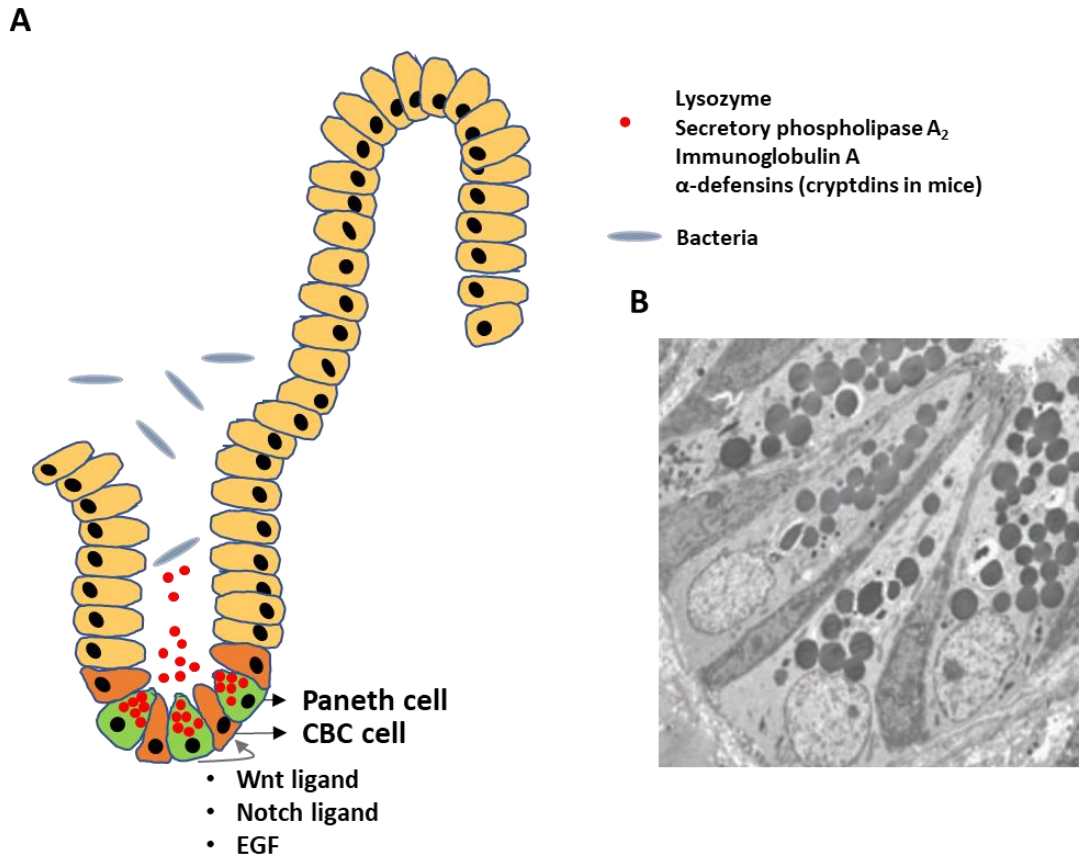

Figure 1. 2: Paneth cells in the small intestine. Paneth cells release antimicrobials and produce EGF, Wnt and Notch ligand (A). Electron microscopy image of the large and abundant apical vesicles of Paneth cells. Image from 13 (B).

The requirement of Paneth cells for intestinal homeostasis has been studied using various genetic-based methods for Paneth cell ablation. An *in vivo* study, utilising a mouse model for Paneth cell ablation (*Sox9*$^{fl/fl}$), showed that loss of Paneth cells results in concomitant loss of stem cells [15]. In this study, crypts that maintained *Sox9* expression, retained Paneth cells, leading to the conclusion that Paneth cells are essential for stem cell maintenance. However, more recently, the requirement of Paneth cells for the maintenance of the stem cell niche was challenged by two studies, showing that Paneth cell depletion *in vivo* does not affect the intestinal stem cells [19,20]. Both studies utilised a transcription factor important for determining the secretory cell fate, *Atoh1* (atonal homologue 1), for genetic ablation of Paneth cells. The authors showed that in *Atoh1*$^{fl/fl}$ mice, upon Cre activation, complete loss of Paneth cells was apparent, however the intestinal stem cells were present and functional. The authors of the studies concluded that Paneth cells are dispensable for the survival and proliferation of stem cells *in vivo*. However, *Atoh1* deletion mimics continuous activation of the Notch pathway,

removing stem cell dependence on Notch signalling, and it is therefore not an accurate approach to study the requirement of Paneth cells [1].

1.2 Colon cancer

The intestinal epithelium is tightly controlled, balancing rapid cellular proliferation, cell loss and organisation of the epithelial monolayer. Malignant transformation of the intestinal epithelium compromises tissue organisation and can be achieved through mutational inactivation of the tumour suppressor gene *adenomatous polyposis coli* (*APC*). In particular, oncogenic mutations in *APC* are sufficient to initiate intestinal epithelial tumorigenesis that, in the colon, precedes the acquisition of other driver mutation during the development of colon adenocarcinoma [21]. In 1990, Fearon and Vogelstein first proposed a multistep genetic model of colorectal neoplasia progression that has remained as a paradigm for disease development [22]. Colon cancer development proceeds with the acquisition of frequently occurring oncogenic mutations in *KRAS* and in three tumour suppressor genes: *APC, SMAD4* and *TP53* (Figure 1.3). Somatic mutations in the *APC* gene are widely regarded as the initiating event of 80-90 % of sporadic colon cancers. Moreover, germline mutations in the *APC* gene result in the familial adenomatous polyposis (FAP) condition, which predisposes a person to colorectal cancer (CRC) [23]. Germline and somatic *APC* mutations are typically nonsense mutations in a region termed the "mutation cluster region" (MCR), leading to the loss of the central and C-terminal domains of the protein [24]. The significance of the loss of these regions defines the basis of my thesis and is discussed below in the section "APC protein".

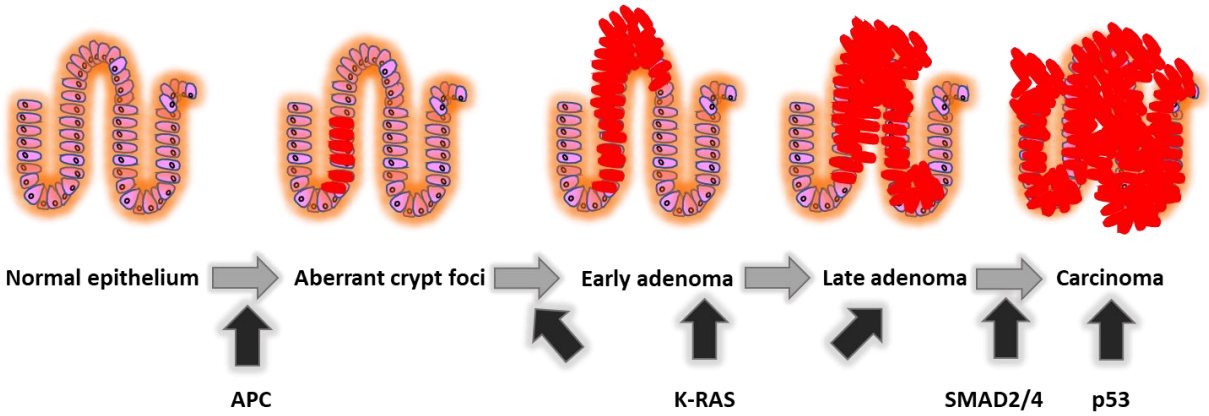

Figure 1. 3: Multistep genetic model of colon carcinogenesis. Molecular events associated with the adenoma–carcinoma sequence first proposed by Fearon and Vogelstein [22,25].

The origin of CRC has long been discussed within the so called top-down versus bottom-up debate, where the cell of origin of cancer is thought to be located either at the top of the crypt or originate from stem cells at the bottom of the crypt, respectively [26,27]. Using a Cre-lox mouse model of *Apc*, it has been postulated that the crypt stem cell is the origin of colorectal cancer [28]. However, as more studies are showing plasticity within the intestinal epithelial cells, the paradigm has started to shift towards potentially other cells for origin of initiation of tumorigenesis [29].

1.2.1 Mouse models of intestinal tumorigenesis

Mouse models have remained as the principal model to study the onset and progression of colon cancer, with various mouse models baring different germline modifications. Most of the models allow studying early stage intestinal tumorigenesis. However, models that more closely mimic late-stage disease with metastasis have also started to emerge, though they are still lagging behind due to problems including the high tumour burden in mice before they have had the opportunity to metastasise [30,31].

In my thesis work, I focus on understanding the onset of intestinal tumorigenesis and therefore only use models that inactivate *Apc*, to mimic the initiation of CRC. APC is well conserved between mouse and human with 92 % similarity on an amino acid level making mice deficient in APC relevant to human disease development [32]. There are over 20 mouse models with different germline *Apc* mutations that differ in their phenotype [30]. In this study I use a well characterized $Apc^{Min/+}$ mouse due to its full loss of the central and C-terminal regions for APC domain specifications and the $Apc^{fl/fl}$ mouse to model acute depletion of the protein.

1.2.1.1 $Apc^{Min/+}$ mouse

The first link between mutations in *Apc* gene and intestinal neoplasia originates from studying the $Apc^{Min/+}$ mouse model [32–34]. Min (multiple intestinal neoplasia) is a mutant allele of the murine *Apc* generated by random germline mutagenesis that encodes a nonsense mutation at codon 850, leading to the loss of the central and C-terminal domains of the protein [35]. $Apc^{Min/+}$ mice are heterozygous for *Apc* with loss of heterozygosity (LOH) of the other allele manifesting spontaneously during development. The $Apc^{Min/+}$ mouse model is regarded as a model for the human FAP condition, due to the similarity in the localisation of polyps within

the intestine. Colon cancer patients develop tumours normally only in the colon, while human FAP patients develop hundreds of small adenomatous polyps throughout the colon that also present in the small intestine [36]. *Apc*$^{Min/+}$ mice in a C57BL/6J background develop more than 40 tumours by 110 days of age, mostly throughout the small intestine, but with also some present in the colon [37]. The tumours do not progress to adenocarcinoma, presumably due to the short lifespan of these mice [38]. *Apc*$^{Min/+}$ model has been used to characterise adenoma development in intestinal tumorigenesis, however due to the difference in localisation of polyps, care must be taken when extrapolating results to the human disease.

1.2.1.2 *Apc*$^{fl/fl}$ mouse

The advent of Cre-lox technology in the 1990s allowed researchers to delete genes in a tissue-specific manner, on demand [39]. A previous study describes the construction of a mouse model engineered so that *loxP* recombination sites flank exon 14 of the *Apc* gene. Excision of exon 14 via Cre recombinase expression leads to a frameshift mutation at codon 580 (hereafter *Apc*$^{fl/fl}$) and expression of a truncated protein [40]. Depending on the promoter used to drive Cre expression, these mice develop adenomas in the colon and small intestine [40,41]. In this work, I describe the use of the *Apc*$^{fl/fl}$ mouse model to determine the primary and direct consequence of loss of APC in an otherwise normal intestinal epithelium.

1.2.2 Organoids to model intestinal tumorigenesis

The use of fixed intestinal epithelial sample to study the initiation of tumorigenesis provides a snapshot of the tissue. However, this does not allow for monitoring changes taking place in real time. In addition, 2-dimensional colorectal cancer cell lines poorly maintain *in vivo* cell characteristics, failing to recapitulate tissue-specific architecture, mechanical and biochemical cues, and cell-cell communication. In 2009 Sato *et al* made a breakthrough achievement in establishing the minimal stem cell niche requirements in a media formulation to grow self-organising miniguts from crypts, termed intestinal organoids [42]. Organoids are grown in a 3-dimensional collagen/laminin/fibronectin matrix and faithfully recapitulate the 3-dimensional (3D) architecture and cellular composition of the epithelial monolayer (Figure 1.4). They consist of an epithelium, complete with crypts harbouring a stem cell niche at their base [42]. A key advantage over the use of *in vivo* models is that organoids can be genetically modified to monitor alterations dynamically. The growth of intestinal organoids requires three essential

stem cell niche promoting growth factors: R-spondin to potentiate Wnt signalling, epidermal growth factor (EGF) to stimulate mitogen signalling and noggin/gremlin, inhibitors of the differentiation cues driven by bone morphogenic protein (BMP) signalling [42]. Intestinal epithelial organoids can be derived from whole crypts or individual $Lgr5^{+}$ stem cells. Isolation of individual stem cells bound to a Paneth cell dramatically improves the efficiency of organoid derivation from $Lgr5^{+}$ stem cells up to 7-fold, demonstrating the requirement of Paneth cells in supporting the stem cell niche [15]. In this thesis, I use mouse small intestinal organoids derived from crypts from the later section of the intestine, the ileum. I also derive organoids from the polyps of $Apc^{Min/+}$ mice (I term them tumoroids) which form cystic organoid structures that lack defined crypt structures as a model of *in vitro* tumours [43].

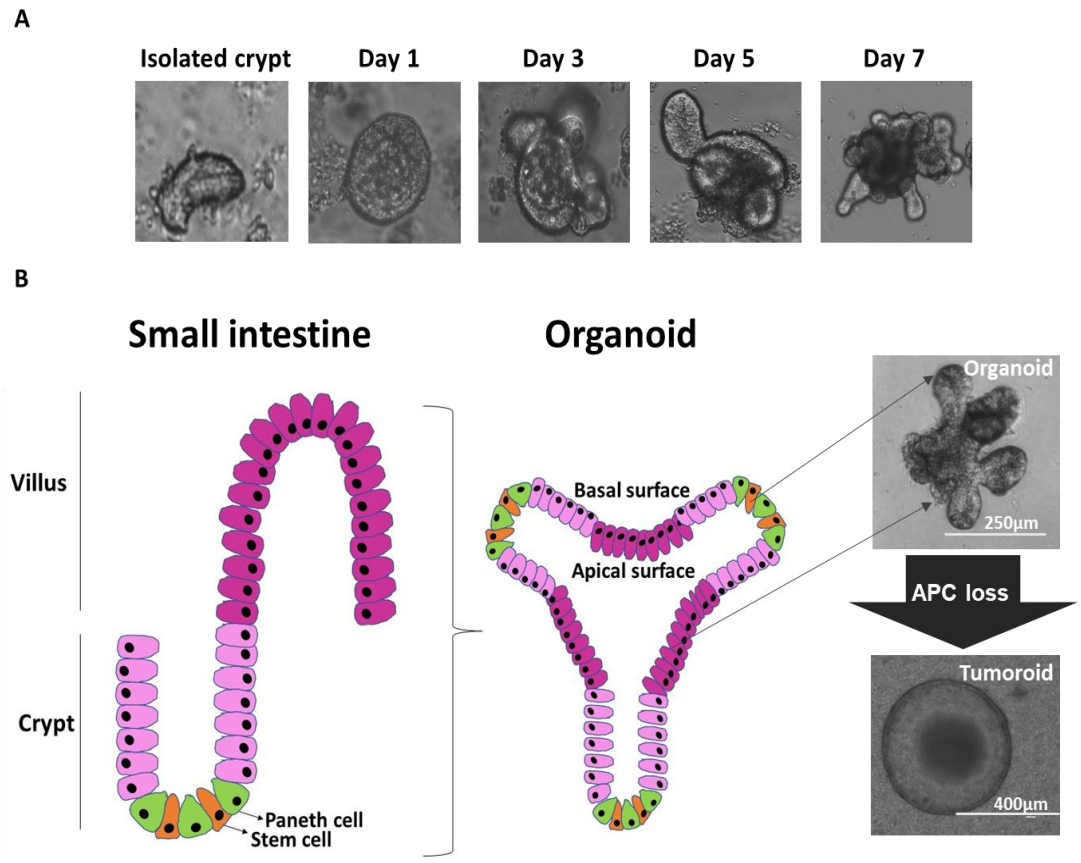

Figure 1. 4: Small intestinal organoids recapitulate the cellular composition and tissue morphology of the intestinal epithelial monolayer. Time-line of a single crypt developing into a budding organoid in culture (A). Small intestinal organoids grow as budding structures where the bud is representative of a crypt in the tissue. Organoids made from the adenomas of an $Apc^{Min/+}$ mouse (tumoroids) grow as spheres and show increased proliferative capacity (B).

1.3 Polarised epithelial cell

Epithelial cells, like intestinal cells, exhibit apical-basolateral polarity (AB) polarity. AB polarity represents cellular polarity, where a distinct domain identity is present, allowing a cell to determine where is up (apical) and where is down (basolateral) [44]. Functionally, AB polarity is important to regulate the asymmetrical distribution of components within a cell and maintain apically located intercellular junctional complexes [45]. Epithelial cells must maintain stable polarity in order to preserve their differentiated states and carry out their functional roles in the digestive, respiratory, vascular, hormonal, reproductive, neural and sensory systems [46].

There are three main polarity complexes that maintain and establish the apical, basal and lateral identity: apically localised Crumbs and Par complexes, and the laterally localised Scribble complex (Figure 1.5). Studies have linked the deregulation of core polarity proteins with cancer and many polarity proteins are regarded as either tumour suppressors or proto-oncogenes [45].

Apical junctional complexes comprised of tight and adherens junctions establish the apical and basolateral domains [44]. The junctional complexes are composed of transmembrane proteins that interact with the neighbouring cell via homotypic protein-protein interactions; in addition, they include numerous cytoplasmic proteins that connect with the cytoskeletal network. The primary function of adherens junctions is to provide strong adhesion between neighbouring cells, while tight junctions create a seal between epithelial cells and produce a selectively permeable diffusion barrier for proteins, lipids and solutes. Importantly, defects in cell–cell adhesion and AB polarity have been linked to tumorigenesis [47].

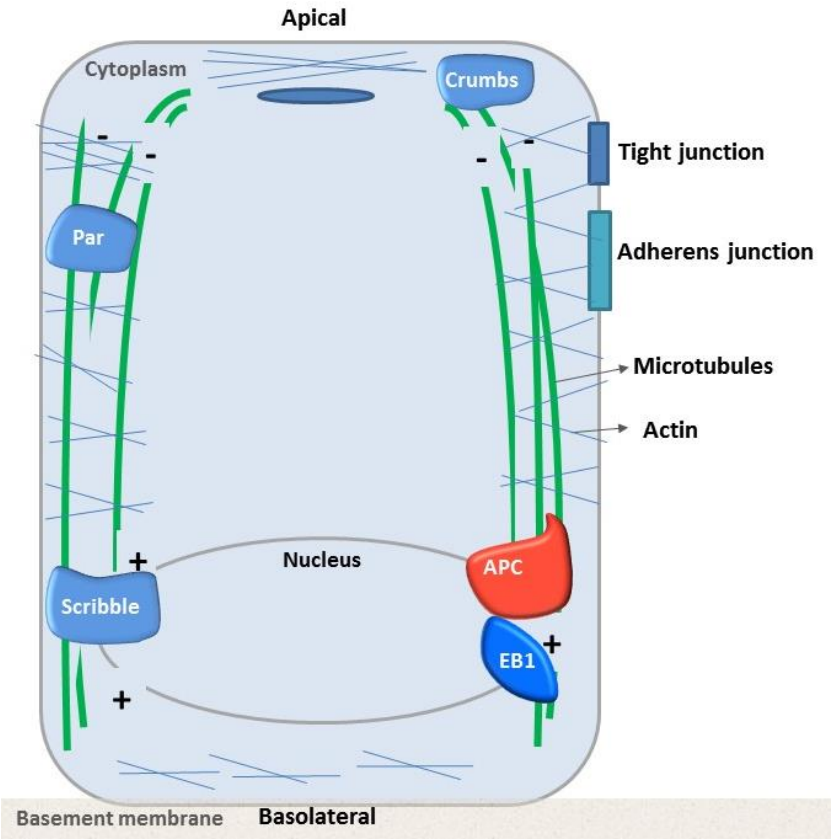

Figure 1. 5: Polarised epithelial cell. Epithelial cells exhibit apical-basolateral polarity with the apical side facing the lumen and the basolateral domain facing the extracellular matrix. Apically localised tight and adherens junctions and Crumbs and Par complexes, and the laterally localised Scribble complex establish and maintain the polarisation of a cell.

1.3.1 The cytoskeleton

Polarised cells, like the intestinal epithelial cells, are highly dependent on the cytoskeleton to carry out their specialised functions. The cytoskeleton is responsible for the establishment and maintenance of the internal order within a polarised cell. It provides shape and structure for the cell to function properly [48]. The three cytoskeletal filaments actin, microtubules and intermediate filaments, cooperate to regulate the cells' spatial organisation and mechanical properties. Intermediate filaments offer mechanical strength, actin filaments determine the shape and movement of the cells, and microtubules regulate the positioning of organelles and direct intracellular transport [46]. For the purpose of this thesis work, I focus on the microtubule cytoskeleton to describe its roles in a polarised epithelial cell and the significance of its correct functioning.

1.3.2 The microtubule cytoskeleton

Microtubules are long hollow cylinders with an outer diameter of 25 nm and are formed of 13 microtubule protofilaments, aligned laterally, each composed of alternating α- and β-tubulin subunits (Figure 1.6) [49]. The two ends of microtubules polymerise at different rates with the faster growing end referred to as the plus end. Both microtubule ends exhibit dynamic instability, alternating between slow growth and rapid disassembly [50]. Hydrolysis of the bound GTP nucleotide to GDP dictates the speed of depolymerisation—depolymerisation is approximately 100 times faster from a microtubule end containing GDP tubulin compared to an end containing GTP, favouring disassembly over growth of microtubules [48].

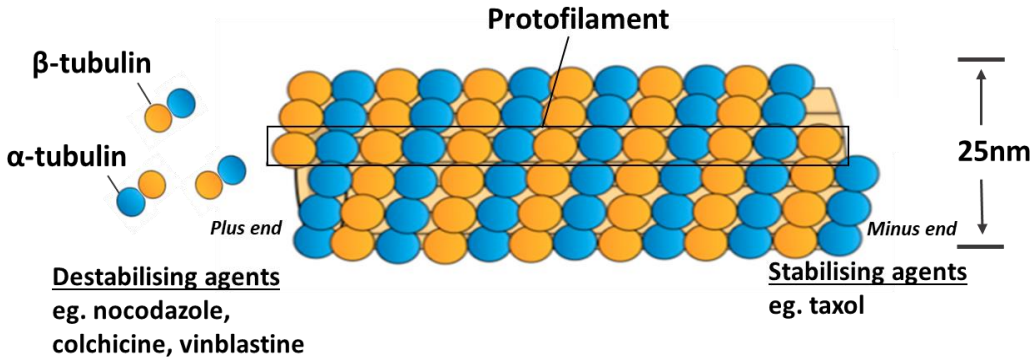

Figure 1. 6: The structure of a microtubule polymer. Microtubules are composed of subunits made from tubulin. Each subunit of the microtubule is made of α- and β-tubulin which are bound together to form heterodimers. The subunits all point to the same direction to form parallel protofilaments giving the structure polarity, with only the α-tubulin proteins exposed at minus end and only β-tubulin proteins at the plus end. Microtubule-specific drugs bind to different sites on the microtubule polymer, affecting the inherent dynamic instability of microtubules.

De novo formation of microtubules (nucleation) in non-polarised cells is coordinated by a microtubule-organising centre (MTOC). The primary MTOC in animal cells is the centrosome [51]. There, the microtubules grow from a multi-protein complex localised at the centrosome, called γ-tubulin ring complex (γ-TURC), with their minus ends embedded in the centrosome and the plus ends emanating outward towards the cell periphery [49]. However, in many differentiated cell types such as polarised epithelial cells, skeletal muscle and neurons, the function of MTOC is reassigned to non-centrosomal sites (ncMTOC), where microtubules are organised in non-radial arrays. Studies have suggested that the microtubules emanating

from ncMTOCs can instead be associated with adherens junctions [52]. The correct assembly, positioning and preservation of these non-centrosomal microtubules, is vital for many of the cells' specialised functions (Figure 1.7) [52–54].

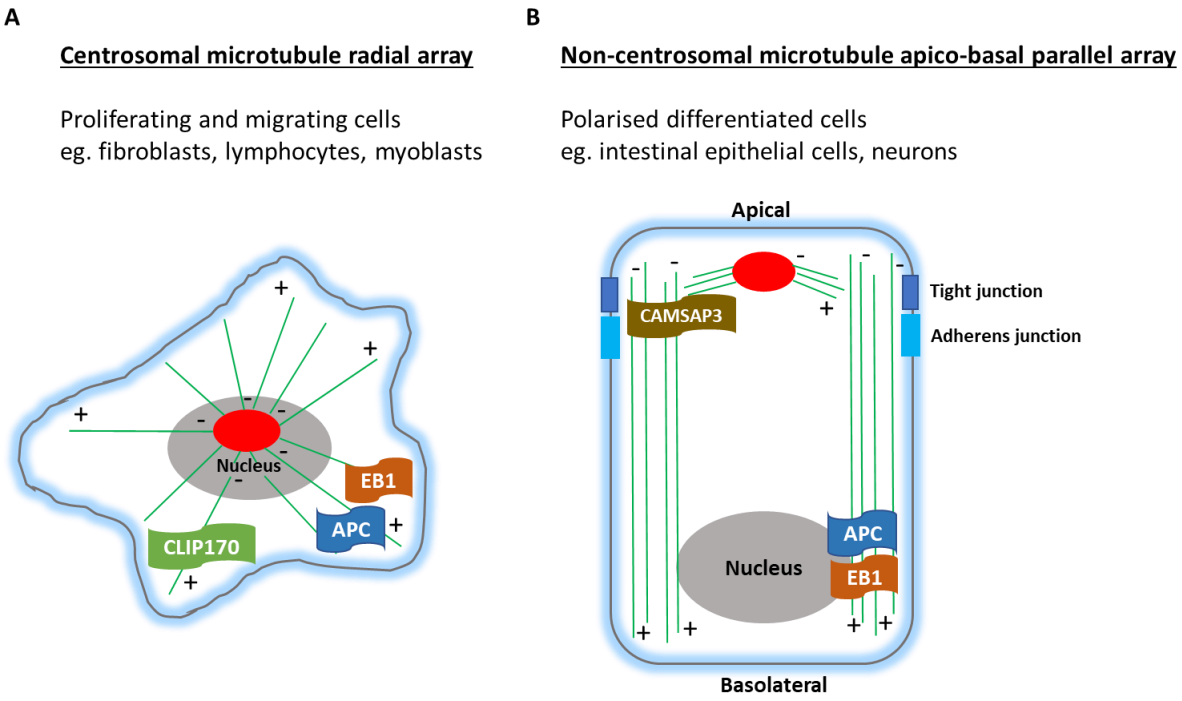

Figure 1. 7: Arrangement of microtubules in non-polarised versus polarised cells. In non-polarised cells, the centrosome serves as the main MTOC from where the microtubules emanate. +TIPs like CLIP170 regulate microtubule dynamics [52] (A). In polarised cells, the microtubules are not anchored to the centrosome [55]. It is thought that most microtubules anchor to the adherens junctions and involve proteins like CAMSAP3 which capture the minus ends of microtubules [56,57] (B). Centrosome is in red. The proposed localisation of APC and EB1 is depicted [53,58–61].

1.3.3 Microtubule functions in polarised epithelial cells

In a polarised epithelial cell, like the intestinal epithelial cell, microtubules provide the structural basis for cell polarisation, and are vital for cell division by being the main constituent of the mitotic spindle. In a non-dividing polarised cell, microtubules run vertically from the apex to the base of the cell to form parallel arrays with the minus end of microtubules at the apex of the cell [48].

A key function of microtubules is to coordinate the localisation of intracellular components, including organelles such as the nucleus, the Golgi complex, mitochondrion, the endoplasmic reticulum (ER), endosome, lysosome and peroxisome [49]. Microtubules also organise the membranous systems of the Golgi complex and ER [62]. The Golgi complex consists of flattened, membrane enclosed compartments, called cisternae that are linked by microtubules into Golgi stacks [63]. The ER also contains cisternae that are held together by microtubules [62]. The trafficking of cargo along microtubules relies on the kinesin and dynein motor proteins; most kinesins move towards the plus end of microtubules and dynein in the opposite direction [46]. Defects in microtubules can influence motor protein based transport *in vitro* [64]. Thus, an intact microtubule cytoskeleton is vital for both the localisation and integrity of intracellular organelles.

Post-translational modifications of microtubules are thought to play a role in coordinating functions of microtubules in the cells [65]. These post-translational modifications include acetylation, polyglutamylation, polyglycylation, tyrosination/detyrosination, phosphorylation and palmitoylation. With the exception of acetylation, these modifications localise to the outer face of microtubules and can presumably affect interactions with binding proteins [66]. Proteins that bind to the growing plus end of microtubules, called microtubule plus-end tracking proteins (+TIPS), further control the different aspects of microtubules by regulating their dynamics and their interactions with proteins [67]. Proteins binding to the minus end of microtubules (-TIPs) like the CAMSAP/Patronin/Nezha family members have been shown to function in contributing to the non-centrosomal microtubule organisation, in cell division, migration and differentiation [68].

Microtubule-specific drugs can be used to manipulate and study microtubule-dependent functions. Several anti-microtubule drugs have important medical uses, particularly colchicine, which is used to treat gout, and vinblastine and taxol, which are used as chemotherapeutic agents to treat cancer [69]. The exact mechanism of action for many of the drugs is yet to be exactly defined, although they can be divided into two groups: microtubule stabilising and destabilising agents. Colchicine, vinblastine and nocodazole cause microtubule depolymerisation and destabilisation, while taxol binds to and stabilises microtubules, causing a net increase in polymerisation (Figure 1.6). The binding sites for the different drugs vary,

with vinblastine binding to the plus ends of microtubules, colchicine and nocodazole to soluble tubulin dimers and taxol to the interior surface of microtubules [70].

1.4 The APC protein: structure and function

The APC protein has crucial functions that impact homeostasis of polarised intestinal epithelial tissue—mutational inactivation of *APC* is the sole genetic lesion required to initiate intestinal epithelial tumorigenesis [21]. Interestingly, in colon cancer, mutations invariably occur within a discrete region of the protein (termed the mutational cluster region or MCR), leading to the expression of a truncated protein encoded by at least one of the inactivated *APC* alleles. The truncated protein lacks the central and C-terminal domains of APC. Understanding the specific phenotypic and molecular consequences of truncated APC is the primary focus of my thesis work.

1.4.1 Structure

APC is a large, multi-functional protein harbouring several domains for interactions with various proteins. The N-terminal region of APC contains seven armadillo repeats through which it interacts with the actin cytoskeleton [71,72], as well as indirectly with the microtubules via Kap3, a linker protein for kinesins (Figure 1.8) [73]. The central region of APC contains domains that interact with proteins regulating the Wnt signalling pathway (described below). The region is composed of (i) seven 20 amino acid repeats (20R) and three 15 amino acid repeats (15R) that, together, function to bind and promote the degradation of β-catenin [74], (ii) the so called β-catenin inhibitory domain (CID), located between the second and third 20R, that down-regulates the transcriptional activity and the levels of β-catenin [75]; and (iii) three Ser-Ala-Met-Pro-rich repeats (SAMP repeats) that bind to Axin [76]. The C-terminal region of APC contains domains for direct interaction with microtubules and for binding the microtubule plus end-binding protein 1, EB1 [60,77]. The final 15 amino acids of the C-terminus of APC has been shown, by a single study, to contain a binding site for PDZ domains and bind hDLG, the human homolog of the Drosophila discs large protein, implicated in cell junction structure and polarity [78].

MCR mutations lead to the expression of a truncated protein that lacks 1-3 of the 20R domains involved in interaction with β-catenin, all SAMP repeats which are required for binding to Axin

and the interaction domains with the microtubule cytoskeleton. Therefore, APC's functions in controlling Wnt pathway activity and interactions with the microtubule cytoskeleton are compromised.

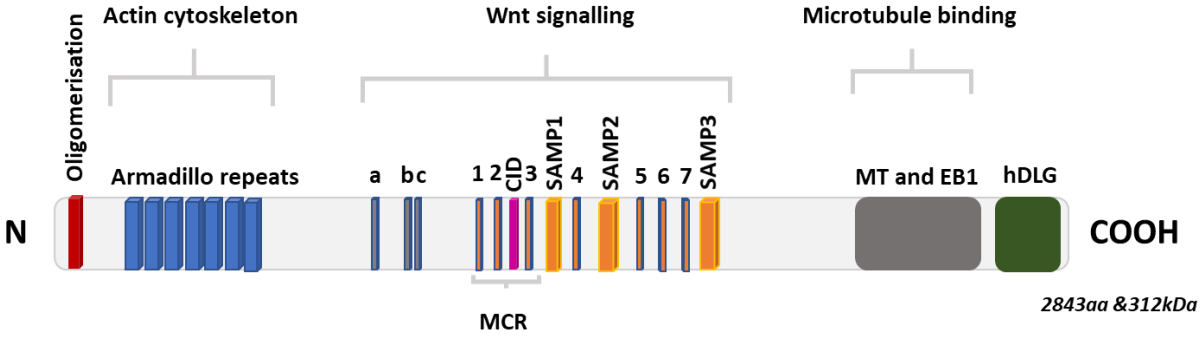

Figure 1. 8: Primary structure of APC protein. The majority of oncogenic mutations in APC are nonsense mutations in the MCR resulting in a truncated protein. The C-terminal portion of the protein is involved in binding to microtubules and to EB1. The central part of the protein has binding domains involved in regulating the Wnt pathway activity: the 15 amino acid β-catenin-binding repeats are labelled a, b and c, the 20 amino acid β-catenin-binding repeats 1–7 and the Axin-binding repeats SAMP1–3. CID marks the β-catenin inhibitory domain. Interactions with the actin cytoskeleton occur in the N-terminal domain via the armadillo repeats.

1.4.2 Functions

APC is reported to be localised to the cytoplasm, but also to membrane pools and the nucleus [79–82]. The distinct localisations and the multitude of interaction domains are responsible for the complexity and diversity of the biological functions of the APC protein [83]. Given the breadth of binding partners that overlap in their interaction domains within APC, it is possible that the different functions of APC cooperate or compete against each other. However, the hierarchy or collaboration of the different APC functions remains largely unknown [2,83]. Findings that APC is also able to self-associate and affect its functions complicates the stratification of its specific cellular functions even further [84,85].

1.4.2.1 APC in Wnt signalling

The most studied and well-known role of APC is in its regulation of the canonical Wnt pathway (Figure 1.9). Wnt pathway activity is required for the maintenance and regulation of intestinal epithelial stem cell proliferation and multipotency [86]. Specifically, APC attenuates Wnt

pathway activity by participating in the destruction complex that earmarks β-catenin, the primary Wnt pathway effector, for proteasome-mediated degradation [87]. In the presence of a Wnt ligand, the ligand binds to the cell-surface receptor Frizzled and low-density lipoprotein receptor-related protein (LRP) 5/6. The ligand-receptor complex triggers a series of events that result in the stabilisation of β-catenin. Stabilised β-catenin can then enter the nucleus to interact with LEF-TCF transcription factors and activate transcription of the Wnt target genes, including *c-Myc, Axin2, Ephrins* and many others [86,88]. A key regulatory feature of the Wnt pathway is the β-catenin destruction complex (βDC), a multiprotein complex that targets β-catenin to the proteasome [89]. The βDC is composed of Glycogen Synthase Kinase 3 β (GSK3β), Casein Kinase 1 α (CK1α) and the scaffold proteins Axin and APC. In the absence of a Wnt ligand, Axin binds to β-catenin and bridges the kinases GSK3β and CK1α. This leads to the phosphorylation of β-catenin triggering the recruitment of E3 β-TrCP ubiquitin ligase [89]. The ubiquitination of β-catenin results in its proteasomal degradation [87]. In the presence of a Wnt signal, Dishevelled (Dsh) protein inactivates GSK3β, leading to a decrease in the kinase activity in the complex. This results in a decrease in the amount of β-catenin targeted for degradation and thus increases the availability of β-catenin to enter the nucleus and activate context-specific Wnt target genes [90,91]. Many of the Wnt target genes, including *c-Myc, CD44, Axin2 and Sox17*, are involved in proliferation, differentiation and migration; thus their proper regulation is important for tissue homeostasis [41].

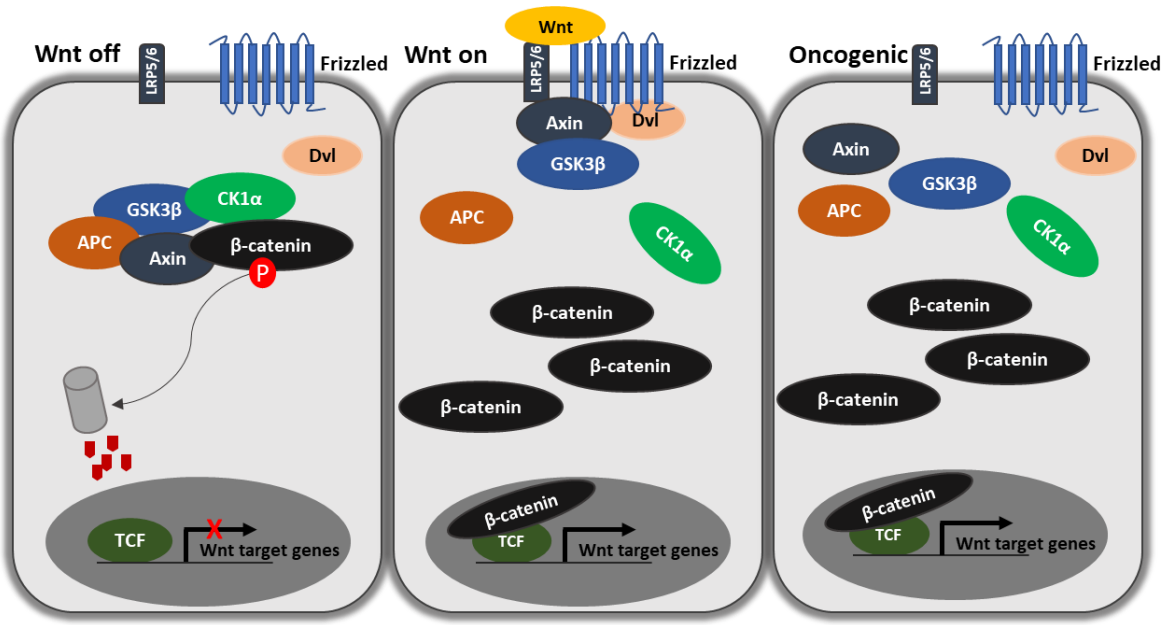

Figure 1. 9: Canonical Wnt signalling in normal and oncogenic setting. In the absence of a Wnt ligand, β-catenin is phosphorylated by the βDC leading to its proteasomal degradation. In the presence of a Wnt ligand, βDC is inhibited and β-catenin translocates to the nucleus to drive the transcription of Wnt target genes. Mutational inactivation of APC results in constitutively elevated β-catenin levels and uncontrolled expression of Wnt target genes.

How, specifically, APC drives the destruction of β-catenin is still unclear. Studies have suggested that it may act as a de-repressor of the complex [92], enhancer of β-catenin binding to the complex [93], or be directly involved in gathering β-catenin from the nucleus and cytoplasm and deliver it to the complex [94]. Consequently, mutational inactivation of APC leads to deregulated activation of the Wnt-dependent transcriptional program and drives uncontrolled proliferation and transformation of intestinal epithelia [95]. Importantly, it has been shown that the Wnt target gene *c-Myc* is the main mediator of murine intestinal epithelial tumorigenesis following inactivation of APC [96].

1.4.2.2 APC as a cytoskeletal regulator

Several studies have established that APC interacts with proteins associated with the microtubule and actin cytoskeletons and may play a key role in establishing AB cell polarity [97]. The apical-basal domain identity and the function of cells is maintained by the establishment of specific cytoskeletal arrangements [47]. Therefore, the correct functioning of proteins, like APC, which play a role in regulating the cytoskeletal network, is especially important for intestinal epithelia.

1.4.2.3 APC interaction with actin cytoskeleton

The armadillo repeats at the N-terminal domain of APC have been shown to interact with and stimulate the activity of Asef (APC-stimulated guanine nucleotide exchange factor), an exchange factor for small GTPases [71]. Small GTPases control cell shape and migration by regulating downstream effectors that influence the actin cytoskeleton [98]. Truncated APC leads to constitutively active Asef resulting in increased migration and decreased cell adhesion [71]. It has been recently shown that unregulated signalling of Asef leads to fragmentation of the Golgi complex [99]. However, my results in Chapter 4 contradict this finding. In addition, another effector of small GTPases, IQGAP1 (IQ Motif Containing GTPase Activating Protein 1), has been shown to interact directly with the armadillo repeats in APC [72]. This interaction is thought to be important for regulating actin dynamics in cell migration and polarisation [100]. Finally, a study demonstrating the localisation of APC at the lateral plasma membrane suggests a close association of APC with filamentous actin (F-actin) [80]. These findings show that the interactions between APC with the actin cytoskeleton regulate epithelial cell morphology, adhesion and migration.

1.4.2.4 APC interaction with microtubule cytoskeleton

APC interacts with the microtubule cytoskeleton directly and indirectly. APC is shown to bind to microtubules via its C-terminus [77]. APC interacts with microtubules at the growing plus ends and thus falls into the category of +TIPs [67]. The binding of APC to microtubules stabilises the microtubule ends [101]. Specifically, the deletion of the microtubule binding domain does not eliminate APC's binding to microtubules, but rather decreases the ability of APC to stabilise them. In addition, the interaction between microtubules and APC has been shown to be decreased by phosphorylation of APC by GSK3β [101]. This finding is opposite to the effect of APC binding to β-catenin, suggesting that the binding of APC to microtubules and β-catenin is mutually exclusive. Further, APC regulates the microtubule cytoskeleton indirectly via EB1 [60]. APC-EB1 interaction is suggested to involve the C-termini of both proteins [102]. EB1 is thought to recruit APC to the growing, plus ends of microtubules located at the base of the cell [59]. The association of APC with the growing ends of microtubules supports the establishment of parallel arrays of microtubule bundles in a polarised cell [53]. Studies on Drosophila neurons have implicated APC in the guidance of growing microtubules at their plus ends [103,104]. It was proposed that the microtubule plus-end walking motor protein, kinesin-2, is recruited to the

plus ends of growing microtubules by EB1 through APC, where it steers growing microtubules to maintain polarised arrays of microtubules [103]. APC has also been suggested to function in microtubule nucleation and growth [105]. APC was shown to bind to the microtubule nucleation factor γ-tubulin through its N-terminal domain and suggested to help target APC to the centrosome. While not necessary for binding to γ-tubulin, the C-terminal domain of APC was shown to be required to stimulate and stabilise microtubule growth [105]. APC has also been shown to accumulate in clusters near the plus ends of microtubules at the edges of migrating epithelial cells [106,107]. Finally, via interactions with its N-terminal domain, APC has been linked to microtubules via Kap3, a linker protein for microtubule motor proteins, kinesins [73]. However, this interaction is not sufficient for microtubule cluster formation. Therefore, APC has several ways of binding to microtubules, with the C-terminal domain of APC being essential for the functional interaction with the microtubule cytoskeleton. In the context of early intestinal tumorigenesis, the loss of the C-terminal domain of APC bearing interaction domains with the microtubule cytoskeleton could therefore alter this tightly regulated intracellular organisation.

1.4.2.5 APC in chromosome segregation

APC localises to kinetochores of metaphase chromosomes and to mitotic spindles of anaphase cells [108]. Truncating mutations in APC and loss of the C-terminal domain have been linked to spindle aberrations and aneuploidy, providing evidence for the link between APC-microtubule interactions and chromosomal instability (CIN) [108–111]. Indeed, 65 %-70 % of sporadic colorectal cancers exhibit CIN and previous reports have found evidence that this could be due to loss of APC's C-terminal microtubule interaction domain [108,112].

1.4.2.6 APC interaction with microtubules in tumorigenesis

The consequence of the loss of the microtubule binding domain of APC on the intestinal epithelial homeostasis has been studied *in vivo* (Figure 1.10). A mouse model was developed that expresses a mutant form of *Apc*, truncated at codon 1638 ($Apc^{1638T/+}$), resulting in the loss of the four 20aa repeats, two SAMP repeats and the rest of the C-terminal domain including the microtubule interaction domains [113]. $Apc^{1638T/+}$ and $Apc^{1638T/1638T}$ mice are tumour free, and the authors of the study concluded that the C-terminus of APC is not required for tumour formation [113]. βDC activity was only moderately affected in these mice owing to the retention

of one SAMP repeat in the truncated Apc [113]. Another study showed that mice lacking six 20 aa repeats, all SAMP repeats and the rest of the C-terminal domain of APC (*Apc*$^{1322T/+}$) develop adenomas [114]. These mice had increased nuclear β-catenin levels, indicative of the loss of APC's down-regulating capacity of β-catenin. In addition, the authors developed a mouse model identical to *Apc*$^{1322T/+}$ but with an intact C-terminus (*Apc*$^{SAMP/+}$) and showed that these mice also developed adenomas, indistinguishable from *Apc*$^{1322T/-}$. Taken together, the two studies indicate that the loss of the C-terminal microtubule interaction domain of APC is not sufficient to drive the formation of intestinal tumours. However, the cellular implications due to the loss of the C-terminal domain of APC beyond CIN have not been determined in the intestinal epithelia.

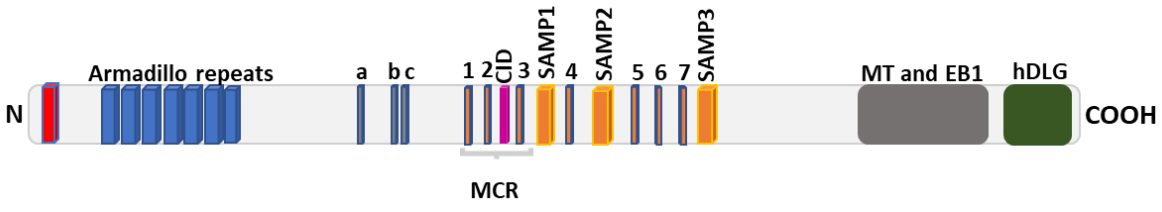

Mouse model	Adenomas?	Domains present
Apc$^{Min/+}$	yes	
Apc$^{fl/fl}$	yes	
Apc$^{1638T/1638T}$	no	
Apc$^{1322T/+}$	yes	
Apc$^{\Delta SAMP/+}$	yes	

Figure 1. 10: APC truncation in various mouse models of intestinal epithelial tumorigenesis. Different mouse models carrying mutations in the Apc gene have been developed to study intestinal tumorigenesis and APC domain specific roles.

1.5 Aims of the thesis

The role of APC in the intestinal epithelia with regards to the Wnt signalling pathway has been extensively studied. However, the phenotypic and functional consequences of the loss of APC's interaction with the microtubule cytoskeleton have not been determined. The aims of my thesis are as follows:

- Phenotypically characterise the intracellular organisation and tissue morphology of intestinal epithelia upon APC inactivation

- Determine the functional roles of the central and the C-terminal domain of APC that are lost upon APC inactivation leading to intestinal tumorigenesis

- Investigate the specific consequence of APC loss in a stem cell supporting cell, identifiable by a distinct cellular morphology—the Paneth cell—on intestinal epithelial homeostasis

Chapter 2:

Materials and methods

2.1 Organoid technology development

The protocols to generate and manipulate organoids and tumoroids were developed from previously published guidelines. I have therefore provided detailed protocols describing each step.

2.1.1 Derivation of organoids

The small intestinal ileum from wild-type C57BL/6 mice was used to derive wild-type organoids. Organoids were generated from crypts following a published protocol with some modifications [42].

I received the small intestine with cecum on ice in PBS with no Ca^{2+}/Mg^{2+} (PBS). The following were carried out under non-sterile conditions, unless stated otherwise. The small intestine was cut into three equal parts with pre-sterilised scissors, keeping only the distal part of the small intestine (ileum) for organoid culture, using the position of cecum for orientation. The reason for using only ileal organoids was two-fold. Firstly, given differences within the small intestine [115], I decided to restrict experiments to only ileum as *Apc*$^{Min/+}$ mice preferentially develop tumours there [116] allowing me to directly compare organoids to tumoroids. Secondly, the Paneth cell specific prompter developed in Chapter 5 was indicated to have highest expression in the ileum and therefore I decided to utilise only ileal organoids for highest control over Paneth cells.

Using a 10 ml syringe with a 25-gauge needle ice-cold PBS was used to remove the faeces from the ileum. Tweezer were then used to remove the fatty tissue around the intestine. The intestine was opened longitudinally using scissors and spread by tweezers. The intestine was cut into 2-4 mm pieces and placed into a 50 ml falcon filled with 25 ml ice-cold PBS. The tube was shaken 50 times to remove the villi. The intestinal pieces were left to settle, and the tissue pieces transferred to a new 50 ml falcon tube with ice-cold PBS. The tube was shaken 50 times and again transferred to a new tube as before. This procedure, with the aim to remove villi and clean the tissue, was repeated total of 5 times. After the last wash, the tissue pieces were transferred to a 50 ml falcon containing 25 ml of 2 mM ethylenediaminetetraacetic acid (EDTA) in PBS and placed on a roller in 4°C for 30 minutes to release the crypts from the mesenchyme. The tube was shaken 3 times, the EDTA medium discarded and then 10ml of

ice-cold PBS added onto the settled tissue pieces. Using a 10 ml stripette, the tissue pieces were pipetted up and down in PBS, let to settle and then the supernatant removed to a new tube. This was fraction 1. This procedure was repeated five times, ie 5 fractions in total were collected, with the aim of enriching crypts with each fraction. 10 µl of each fraction was pipetted onto a petri dish to check for the presence of crypts under the microscope. All the fractions with crypts in them were pooled into a 50 ml falcon tube (usually fractions 2-4), topped up with ADF (Table 2.1) and passed through a 70 µm cell strainer into a new 50 ml falcon tube. The tube was centrifuged at 200 RCF for 5 minutes at 4°C. The supernatant was carefully removed, and the pellet was taken up in 10 ml ADF. The tube was then centrifuged at 450 RCF for 5 minutes at 4°C.

All subsequent steps were carried out under sterile conditions in a tissue culture grade Laminar flow hood. The supernatant was removed with minimal disturbance to the pellet. When the whole ileum was used, the pellet that formed was taken up in 400 µl of 100 % phenol-red free Matrigel that had been thawed on ice (Table 2.1) and plated out 40 µl/well into a pre-heated 24-well plate (plate in 37°C for 24 h prior to use). This yielded on average 100 crypts/40 µl Matrigel dome. The plate was placed into a 37°C incubator with 5% CO_2 for 10 minutes to allow the Matrigel to solidify. The plate was then taken out and 600 µl of pre-warmed WENR media with 10 µm ROCK inhibitor was added per well (Table 2.1). The plate was placed back into the 37°C incubator. The media was switched to ENR (Table 2.1) on day 3 and grown in this media unless genetic manipulation was to be carried out (see section 2.1.5). Media was changed every 3rd day and organoids passaged every 5-7 days (see section 2.1.3).

2.1.2 Derivation of tumoroids

Tumoroids were derived from the polyps of an 8-10-week-old *Apc*$^{Min/+}$ mouse where the loss of heterozygosity causes adenomatous polyps to form preferentially in the ileum of the small intestine [116]. Tumoroids were generated from the ileal polyps following a published protocol with several modifications [43].

I received the small intestine with cecum on ice in PBS with no Ca^{2+}/Mg^{2+} (PBS). The following were carried out under non-sterile conditions, unless stated otherwise. The intestine was laid longitudinally onto a Petri dish filled with ice-cold PBS and cut the intestine into three equal

parts with pre-sterilised scissors, keeping only the ileum. Tweezer were used to remove the fatty tissue around the intestine making it easier to spot the polyps. Using a 10 ml syringe with a 25-gauge needle ice-cold PBS was used to remove the faeces from the ileum. The intestine was then opened up longitudinally using scissors and spread by tweezers. The polyps (ranging from 5-20) were cut away from the small intestine using a scalpel while avoiding taking the surrounding tissue along. The polyps were pooled into a 1.5 ml Eppendorf tube with 1 ml of PBS+ 2 % BSA. Using scissors, the polyps were cut into small pieces inside the Eppendorf tube. The pieces were allowed to settle, supernatant removed and 1 ml of fresh PBS+ 2 % BSA added to wash the adenoma cells. This step was repeated three times. After the last wash, the pieces were let to settle, supernatant removed, and the pellet was taken up in 1 ml of 5 mM EDTA in PBS. The Eppendorf tube was placed on a roller in 4°C for 30 minutes to release the normal intestinal cells from the mesenchyme. The tube was then shaken, pieces let to settle, and the supernatant carefully removed. 1 mL of TrypLE Express (Table 2.1) was added to the pellet and incubated for 15 minutes at 37°C to release the adenoma fragments.

All subsequent steps were carried out under sterile conditions in a tissue culture grade Laminar flow hood. The Eppendorf tube was shaken, the supernatant removed, and the adenoma fragments washed with 1 ml ADF + 100 µg/ml Primocin™ (Table 2.1). The wash was repeated three times, each time transferring the supernatant to a 15 ml falcon tube. The 15 ml falcon tube was centrifuged at 650 RCF for 5 minutes at 4°C. The supernatant was removed, and the pellet was again washed with 5 ml ADF + 100 µg/ml Primocin™ followed by centrifugation at 650 RCF for 5 minutes at 4°C. To note, extensive washing in the presence of the antimicrobial/antifungal was necessary as not doing so resulted in contamination of the culture on day 2. The supernatant was carefully removed from the 15 ml falcon tube and the pellet taken up in 120 µl of Matrigel that had been thawed on ice. To note, this amount of Matrigel was suitable for when initially 10-20 adenomas were collected. The amount of Matrigel was lowered when the polyp collection was less efficient. Adenoma cells in Matrigel were plated out 40 µl/ well into a pre-heated 24-well plate (plate in 37°C for 24 h prior to use). The plate was placed into a 37°C incubator with 5% CO_2 for 10 minutes to allow the Matrigel to solidify. The plate was then taken out and 600 µl of pre-warmed EN media with 10 µm ROCK inhibitor (Y-27632) and 100 µg/ml Primocin™ was added per well (Table 2.1). The plate was placed back into the 37°C incubator. Upon successful tumoroid formation, small spheres were

apparent the next day. The media was switched to only EN on day 3. To note, R-spondin 1 addition to tumoroids was dispensable because the loss of APC constitutively activates the Wnt pathway. Media was changed every 3rd day to EN and tumoroids passaged every 5-7 days (section 2.1.3).

Advanced DMEM/F12 +++ (ADF)	**Final concentration**	**Company**	**Catalogue nr**
Glutamax 100X	1X	ThermoFisher	35050061
Hepes 1 M	10 mM	ThermoFisher	15630080
Pen Strep	1X	ThermoFisher	15140122
Advanced DMEM/F12		ThermoFisher	12634028
ENR medium			
Into ADF	**Final concentration**	**Company**	**Catalogue nr**
N21-MAX (B27)	1X	R&D	AR008
N2	1X	ThermoFisher	17502048
mouse EGF	50 ng/ml	R&D	2028-EG
R-spondin 1- MBP	25 nM	de la Roche lab	
Gremlin 1	25 nM	Hyvonen lab	
n-Acetylcysteine	1.25 mM	Sigma	A9165-5G
WENR medium			
Into ADF	**Final concentration**	**Company**	**Catalogue nr**
N21-MAX (B27)	1X	ThermoFisher	AR008
N2	1X	ThermoFisher	17502048
mouse EGF	50 ng/ml	R&D	2028-EG
R-spondin 1- MBP	25 nM	de la Roche lab	
Gremlin 1	25 nM	Hyvonen lab	
n-Acetylcysteine	1.25 mM	Sigma	A9165-5G
Nicotinamide	10 mM	Sigma	N3376
Advanced DMEM/F12	50 % -additives	ThermoFisher	
Wnt3A conditioned media	0.5	From L Wnt3A cells	
EN medium			
Into ADF	**Final concentration**	**Company**	**Catalogue nr**
N21-MAX (B27)	1X	ThermoFisher	AR008
N2	1X	ThermoFisher	17502048
mouse EGF	50 ng/ml	R&D	2028-EG
Gremlin 1	25 nM	Hyvonen lab	
n-Acetylcysteine	1.25 mM	Sigma	A9165-5G
Primocin	100 ug/ml	InvivoGen	ant-pm-1

Reagents	Final concentration	Company	Catalogue nr
TrypLE Express	1X	ThermoFisher	12604013
Matrigel	1X	Corning	356237
ROCK inhibitor (Y-27632)	10 µM	Sigma	SCM075
GSK3 inhibitor (CHIR99021)	5 µM	Sigma	SML1046
Opti-MEM + GlutaMAX Reduced Serum Medium	1X	ThermoFisher	11574506
BTXpress electroporation buffer	1X	BTX	45-0802

Table 2. 1: Media components and reagents used for derivation and manipulation of organoids and tumoroids. R-spondin 1 and Gremlin in-house production described in [117].

2.1.3 Passaging organoids and tumoroids

Organoids and tumoroids were passaged identically, every 5-7 days, and kept in culture for no more than 10 passages. The media was removed, cold ADF added onto the Matrigel dome and the plate placed on ice for 2 minutes to dissolve the Matrigel. The dome was then released from the plate bottom by pipetting up and down using a p1000 pipette tip and the contents transferred to a 15 ml falcon tube. Using a p200 pipette tip, the organoids/tumoroids were broken up into chunks by pipetting up and down until there were visually no white “dots” (around 50 times). The tube was centrifuged at 600 RCF for 5 minutes at room temperature. The supernatant was removed, and the pellet taken up in an appropriate volume of Matrigel. Organoids/tumoroids were split 1:3 to 1:5, depending on their initial size. Cell clusters in Matrigel were plated out 40 µl/well into a pre-heated 24-well plate (plate in 37°C for 24 h prior to use). The plate was placed into a 37°C incubator with 5% CO_2 for 10 minutes to allow the Matrigel to solidify. The plate was then taken out and 600 µl of pre-warmed WENR/ENR/EN media was added, depending on the application/genotype of the organoid. The plate was placed back into the 37°C incubator.

2.1.4 Freezing/thawing organoids and tumoroids

At a minimum of three days prior to freezing, organoids were grown in WENR media to enrich for stem-like cells that allowed for improved survival upon thawing. Tumoroids, given their APC status, were continued to be grown in EN before freezing. Organoids and tumoroids were frozen identically. The media was removed, cold ADF added onto the Matrigel dome and the plate placed on ice for 2 minutes do dissolve the Matrigel. The dome was then released from

the plate bottom by pipetting up and down using a p1000 pipette tip and the contents transferred to a 15 ml falcon tube. Using a p200 pipette tip, the organoids/tumoroids were broken up into chunks by pipetting up and down until there were visually no white “dots” (around 50 times). The tube was centrifuged at 600 RCF for 5 minutes at room temperature. The supernatant was removed, and the pellet taken up in an appropriate volume of freezing media containing 90 % fetal bovine serum (FBS; Sigma) and 10 % dimethyl sulphoxide (DMSO; Sigma). 1 ml of the freezing media was used to freeze 2 confluent wells of a 24-well plate and then placed into a 1.5 ml cryovial (Greiner Bio-One). The vial was placed into a cell freezing container (CoolCell; Sigma) and put into a -80°C freezer for 24 hours. The next day, the vial was transferred to a liquid nitrogen tank for short- and long-term storage.

To thaw organoids/tumoroids, a 15 ml falcon tube was filled with 5 ml pre-warmed ADF. The cryovial was thawed in a 37°C water bath, not allowing the sample to warm-up. The contents of the cryovial were then pipetted into the ADF and the tube centrifuged 600 RCF for 5 minutes at room temperature. The supernatant was removed, the pellet taken up in 40 µl Matrigel and plated out to 1 well of a pre-heated 24-well plate (plate in 37°C for 24h prior to use). The plate was placed into a 37°C incubator with 5 % CO_2 for 10 minutes to allow the Matrigel to solidify. The plate was then taken out and 600 µl of pre-warmed WENR or EN media with 10 µM ROCK inhibitor was added to organoids and tumoroids, respectively. The plate was placed back into the 37°C incubator. Media was changed to ENR for organoids and to EN for tumoroids after 3 days and cultured as normally.

2.1.5 Genetic manipulation of organoids and tumoroids

2.1.5.1 Transfection by electroporation

Electroporation of organoids/tumoroids was carried out using a published protocol with several modifications [118]. Organoids and tumoroids were cultured in different media compositions before and after electroporation following the time-line shown in Figure 2.1A. The procedure for electroporation of organoids and tumoroids was identical. For a successful electroporation the following parameters are essential: cell count per reaction, DNA amount and incubation time after electroporation.

A minimum of three confluent wells of organoids/tumoroids of a 24-well plate were collected per electroporation. Cold ADF was added onto the wells and left on ice for 2 minutes to allow the Matrigel to dissolve. After pooling the contents of wells into a 15 ml falcon tube (maximum 5 confluent wells of a 24-well plate/tube), the organoids/tumoroids were broken down using a p200 pipette tip until no white "dots" were apparent. The tube was then centrifuged 500 RCF for 5 minutes at room temperature. The supernatant was removed, and the pellet resuspended in 1 ml TrypLE Express with 10 µM ROCK inhibitor. After pipetting up and down using a p200 pipette tip, the tube was placed into a 37°C water bath for 5 minutes. After 5 minutes a small aliquot (10 µl) of the suspension was checked under the microscope for cell cluster size-ideally the organoids/tumoroids were in 3-6 cell clusters. If the clusters were bigger, the tube was placed back into the water bath, for maximum 10 more minutes. To note, when organoids/tumoroids were broken down to single cells, the survival of cells after electroporation was very low. Equally, if the cell clusters were bigger than 20 cells, the organoids/tumoroids that grew up after electroporation often expressed the gene in a mosaic pattern. 9 ml of ADF with 10 % FBS was added onto the cell suspension and centrifuged at 650 RCF for 5 minutes at room temperature. The supernatant was removed, and the pellet taken up in 1 ml of Opti-MEM + GlutaMAX Reduced Serum Medium (Opti-MEM; ThermoFisher). The number of cells was then counted using Countess Automated Cell Counter (Invitrogen). Optimal cell count for a successful electroporation was approximately 500 000 cells/ reaction (minimum 250 000cells/ reaction). The cell suspension was pelleted down at 650 RCF for 5 minutes at room temperature, supernatant carefully removed, and pellet taken up in 90 µl of Opti-MEM or 90 µl of BTXpress electroporation buffer (BTX). To note, survival of cells after electroporation was higher with BTXpress buffer, however due to cost Opti-MEM was used routinely. The 90 µl of cell suspension was transferred to a 1.5 ml Eppendorf tube and placed on ice. 10 µl of 14 µg of DNA in Opti-MEM or BTXpress buffer was added to the cell suspension on ice. NEPA21 electroporator (Nepagene) was used for electroporation. This electroporator allows for short duration poring and transfer pulses leading to high transfection and viability [118]. Electroporation was carried out at room temperature using published settings [118] (Figure 2.1B) and following the manufacturer's guidelines. Before electroporation, the impedance in the sample was checked to be in the range 30-55 Ω, adjusting it to the range with dilution or removal of cell suspension, as necessary. After electroporation was carried out, 400 µl of Opti-MEM or BTXpress buffer with 10 µM ROCK inhibitor was added to the sample and incubated

at room temperature for 30 minutes. To note, incubation over 30 minutes showed a decrease in survival of cells. The tube was then centrifuged at 800 RCF for 3 minutes. The supernatant was very carefully removed, taking care not to disturb the lose pellet, and taken up in 40 µl Matrigel. The cell suspension in Matrigel was plated out as described in sections 2.1.1 and 2.1.2 with media additions as depicted in Figure 2.1A. For constructs transferred via electroporation in this thesis, Hygromycin B (ThermoFisher) was the antibiotic used for selection for positive clones. The concentration of Hygromycin B used was 150 µg/ml for organoids and 100 µg/ml for tumoroids for 7 days.

A

Day	-4	-2	-1	0	2	5	7	10	13	14
Organoid	WENR	EN GSK3i ROCKi	EN GSK3i ROCKi DMSO	EN GSK3i ROCKi DMSO	EN GSK3i ROCKi	WENR	WENR + antibiotics	WENR + antibiotics	WENR + antibiotics	ENR
Tumoroid	EN	EN ROCKi	EN ROCKi DMSO	EN ROCKi DMSO	EN ROCKi	EN	EN + antibiotics	EN + antibiotics	EN + antibiotics	EN

Component	Final concentration
ROCKi (inhibitor)	10uM
GSK3i (inhibitor)	5uM
DMSO	1.25% vol/vol

B

Setting	Poring pulse	Transfer pulse
Voltage	175V	20V
Pulse length	5msec	50msec
Pulse interval	50msec	50msec
Number of pulses	2	5
Decay rate	10%	40%
Polarity	+	+/-

Figure 2. 1: Electroporation of organoids and tumoroids. Electroporation time-line with required media changes depicted for days before and after electroporation for organoids and tumoroids. Media components for WENR, EN and ENR are described in Table 2.1. (A). Settings for electroporation with NEPA21 (B).

2.1.5.2 Lentiviral transduction

Lentiviral transduction of organoids/tumoroids was carried out using a published protocol with several modifications [119]. Lentivirus was generated and pelleted by high-speed ultracentrifugation as described in section 2.2.2. Viral pellet was taken up in 250 µl of infection media: WENR for organoids and EN for tumoroids, supplemented with 10 µM ROCK inhibitor and 8 µg/ml Polybrene (Sigma). Viral suspension was stored at -80°C, if not used directly. Prior to transduction, organoids were grown in WENR media for one passage (5-7 days). Tumoroids were grown as usual in EN media. Transduction procedure was identical for organoids and tumoroids. Minimum one confluent well of organoids/tumoroids of a 24-well plate was required per reaction. Organoids and tumoroids were broken into 3-6 cell clusters with TrypLE as described in section 2.1.5.1. 9 ml of ADF with 10 % FBS was added onto the cell suspension, centrifuged at 650 RCF for 5 minutes at room temperature and the supernatant carefully removed. The cell pellet was taken up in 250 µl of the infection media containing lentivirus and transferred to a pre-warmed 48-well plate. The plate was centrifuged at 32°C for 1 hour at 650 RCF (spinoculation). The plate was then placed to 37°C 5 % CO_2 incubator for 6 hours. Next, the cells were transferred into a 1.5 ml Eppendorf tube and spun down 800 RCF for 5 minutes at room temperature. The supernatant was carefully removed, taken up in 40 µl Matrigel and plated out as described in sections 2.1.1 and 2.1.2. The Matrigel dome was laid over with infection media without Polybrene. 48 hours after transduction, the media was changed to WENR (for organoids) or EN (for tumoroids) containing the relevant antibiotic. The media was changed to normal media (ENR for organoids; EN for tumoroids) after the antibiotic selection was finished. The lentiviral constructs used in this thesis contained puromycin resistance gene. Puromycin (Sigma) selection of organoids and tumoroids was carried out at 2 µg/ml for 7 days.

2.1.5.3 Transfection with Lipofectamine 2000

Transient transfection of organoids and tumoroids in this thesis was carried out to test if promoters in the constructs were expressed in the mouse system. Transfection was done following a published protocol with minor modifications [120].

Organoids and tumoroids were grown and broken into 3-6 cell clusters following the same procedure as for lentiviral transduction (see section 2.1.5.2). Following TrypLE incubation and

subsequent centrifugation, the cell pellet was taken up in 450 µl of WENR (organoids) or EN (tumoroids) media supplemented with 10 µM ROCK inhibitor. The cell suspension was plated into one well of a 48-well plate. 4.5 µg of plasmid DNA and 12 µl of Lipofectamine 2000 were each diluted in 50 µl Opti-MEM and mixed together and incubated according to the manufacturer's protocol. The DNA-reagent complex was then added to the cell suspension (50 µl) and the plate centrifuged at 650 RCF for 1 hour at 32°C. The plate was then incubated for a further 4 hours in the 37°C 5 % CO_2 incubator. Cells were transferred into a 1.5 ml Eppendorf tube and spun down 800 RCF for 5 minutes at room temperature. The supernatant was carefully removed, taken up in 40 µl Matrigel and plated out as described in sections 2.1.1 and 2.1.2. The Matrigel dome was laid over with WENR (organoids) or EN (tumoroids) media supplemented with 10 µM ROCK inhibitor. Successful transfection was evident 48 hours later.

2.1.5.4 Picking

Organoids and tumoroids that were electroporated went through a round of antibiotic selection to enrich for integrants. The piggyBac vector system used in this thesis contained three plasmids, including transposase-expressing plasmid (see section 2.2.10 and Appendix). A negative selection marker was only carried by one of the plasmids. Therefore, antibiotic selection did not select for organoids/tumoroids that incorporated both constructs. Thus, organoid/tumoroid picking was carried out using the positive selection marker, mCherry fluorescence. Cold PBS was added to the appropriate well and left on ice for 2 minutes. Then, using a 1 ml pipette, the Matrigel dome with PBS was transferred to a small tissue culture dish (2 cm diameter). In order to not disrupt the organoids/tumoroids, it was important that pipetting was done very carefully and a tissue culture dish with a small surface area used for easier picking. The dish was then taken under a fluorescent microscope (EVOS fl) and positive organoids/tumoroids picked using a p20 pipette tip under appropriate fluorescence. It was important to pre-coat the pipette tip with FBS to avoid picked organoids/tumoroids from getting stuck inside the tip. Positive clones were pipetted into a pre-thawed Matrigel and plated out as described in sections 2.1.1 and 2.1.2.

2.1.5.5 Sorting using flow cytometry

Lentiviral transduction generated organoids that often expressed the positive fluorescent marker in a mosaic manner (see Chapter 5) or fluorescence that was expressed was too dim

for picking under the microscope (see Chapter 4). In order to overcome this, fluorescence-activated cell sorting (FACS) was utilised. Three confluent wells of a 24-well plate were collected and organoids/tumoroids were made into single cells using TrypLE incubation for 10 minutes, as described in section 2.1.5.3. The pellet was taken up in PBS + 5 % FBS and placed on ice. Up to 10 000 cells were collected by FACS (BD Aria, BD Bioscience). The sorting was carried out by Dr. Hung-Chang Chen from Cancer Research UK Cambridge Institute. The tube with single cells was then centrifuged at 1000 RCF for 3 minutes. The supernatant was very carefully removed and taken up in 40 µl Matrigel containing 1 µM Jagged-1 (AnaSpec), a Notch ligand to support single-cell cultures in the absence of Notch signalling from adjacent supportive cells. The cells were then plated out as described in sections 2.1.1 and 2.1.2. Single organoid cells were grown in WENR for up to 14 days, single tumoroid cells were grown in EN. Growth media for both was supplemented with 10 µM ROCKi for the first three days only.

2.1.6 Immunofluorescent labelling

Organoids and tumoroids were seeded onto eight-well chamber slides (ThermoFisher; 154526) 48 hours before immunofluorescent (IF) staining. IF staining was carried out directly within the slide, with the organoids/tumoroids in Matrigel. Depending on the antibody used, the fixative solution used was either 4 % paraformaldehyde or 92 % methanol plus 8 % formaldehyde (Table 2.2).

Slides fixed with 4 % paraformaldehyde were stained following a published protocol with some modifications [121]. Briefly, organoids/tumoroids were fixed in warm fixative containing 4 % paraformaldehyde (pH 7.4) for 1 hour, permeabilised using permeabilisation buffer (PBS, 1 % triton X-100) and blocked with blocking buffer (PBS, 1 % BSA, 3% normal goat serum, 0.2 % Triton X-100). Primary antibodies were diluted in working buffer (PBS, 0.1 % BSA, 0.3 % normal goat serum, 0.2 % Triton X-100) and incubated for 6 hours at room temperature. After three washes in working buffer, the secondary antibody diluted in working buffer was added onto the wells for 2 hours at room temperature, followed by three washes in PBS. Nuclei were stained and organoids/tumoroids mounted using DAPI Fluoromount-G (SouthernBiotech).

Slides fixed with 92 % methanol plus 8 % formaldehyde (MeOH+F) were stained following a published protocol with some modifications [122]. Briefly, organoids/tumoroids were fixed in

ice-cold MeOH+F for 15 minutes in -20°C. The wells were then washed with washing solution (PBS, 0.1 % Triton X-100, 1 % normal goat serum) three times at room temperature and blocked in blocking buffer (PBS, 0.1 % Triton X-100, 10 % normal goat serum) for 1 hour at room temperature. Primary antibodies were diluted in washing solution and incubated at 4° C over night. The next day the slides were brought back to room temperature and left there for 1 hour in order to allow the Matrigel to harden. Wells were then washed in washing solution for three times, followed by incubation for 1 hour at room temperature in the secondary antibody diluted in washing solution. The wells were washed three times in washing solution and nuclei were stained and slides mounted as above. Imaging was done using Nikon C2 plus confocal microscope using the 20X and 40X objectives. Z-stacks were taken at 1 µm steps. Images were processed and published using ImageJ software. Staining for each antibody was repeated a minimum of three times.

Target	Conjugate	Species	Company	Cat.no	Dilution	Fixative in IF
Lysozyme		rabbit	Dako	A0099	1:200	PFA
UEA-1	Rhodamine		Vector laboratories	RL-1062	1:2000	PFA
ZO-1		rat	Millipore	MABT11	1:200	MeOH+F
Pericentrin		rabbit	Abcam	ab4448	1:200	MeOH+F
ZFPL1 (Golgi)		rabbit	Sigma	HPA014909	1:200	MeOH+F
Phalloidin	Alexa Fluor 488		ThermoFisher	A12379	1:500	MeOH+F
β4-integrin		rat	Abcam	ab25254	1:200	MeOH+F
Total β-catenin		mouse	BD Transduction Laboratories	610153	1:200	PFA
β-tubulin		rabbit	CST	2128	1:200	MeOH+F
Acetylated tubulin	Alexa Fluor 647	mouse	clone C3B9, from Emmanuel Derivery		1:300	MeOH+F
DAPI			SouthernBiotech	0100-20		PFA/MeOH+F
Ki67		rabbit	ThermoFisher	MA5-14520	1:200	PFA
PH3		mouse	CST	9701	1:200	PFA
Rat IgG	Alexa Fluor 488; 555	goat	ThermoFisher	A-11006, A-21434	1:500	PFA/MeOH+F
Rabbit IgG	Alexa Fluor 488; 555	goat	ThermoFisher	A-11008, A-21428	1:500	PFA/MeOH+F
Mouse IgG	Alexa Fluor 488; 555	goat	ThermoFisher	A-21422, A-11001	1:500	PFA/MeOH+F

Table 2. 2: Antibodies used for immunofluorescent labelling of organoids. Fixative used for an antibody is marked. PFA stands for 4 % paraformaldehyde and MeOH+F for 92% methanol plus 8 % formaldehyde.

2.1.7 Live imaging

Live imaging of organoids was carried out in AstraZeneca (AZ) facilities. An automated spinning disc confocal microscope (YOKOGAWA Cell Voyager CV8000) was used for its high-speed image acquisition and minimal photo-bleaching and photo-toxicity. Dr. Samantha Peel from AZ handled the microscope and the settings. Organoids were grown in 10 µl Matrigel drops in a clear flat bottom black 96-well plate (Cell Carrier Ultra, Perkin Elmer). Organoids were seeded onto the plate 48 hours before imaging in ENR and 2 µg/ml doxycycline. Fresh media with doxycycline was replaced 1 hour prior to imaging. Confocal fluorescent and brightfield images of single organoids were captured using a 40X objective (Olympus, 1.0 NA) and a Hamamatsu SCMOS camera with a 2 x 2 bin. Organoids were imaged under full environmental control (5 % CO_2, 37°C) every hour over a 72-hour period. Images were captured over a 50-100 µm Z range at 2 µm spacing intervals. GFP was imaged using a 488 nm excitation laser with a 525/50 nm band pass emission filter. DAPI was imaged using a 405 nm excitation laser with a 445/45 nm band pass emission filter. RFP was imaged using a 561 nm excitation laser with a 600/37 nm band pass emission filter and Far Red was imaged using a 640 nm excitation laser with a 676/37 nm band pass emission filter. Laser power and exposure settings were optimised to reduce phototoxicity. 3 dimensional reconstructions of single Paneth cells labelled with GFP was done by Yinhai Wang in AZ using computational modelling. The spinning disc confocal microscope was also used for quantification of Golgi complex, centrosome and Paneth cell vesicles in organoids and tumoroids fixed on slides using a 20X objective (Olympus, 0.75 NA) and 1 µm stacks.

2.1.8 Protein extraction and western blotting

Two confluent wells of a 24-well plate of organoids/tumoroids were used for protein extraction. Organoids/tumoroids were recovered from Matrigel using several rinses of ice-cold PBS (tube was spun down at 650 RCF for 5 minutes at 4°C between each wash). The pellet was then lysed with 50 µl 1X RIPA buffer (Millipore) containing protease (Sigma) and phosphatase inhibitors (Roche). The sample was sonicated for 15 minutes at cold followed by centrifugation at 20 000 RCF for 30 minutes at 4°C. The supernatant was collected, and the protein measured using Pierce BSA Protein Assay kit (ThermoFisher). Samples containing 5-10 ng of protein, 100 nM DTT and 1:4 NuPage LDS sample buffer (ThermoFisher) were denatured at 95°C for 5 minutes and loaded onto NuPAGE 3-8 % Tris-Acetate gradient gel (ThermoFisher).

Wet electroblotting (Biorad Mini Transblot) was used to transfer proteins onto a PVDF membrane with 0.45 µm pore size for 1 hour at 100 V at 4°C. Pierce ECL substrate was used for development. The primary and secondary antibodies used are shown in Table 2.3.

Target	Conjugate	Species	Company	Catalogue nr	Dilution
APC-H290		rabbit	Santa Cruz	sc-7930	1:1000
Non-phosho-β-catenin		rabbit	CST	8814	1:1000
HA		mouse	Sigma	H3663	1:2000
AXIN2		rabbit	CST	2151	1:1000
c-MYC		rabbit	Abcam	ab32072	1:1000
Vinculin		rabbit	CST	4650	1:5000
Rabbit IgG	HRP	goat	Abcam	ab6721	1:10 000
Mouse IgG	HRP	goat	Abcam	ab6789	1:10 000

Table 2. 3: Antibodies used in this study for western blotting.

2.1.9 RT-qPCR

RNA from organoids and tumoroids was isolated using ReliaPrep RNA Cell Miniprep System kit (Promega). Organoids and tumoroids were harvested by adding ice-cold PBS to the Matrigel dome (usually two wells of a confluent 24-well plate/reaction). The organoids/tumoroids in Matrigel were collected using a p1000 pipette tip, transferred to a 15 ml falcon and centrifuged at 400 RCF for 5 minutes at 4°C. The supernatant was carefully removed, and the pellet taken up in 100 µl of BL+TG Buffer. RNA isolation was carried out according to the manufacturer's protocol with final elution of RNA in 15 µl of Nuclease-free water. RNA concentration and A260/280 and A260/230 ratios were determined. A ratio of 1.7-2.1 for A260/280 and 1.8-2.2 for A260/230 were considered acceptable limits for proceeding with cDNA synthesis.

cDNA was prepared using the High Capacity cDNA Reverse Transcription kit (ThermoFisher) and RNase inhibitor (ThermoFisher). 500 ng-1 µg RNA was used per reaction. 20 µl of final mix was prepared on ice and transferred to a PCR machine. The following programme was used: 25°C for 10 minutes, 37°C for 120 minutes, 85°C for 5 minutes. cDNA was kept at -20°C until use. Quantitative reverse transcription PCR (RT-qPCR) was done using Fast SYBR Green Master Mix (Applied Biosystems). The following mix was prepared per sample: 5 µl Fast SYBR Green Master Mix, 1 µl of forward and reverse primer at final concentration of 0.4 µM, 0.5-1 µl of

cDNA and RNase-free water to make a total volume of 10 µl. QuantStudio 5 Real-Time PCR System (Applied Biosystems) was used with amplification for 40 cycles at 95°C for 15 seconds and 60°C for 20 seconds. The specificity of the amplified products was confirmed by melting curve analysis. PCR threshold cycle (Ct) was automatically determined by the software. *B2m* was used as a housekeeping gene and the ΔΔCT method for calculating relative fold changes in expression. The list of primers used are in Table 2.4.

RT PCR primers	Forward (5')	Reverse (5')
Axin2	GCAGCTCAGCAAAAAGGGAAAT	TACATGGGGAGCACTGTCTCGT
Apc 1	AGCCATGCCAACAAAGTCATCACG	TTCCTTGCCACAGGTGGAGGTAAT
Apc 2	CCTCATCCAGCTTTTACATGGC	GCCCGAGCCTCTTTACTGC
mCherry	CACGAGTTCGAGATCGAGGG	CAAGTAGTCGGGGATGTCGG
Gapdh	AAGGTCATCCCAGAGCTGA	CTGCTTCACCACCTTCTTG
B2m	ACCCCCACTGAGACTGATAC	ATCTTCAGAGCATCATGATG

Table 2. 4: RT-qPCR primers used in this study.

2.2 Materials & Methods

2.2.1 Cell lines, cell culture and Wnt3a conditioned media

Cell lines were maintained in DMEM (ThermoFisher) with 2 mM Glutamine, 10 % foetal bovine serum (FBS) and 1 % penicillin/streptomycin (ThermoFisher) (DMEM +Q +10 % FBS+ P/S). Cells were maintained at 37°C, 5 % CO_2 and 95 % relative humidity (Table 2.5).

Cell line	Origin
SW480	human colorectal adenocarcinoma
HEK293T	human embryonic kidney, contains SV40 T-antigen
NIH 3T3	murine embryonic fibroblast
L Wnt3A cells	murine fibroblast transfected with a Wnt3a expression vector

Table 2. 5: Cell lines used in this study.

Conditioned media from L-cells stably transfected with Wnt3a expression vector (ATCC, CRL-2647, obtained from Mariann Bienz' laboratory) was collected following a protocol by Nusse laboratory. Briefly, cells were cultured in DMEM+Q +10 % FBS. Cells were grown to confluency,

followed by a 1:10 split. The supernatant was collected after 4 days and the media replenished. After 3 days the supernatant was collected again, the two collections pooled and filtered through a 0.2 μm filter (Minisart, ThermoFisher). The medium was stored for up to two months at 4°C with no detectable loss of Wnt3a activity.

2.2.2 Lentivirus production and cell transduction

HEK293T cells were used to produce lentivirus. Lentivirus was generated using psPAX2 packing and pMD2.G envelope plasmids (both a gift from Dr. Frank McCaughan; Addgene plasmids #1226 and 12259). 12 million HEK293T cells were seeded onto a 150 mm dish 24 hours before transfection in media without Pen Strep. Transfections were performed using Lipofectamine 2000 at a ratio of 3:1 to μg of DNA according to the manufacturer's protocol (Life Technologies). 12 μg of vector DNA, 6 μg of psPAX2 and 6 μg of pMD2.G was added to the cells. After 16 hours, media was changed (media with no Pen Strep), and virus was collected, filtered using a 0.45 μm filter (Minisart, ThermoFisher) and pooled with collections at 48 h and 72 h post-transfection. Viral supernatant was used either directly (for cells) or spun down at 45 000 RCF for 16 hours at 4°C using SW32-Ti rotor in a LE-80K ultracentrifuge (for organoids). For organoid transductions, the lentiviral pellet was taken up in the specific infection media [119] (section 2.1.5.2). Transductions were carried out using 8 μg/ml of Polybrene (Sigma). Virus aliquots were stored at -80°C.

2.2.3 Protein extraction and western blotting

Cells were lysed in RIPA buffer (Millipore) containing protease (Sigma) and phosphatase inhibitors (Roche), spun down at 20 00 RCF for 30 minutes at 4°C and protein was quantified using Pierce BSA protein quantification assay (ThermoFisher). Samples containing 30-50 μg of protein, 100 mM (dithiothreitol) DTT (Sigma) and 1:4 NuPage LDS sample buffer (ThermoFisher) were denatured at 95°C for 5 minutes. The samples were run on a NuPAGE 3-10 % Tris-Acetate gradient gel (ThermoFisher) (for antibodies against APC and HA) or 10 % SDS-polyacrylamide gel. Wet electroblotting (Biorad Mini Transblot) was used to transfer proteins onto a PVDF membrane (Immobilon) with 0.45 μm pore size for 2 hours at 100 V at 4°C. The membrane was blocked with 1XTBS, 0.1 % Tween-20 (TBST) containing 3 % BSA (GE Healthcare) or 5 % non-fat dry milk for 1 hour at room temperature. Primary antibodies were diluted in the blocking solution and incubated overnight at 4°C (Table 2.3). The membrane

was washed three times for 5 minutes each with 1XTBST followed by incubation with secondary antibodies diluted in blocking solution for 1 hour at room temperature. The membrane was washed again and incubated with ECL chemiluminescence (Pierce ECL substrate, ThermoFisher). The membrane was then exposed to X-ray film (Fuijifilm) and developed.

2.2.4 RT-qPCR

RNA was extracted from cells using the RNeasy Plus kit (Qiagen) according to the manufacturer's protocol with final elution of RNA in 50 µl of Nuclease-free water. RNA concentration and A260/280 and A260/230 ratios were determined. A ratio of 1.7-2.1 for A260/280 and 1.8-2.2 for A260/230 was considered acceptable limits for proceeding to cDNA synthesis.

cDNA synthesis and RT-qPCR was carried out as described in section 2.1.8. *Gapdh* was used as a housekeeping gene and the ΔΔCT method used for calculating the relative fold change in expression. The list of primers used are in Table 2.4.

2.2.5 Fluorescence activated cell sorting (FACS)

SW480 cells were made into single cells using TrypLE Express (ThermoFisher) and the pellet was taken up in PBS + 5 % FBS and placed on ice. Up to 10 000 cells were collected based on mCherry expression by FACS (MA900 Multi-Application Cell sorter, Sony). The sorting was carried out with Thomas Foets from the Department of Biochemistry, University of Cambridge. Sorted cells were grown and expanded in normal media including selection antibiotic. SW480 cells transfected with piggyBac constructs were selected with 400 µg/ml Hygromycin B (ThermoFisher).

2.2.6 TOP-Flash assay

The TOP-Flash assay was used to determine the Wnt pathway activity in sorted SW480 cells. Cells were transfected with the plasmids Super16xTOPflash encoding TCF binding sites and firefly Luciferase (Moon R., University of Washington, USA) and pRL-CMV coding for *Renilla* Luciferase under control of the constitutive CMV promoter (Promega, Madison, USA) in a ratio of 10:1. Transfection was carried out using Lipofectamine 2000 according to the manufacturer's protocol. 24 hours after transfection SW480 cells were treated with 2 µg/ml

doxycycline. After 48 hours of treatment the cells were harvested and resuspended in passive lysis buffer (Dual-Luciferase Reporter assay, Promega). Luciferase reporter activity was determined according to the manufacturer´s instructions (Dual-Luciferase Reporter assay, Promega) using PHERAstar FSX microplate reader (BMG Labtech). The relative activity of the Wnt pathway was measured as the ratio of firefly Luciferase activity over *Renilla* Luciferase activity.

2.2.7 Immunofluorescent labelling of tissue

The small intestine from C57BL/6 mice and 10-week old *Apc*$^{Min/+}$ mice was used to prepare the so called "swiss role"—a method, where the intestine is opened longitudinally and rolled with the mucosa outwards, allowing for the examination of the entire length of the small intestine [123]. Tissue was fixed in either 4 % paraformaldehyde and embedded in paraffin or fixed-frozen in 10 % formalin and embedded in optimal cutting temperature (OCT) liquid, followed by snap freezing, depending on the antibody used (Table 2.6). Tissue sections were cut into 4 µm or 20 µm thick sections for immunofluorescent staining (IF). 20 µm thick sections were cut onto poly-L-lysine coated slides and were used only for probing for microtubules and acetylated-tubulin, for all other probes 4 µm sections were used, unless stated otherwise.

Processing and staining of fixed-frozen tissue was carried out as described previously [124]. Paraffin embedded tissue was deparaffinised using three consecutive incubations in xylene and hydrated using incubations in 100 %, 95 %, 70 % and 50 % ethanol washes. Epitope retrieval was performed using sodium citrate buffer (sodium citrate 10 mM, 0.05 % Tween-20, pH 6.0). Primary antibody incubations were carried out at 4°C overnight and secondary antibody incubation for 2 hours at room temperature. DAPI Fluoromount-G (SouthernBiotech) was used for staining the nuclei and mounting. Staining for each antibody was repeated a minimum of three times. Fluorescent imaging was carried out using a Nikon C2 plus confocal microscope using 20X, 40X and 63X objective lens. Z-stacks were taken at 1 µm steps. Images were processed using ImageJ software.

Target	Conjugate	Species	Company	Catalogue nr.	Dilution	Fixation
Lysozyme		rabbit	Dako	A0099	1:200	PFA
UEA-1	Rhodamine		Vector laboratories	RL-1062	1: 10 000	PFA
ZO-1		rat	Millipore	MABT11	1:200	PFA
Pericentrin		rabbit	Abcam	ab4448	1:200	PFA
ZFPL1 (Golgi)		rabbit	Sigma	HPA014909	1:200	PFA
Phalloidin	Alexa Fluor 488		ThermoFisher	A12379	1:500	FF
β4-integrin		rat	Abcam	ab25254	1:200	FF
Total β-catenin		mouse	BD Transduction Laboratories	610153	1:200	PFA
β-tubulin		rabbit	CST	2128	1:200	PFA
Acetylated tubulin	Alexa Fluor 647	mouse	clone C3B9, from Emmanuel Derivery		1:300	PFA
DAPI			SouthernBiotech	0100-20		PFA/FF
Ki67		rabbit	ThermoFisher	MA5-14520	1:200	PFA
PH3		mouse	CST	9701	1:200	PFA
Rat IgG	Alexa Fluor 488; 555	goat	ThermoFisher	A-11006, A-21434	1:500	PFA/FF
Rabbit IgG	Alexa Fluor 488; 555	goat	ThermoFisher	A-11008, A-21428	1:500	PFA/FF
Mouse IgG	Alexa Fluor 488; 555	goat	ThermoFisher	A-21422, A-11001	1:500	PFA/FF

Table 2. 6: Antibodies used for immunofluorescent labelling of tissue. Fixation method of tissue for an antibody is marked. PFA stands for 4 % paraformaldehyde and FF for fixed-frozen in 10 % formalin.

2.2.8 Hematoxylin and eosin (H&E) staining

4 µm sections were cut onto poly-L-lysine coated slides, followed by incubation overnight at 37°C. The sections were then deparaffinised with xylene, hydrated with decreasing concentrations of ethanol and stained with hematoxylin and eosin. The slides were mounted in DPX Mountant (Sigma) and covered with a coverslip.

2.2.9 siRNA transfection and shRNA cloning

Small interfering RNA (siRNA) targeting mouse *Apc* was tested on NIH/3T3 cells by transfection (Table 2.7). Transient transfection of cells was carried out using Lipofectamine 2000 following manufacturer's guidelines. shRNA targeting *Apc* was then designed using the siApc sequence

following guidelines from a previously published protocol with some modifications [125]. Briefly, the two long oligos (top and bottom) were reconstituted in nuclease free water to a concentration of 0.5 µg/ml. The following was mixed for the annealing reaction: 20 µl of each oligo and 10 µl of 5X annealing buffer (500 mM potassium acetate, 10 mM magnesium acetate, HEPES-potassium hydroxide to pH 7.4 (Sigma)). PCR was run with the following settings: 5 minutes at 95°C, 10 minutes at 80 °C, ramp from 80°C to 4°C with -0.5°C every 150 seconds. The annealed oligos were amplified by PCR with cloning primers (30 cycles). The product was run on a 2 % agarose gel, excised and gel purified using QIAquick Gel Extraction-Kit (Qiagen). Gibson cloning followed by transformation was carried out as described in section 2.2.10.

siRNA/shRNA	Oligo (5')
siAPC (sense strand)	CACCAAUAAAUUACAGUCUUA(dT)(dT)
NT siRNA (sense strand)	AAUUCUCCGAACGUGUCACGU[dT][dT]
shApc top oligo	AAGGTATATTGCTGTTGACAGTGAGCGCCACCAATAAATTACAGTCTTATAGTGAAGCCACAGATGTATAAGACTGTAATTTATTGGTGTTGCCTACTGCCTCGG
shApc bottom oligo	CCGAGGCAGTAGGCAACACCAATAAATTACAGTCTTATACATCTGTGGCTTCACTATAAGACTGTAATTTATTGGTGGCGCTCACTGTCAACAGCAATATACCTT

Table 2. 7: siRNA and shRNA sequences used in this study. NT= non-targeting. Green annotates miR30 scaffold, red marks the stem sequence, blue labels loop sequence and brown marks the basal stem sequence of the shRNA targeting *Apc*.

2.2.10 Molecular cloning

The constructs cloned for this study are shown in Table 2.8. Plasmid maps of the constructs can be found in the Appendix. All cloning reactions were carried out using Gibson assembly [126]. Gibson primers were designed using the NEBuilder Assembly tool and tested *in silico* using SnapGene software.

Phusion High Fidelity DNA polymerase (M0530, New England Biolabs) was used for PCR reactions and thermocycler conditions were tested out per cloning step. Restriction enzymes were purchased from New England Biolabs. Depending on the size, PCR products and vectors were run on a 1-2 % agarose gel in 1x Tris-Acetate-EDTA (TAE) buffer and purified from the gel using QIAquick Gel Extraction-Kit (Qiagen).

NEBuilder HiFi DNA Assembly Master Mix (E2621, New England Biolabs) was used to assemble Gibson fragment(s) and vector, according to manufacturer's instructions. Briefly, the following was set up on ice: 10 µl of the 2X NEBuilder HiFi DNA Assembly Master Mix, DNA and deionised water to make up a total volume of 20 µl. A vector:insert ratio of 1:2 was used when 1-3 fragments were assembled, and a ratio of 1:1 when 4-6 fragments were assembled. The mix was incubated at 50°C for 60 minutes followed by transformation into Stbl3 chemically competent *E.coli*. DNA was purified using QIAprep Spin Miniprep Kit or QIAGEN Plasmid Midi kit (Qiagen). Plasmid DNA was sequenced by the DNA Sequencing Facility at the Department of Biochemistry, University of Cambridge. DNA (100 ng/µl) was provided with 10 µM of oligonucleotide sequencing primer [127].

Construct	**pLV-TRE-EGFP-PGK-RFP-DEFA5-rtTA**
Backbone	pLV-Puro-TRE-DEFA5-rtTA (Vector Builder) (BamHI & EcoRV)
Template	pCMV-EGFP & pSLIK-Neo (de la Roche lab)
Primers 5'	(EGFP FOR) TACAAAAAAGCAGGCTGGATCCATGGTGAGCAAGGGCGAG
	(EGFP REV) CTCTATATTTGAATTCGATATCTTACTTGTACAGCTCGTCCATG
	(PGK-RFP FOR) CTGTACAAGTAAGATTTAATTAAGGGTAGGGGAGGCGCTTT
	(PGK-RFP REV) CTATATTTGAATTCGATGATATCTTATCTGTGCCCCAGTTTGC
Construct	**pLV-TRE-EGFP-shApc-DEFA5-rtTA**
Backbone	pLV-TRE-EGFP-DEFA5-rtTA (EcoRV)
Template	shApc
Primers 5'	(shApc FOR) CATGGACGAGCTGTACAAGTAAGATGATCCGAAGGTATATTGCTGTTGACAGTGAGC
	(shApc REV) GAGAGTCTCTATATTTGAATTCGATATCATCCCGAGGCAGTAGGCAACACCA
Construct	**pLV-TRE-shApc-UbC-rtTA**
Backbone	pTRIPZ-Puro (XhoI & EcoRI) (from Evan lab; Dharmacon)
Template	shApc
Primers 5'	(shApc FOR) TCTTCAGGTTAACCCAACAGAAGGCTCGAGGATCCGAAGGTATATTGCTGTTGACAGTGAGCGCC
	(shApc REV) AATTGCTCCTAAAGTAGCCCCTTGAATTCATCCCGAGGCAGTAGGCAACACCAATAAATTACAG
Construct	**pB-TRE-shApc-mCherry**
Backbone	pB-TRE-mCherry (SpeI) (from Bon-Kyoung Koo)
Template	shApc
Primers 5'	(shApc FOR) CCTCGAGATCTCACGCGTGACTAGTCGAGGATCCGAAGGTATATTGCTGT
	(shApc REV) CGTATGGGTAGGCCATGGCAACGCGTCCTAGGTAATACGACT
Construct	**pB-TRE-CRE-IRES-GFP**
Backbone	pB-TRE-mCherry (BsrGI & MluI)
Template	pBABE-Cre-ERT2 (from Evan lab)
Primers 5'	(CRE FOR) CAAAGAATTCCTCGAGATCTCACGCGTACCATGGCCAATTTACTGACCG
	(CRE REV) AGGGGCGGCCTAATCGCCATCTTCCAGCAG
	(IRES FOR) GATTAGGCCGCCCCTCTCCCT
	(IRES REV) CCCTTGCTCACCATGGATCCATTATCGTGTTTTTCAAAGGAAAACCACGTCCC
	(EGFP FOR) TACAAAAAAGCAGGCTGGATCCATGGTGAGCAAGGGCGAG
	(EGFP REV) GCGAGCTCTAGATCATCGGGCCGCTACTTTTTAATTAATTACTTGTACAGCTCG

Construct	**pB-TRE-CRE-ERT2-IRES-GFP**
Backbone	pB-TRE-mCherry (BsrGI & MluI)
Template	pBABE-Cre-ERT2
Primers 5'	(CRE-ERT2 FOR) CAAAGAATTCCTCGAGATCTCACGCGTATGGCCAATTTACTGACCGTACACC
	(CRE-ERT2-REV) ATCGGGCCGCTACTTTTTAATTAATCATCAAGCTGTGGCAGGGAAAC
	(IRES-GFP FOR) GTTTCCCTGCCACAGCTTGATGATTAATGCCGCCCCTCTC
	(IRES-GFP-REV) GCGAGCTCTAGATCATCGGGCCGCTACTTTTTAATTAATTACTTGTACAGCTCG
Construct	**pB-DEFA5-rtTA-CAG-GFP**
Backbone	pB-CAG-rtTA (Xho & NotI) (from Bon-Kyoung Koo)
Template	pLV-TRE-EGFP-shApc-DEFA5-rtTA
Primers 5'	(EGFP FOR) TCTCATCATTTTGGCAAAGAATTCCGGATCCATGGTGAGCAAGG
	(EGFP REV) GAATTCGATATCAAGCTTATCGAGCGATATCTTACTTGTACAGCTCGTCC
Template	(SalI)
	(DEFA5-rtTA FOR)
Primers 5'	TCTTGTTATAGATATCGGATATCGAATTCAAATATAGAGACTCTCCAAGGGCCCAC
	(DEFA5-rtTA REV) ATAACTAGCTAGTCAATAATCAATGTCGACGAAGCCATAGAGCCCACCG
Construct	**pB-TRE-APC-mCherry (de la Roche lab)**
Backbone	pB-TRE-mCherry (SpeI & NotI)
Template	XE68 APC-GFP in CS2+ (Addgene, #16687)
Primers 5'	(APC FOR) TCCTCGAGATCTCACGCGTGATGGCTGCAGCTTCATATG
	(APC REV) CGTATGGGTAGGCCATGGCACTAGTAACAGATGTCACAAGGTAAG
	PCR product digested with DpnI
Construct	**pB-TRE-APCΔMT-mCherry**
Backbone	pB-TRE-mCherry (SpeI & MluI)
Template	pB-APC-mCherry
Primers 5'	(APCΔMT FOR) AAGAATTCCTCGAGATCTCACGCGTATGGCTGCAGCTTCATATG
	(APCΔMT REV) CGTATGGGTAGGCCATGGCACTAGTCATATTTCTGGGACTATGTTTTTC
Construct	**pB-TRE-APCΔWnt-mCherry**
Backbone	pB-TRE-mCherry (SpeI & MluI)
Template	pB-APC-mCherry
Primers 5'	(APCΔWnt 1 FOR) AAGAATTCCTCGAGATCTCACGCGTATGGCTGCAGCTTCATATG
	(APCΔWnt 1 REV) GACTATGTTTACTTCTATCTTTTTCAGAACGAG
	(APCΔWnt 2 FOR) AGATAGAAGTAAACATAGTCCCAGAAATATG
	(APCΔWnt 2 REV) CGTATGGGTAGGCCATGGCACTAGTAACAGATGTCACAAGGTAAG

Table 2. 8: Constructs cloned for this study. Gibson primers and restriction enzymes used for cloning shown. pLV denotes lentiviral construct, pB stands for piggyBac construct.

Chapter 3:

APC inactivation compromises intracellular organisation of intestinal epithelial cells

3.1 Introduction

APC is a large multi-domain protein regulating a plethora of effector pathways involved in cellular and tissue homeostasis. Its roles in the intestinal epithelia have largely been determined by experimentally defining the phenotypic consequences of inactivating APC mutations. Germline and somatic *APC* mutations that drive colon cancer lead to the expression of truncated forms of APC that compromise the ability of the protein to regulate the Wnt pathway activity and interact with the microtubule cytoskeleton [24,60,77]. Extensive investigation of oncogenic Wnt pathway activity in APC-mutant cells has ascribed a key role in the regulation of intestinal epithelial cell proliferation through the Wnt target gene c-*Myc* [128,129]. However, the impact of truncating APC mutations on the microtubule cytoskeleton in intestinal epithelial cells has not been determined. I hypothesise that the loss of the C-terminal domain of APC results in altered functions of the microtubule cytoskeleton. APC has been shown to stabilise microtubules via its C-terminal domain and support the establishment of parallel arrays of microtubules in a polarised cell [53,101]. Microtubule stabilisation and subsequent establishment of apical-basal microtubule arrays is vital for maintaining the shape of the cell and coordinate the localisation of intracellular components, including organelles [52]. In this chapter, I identify a novel role of APC in maintaining microtubule-dependent intracellular organisation in the intestinal epithelium that is compromised in tumorigenesis.

3.2 Chapter methods

A detailed description of methods and materials used in this chapter is covered in depth in Chapter 2. Below is a brief overview of Materials and Methods specific to this chapter.

3.2.1 Imaging

Fluorescent imaging was carried out using a Nikon C2 plus confocal microscope. Z-stacks were taken at 1 µm steps at high resolution. For quantification of Golgi complex and centrosome in organoids and tumoroids AstraZeneca imaging facilities were utilised. In collaboration with Samantha Peel, the spinning disc confocal microscope was used to take Z-stacks at 1µm steps through the sample from 4 different locations within a well of a slide using a 20X objective.

3.2.2 Imaging data analysis

All figures presented are representative images from a single plane within the Z-stack of the imaged specimen. For the quantification of organelle positioning within organoids and tumoroids, approximately 200 cells were counted per experiment manually, using the scoring criteria for apical and basal localisation shown in Figure 3.8 C.

3.2.3 Validation of shApc for *Apc* depletion

NIH/3T3 cells were transduced with a lentivirus expressing shApc or shNT following the virus production and transduction protocols described in Chapter 2. Cells transduced with the virus were selected for construct integration using 2 µg/ml puromycin for 7 days. Organoids were electroporated with piggyBac constructs as described in Chapter 2. Electroporated organoids were selected for integration of constructs using 150 µg/ml Hygromycin B for 7 days.

3.2.4 Compounds and RT-qPCR

In all the experiments, doxycycline was used at 2 µg/ml and ROCK inhibitor Y-27632 at 10 µM. RT-qPCR for *Apc* levels was detected using primer pair *Apc 1* (Chapter 2). Nocodazole (Sigma) was tested at concentrations 100-1000 nM. Wnt3a conditioned media was collected from Wnt3a-expressing L-cells as described in Chapter 2.

3.3 Results

3.3.1 APC inactivation leads to compromised cellular organisation

The *Apc*$^{Min/+}$ (multiple intestinal neoplasia) mouse is a widely used model to study intestinal tumorigenesis. The mice have a single wild-type copy of *Apc*, the other harbouring a nonsense mutation in exon 14 of the *Apc* gene resulting in loss of the central and C-terminal domains in the truncated protein. *Apc*$^{Min/+}$ mice develop up to 40 benign adenomas over the course of 110 days of life in the small intestine due to the spontaneous loss of heterozygosity in the other *Apc* allele [32,35]. *Apc* is haplo-sufficient as a tumour suppressor [130]; haematoxylin and eosin (H&E) staining of cross sections of the small intestine of a 100-day old *Apc*$^{Min/+}$ mouse show the characteristic crypt and villus architecture of wild-type tissue adjacent to APC-deficient intestinal polyps—the consequence of inactivation of the wild-type allele (Figure 3.1). *Apc*$^{Min/-}$ polyps are composed of glandular structures that lack the characteristic crypt-villus axis. Moreover, I consistently observe that, relative to APC-proficient tissue, nuclei

in polyp cells are of variable shapes and sizes and are not properly positioned within the plane of the monolayer. Therefore, the H&E stain shows that APC loss compromises tissue morphology and potentially intracellular organisation.

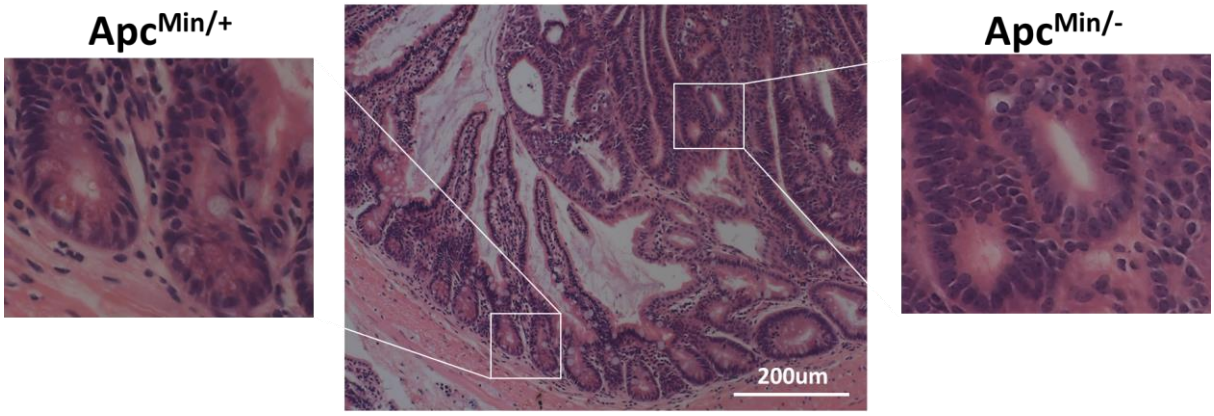

Figure 3. 1: Loss of the crypt-villus axis and altered positioning of nuclei in *Apc*$^{Min/-}$ polyp. Haematoxylin and eosin stain of adjacent haplosufficient and polyp tissue in ApcMin/- mouse.

To determine the extent to which cellular organisation is changed, I stained *Apc*$^{Min/+}$ tissue for Paneth cell granules using the fluorescently-labelled agglutinin molecule—*Ulex europaeus* agglutinin I (UEA). UEA binds to fucose residues that are displayed, specifically, on secretory vesicles in Paneth and Goblet cells. Interestingly, the normally mechanically rigid Paneth cells [17,131] fail to adopt their characteristic pyramidal shape in polyps (Figure 3.2). Intracellular UEA-positive vesicles are no longer apically localised but instead tightly associate with the apical face of the cell and in some cases the lateral face. In the normal small intestine cycling stem cells are interspersed between Paneth cells [13]. In the stained *Apc*$^{Min/+}$ tissue, the adenoma Paneth cells are intermingled with Ki67 positive cells, similar to that in the wild-type tissue, suggesting that the stem cell niche is kept when APC is lost [132]. My data establishes that *Apc*$^{Min/-}$ polyps are compromised for normal epithelial morphology. Moreover, the altered organisation of Paneth cell vesicles and the disposition of nuclei along the epithelial monolayer suggests an effect on intracellular organisation in the polyps.

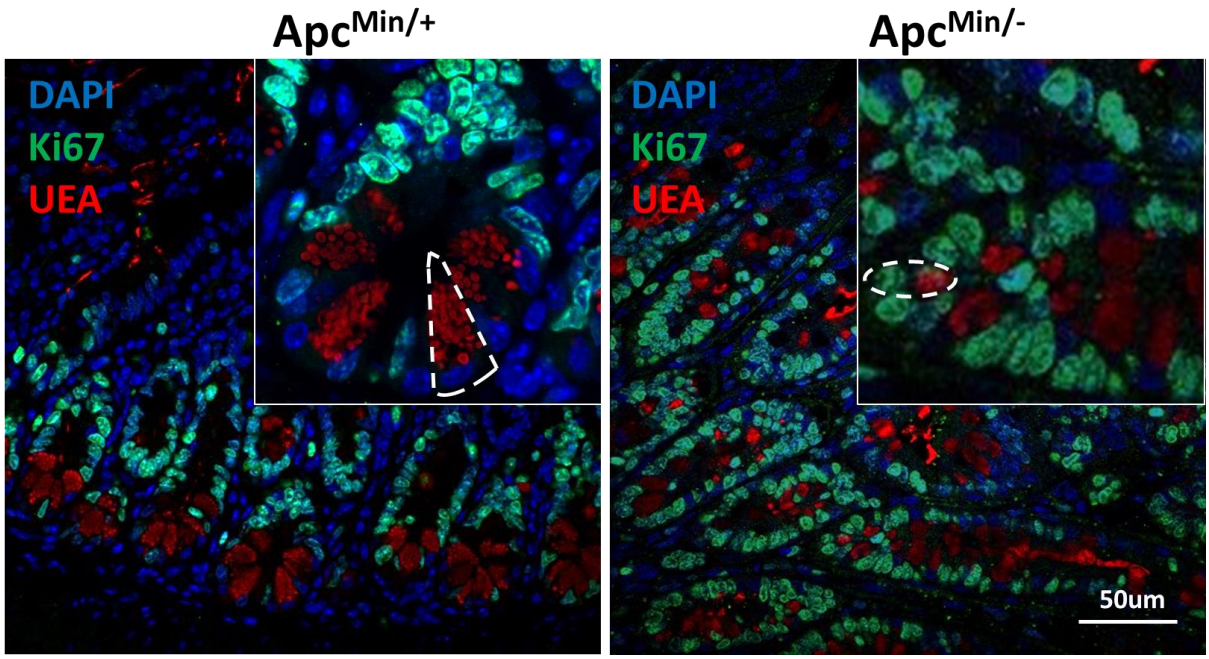

Figure 3. 2: Dispersed positioning of Paneth cell vesicles in *Apc*$^{Min/-}$ polyps. Confocal optical sections from immunofluorescent stains of the small intestinal tissue from *Apc*$^{Min/+}$ mouse displaying haplosufficient tissue (*Apc*$^{Min/+}$; left panel) and polyps (*Apc*$^{Min/-}$; right panel). Paneth cell vesicles are marked with UEA, Ki67 marking cycling cells including stem cells and transient-amplifying cells and DAPI labelling nuclei.

To determine, specifically, how APC loss affects intracellular organisation, I probed for differences in the cytoskeleton between cells in the intestinal epithelia and in the polyps. Cytoskeletal filamentous protein polymers such as filamentous actin (F-actin) and microtubules provide structural support for the shape and organisation of cells [97]. Notably, APC has established roles in the regulation of F-actin and microtubule cytoskeleton [80,101]. I first determined whether APC inactivation altered the localisation of components associated with the actin cytoskeleton. I used fluorescently labelled phalloidin to decorate F-actin in sections of *Apc*$^{Min/+}$ tissue and polyps. Consistent with a previous study [121] , intestinal epithelial cells express F-actin, predominantly, at the apical face. Interestingly, F-actin localised to the apical face of epithelial cells within the polyp monolayer (Figure 3.3). Tight and adherens junctions bridge the actin cytoskeletons of two epithelial cells laterally, while integrins expressed at the base of epithelial cells anchor the actin cytoskeleton to the extracellular matrix [133]. Indirect immunofluorescence using the antibody probes for the tight junction marker ZO-1, the adherens junction marker β-catenin and the basally-localised integrin β4-integrin indicated

the predicted apical- lateral- and basal localisation in all cells of the intestinal epithelial monolayer. Intriguingly, the localisation of all probes was consistent within cells of the APC deficient polyp. My results suggest that the molecular regulation of the actin cytoskeleton is not compromised upon APC inactivation.

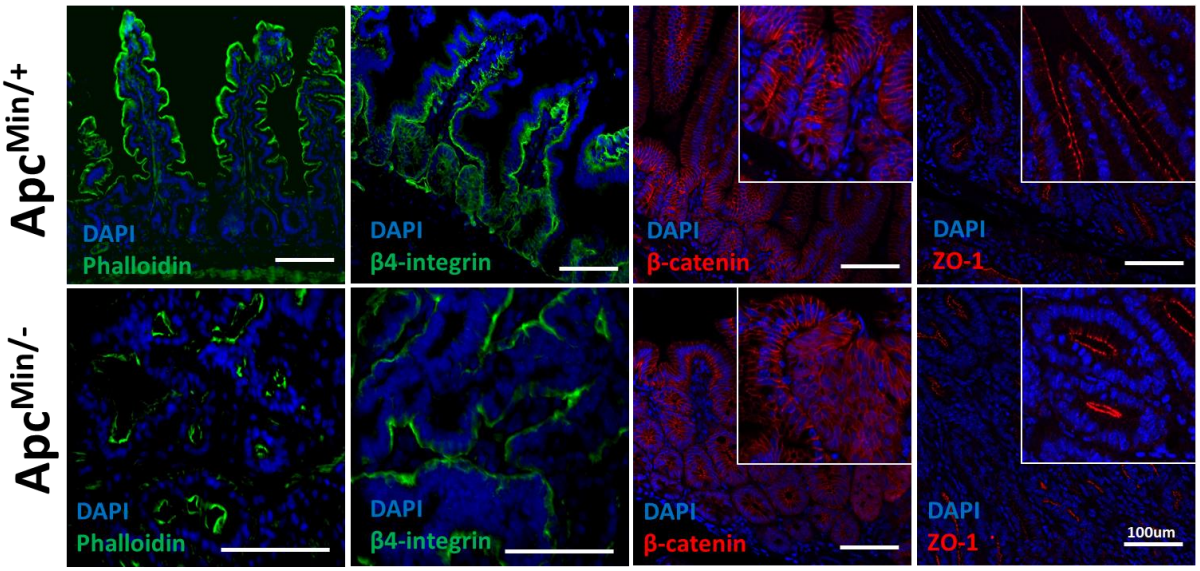

Figure 3. 3: Actin cytoskeleton remains intact in APC inactivation. Confocal optical sections from immunofluorescent stains of the small intestinal tissue from *Apc*$^{Min/+}$ mouse displaying haplosufficient tissue (*Apc*$^{Min/+}$; upper panel) and polyps (*Apc*$^{Min/-}$; lower panel). F-actin is marked by phalloidin, adherens junctions by β-catenin and tight junctions by ZO-1. Nuclei are labelled by DAPI.

Microtubules, a major component of the cytoskeleton, play a vital role in the control of the shape and internal arrangement of cells, and targeting of vesicles and signalling molecules within cells [48,63,97]. I visualised the microtubule cytoskeleton in *Apc*$^{Min/+}$ tissue using an antibody raised against β-tubulin. Within intestinal epithelial cells, microtubules are arranged in parallel arrays (Figure 1.7) [134]. In comparison, microtubules in the adenoma cells were more disorganised compared to wild-type cells with microtubules that were not restricted to parallel positioning (Figure 3.4 A). Post-translational modifications of microtubules are thought to play a role in coordinating functions of microtubules in the cells [65]. Using an antibody raised against the acetylated form of α-tubulin, I found that the signal was concentrated at the apical domain of cells in the intestinal epithelia. In contrast, I failed to

detect any apical concentration of acetylated α-tubulin in the tumour cells (Figure 3.4 B). Taken together, my molecular comparison of cytoskeletal-associated proteins between intestinal epithelial and tumour cells reveals no differences in F-actin or its associated components, yet differences in components of the microtubule cytoskeleton.

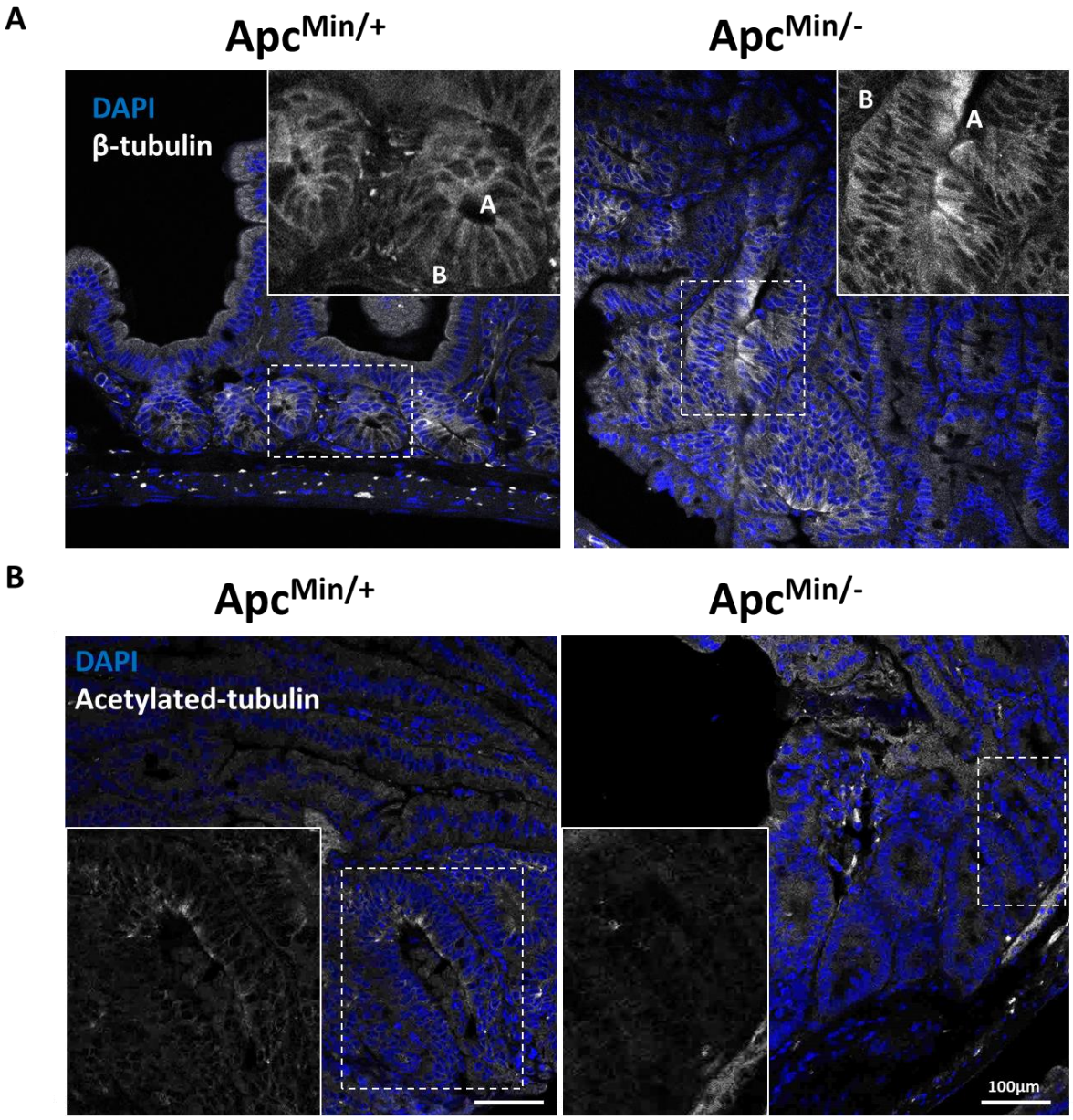

Figure 3. 4: Loss of APC results in altered microtubule cytoskeleton. Confocal optical sections from immunofluorescent stains of the small intestinal tissue from *Apc*$^{Min/+}$ mouse displaying haplosufficient tissue (*Apc*$^{Min/+}$; left panel) and polyps (*Apc*$^{Min/-}$; right panel). β-tubulin marking microtubules in white (A) Acetylated α-tubulin in white (B). Nuclei are labelled by DAPI. "A" marks the apical (top) domain of cells and "B" the basal (bottom) side.

A key role of the microtubule cytoskeleton is the directional transport of cargo mediated by the kinesin and dynein motor proteins [64,65]. In this capacity, microtubules are required for the transport and positioning of organelles and membrane enclosed vesicles [135]. Therefore, correct organelle positioning can be used as a surrogate for the correct regulation and function of the microtubule cytoskeleton. In intestinal epithelial cells, Paneth cell secretory vesicles, the centrosome and the Golgi complex are all positioned apical to the nucleus [44]. I confirmed the positioning of the Golgi complex using an antibody raised against the cis-Golgi protein ZFPL1 and centrosome using an antibody raised against pericentrin. However, when I visualised the Golgi complex and the centrosome in *Apc*$^{Min/-}$ tumours, I observed mislocalisation of both organelles, with the Golgi complex fragmented and dispersed throughout the cell body and the centrosome not restricted to the apical domain (Figure 3.5). Golgi fragmentation has been observed during mitosis [135]. To determine whether Golgi fragmentation in tumour cells was independent of mitosis, I used an antibody for the mitotic marker phosho-Histone 3 (PH3) and co-stained with the Golgi antibody (Figure 3.5). In most PH3 negative cells I observed Golgi fragmentation, suggesting that the fragmentation was not due to an increase of cells in mitosis. Consistent with my results from Figures 3.2 and 3.3, fluorescent UEA-binding vesicles, normally apically localised in Paneth cells, were instead tightly associated with the cell periphery in tumour cells. In contrast, ZO-1 maintained its apical association. In summary, my findings demonstrate that intestinal epithelial cells with inactive APC are compromised for hallmarks of cellular organisation that are specified by the microtubule cytoskeleton.

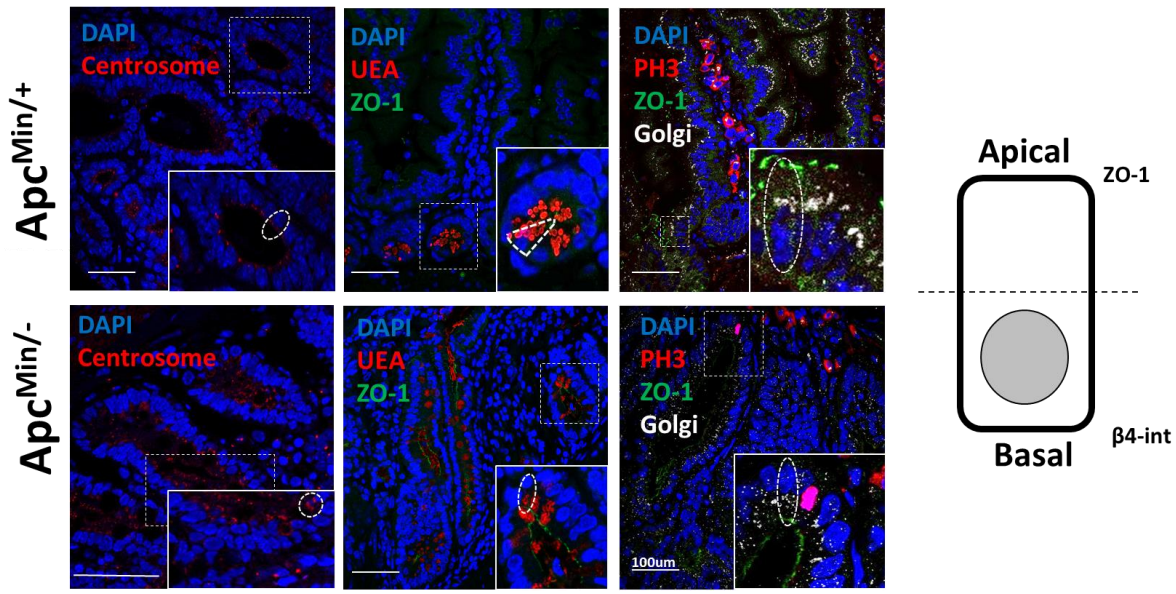

Figure 3. 5: Loss of APC results in mispositioning of the centrosome, Paneth cell vesicles and the Golgi complex. Confocal optical sections from immunofluorescent stains of the small intestinal tissue from *Apc*$^{Min/+}$ mouse displaying haplosufficient tissue (*Apc*$^{Min/+}$; upper panel) and polyps (*Apc*$^{Min/-}$; lower panel). UEA marks Paneth cell vesicles and PH3 marks mitotic cells. Nuclei are labelled by DAPI. ZO-1, labelling tight junctions, is used for orientation to mark the apical domain of cells.

3.3.2 Organoids recapitulate the consequences of APC inactivation in the intestinal epithelia

Studies using tissue sections yield visual snapshots of fixed samples and cannot be used to monitor dynamic changes in intracellular and tissue organisation and morphology. Further, the *in vivo* milieu of the epithelia contains secreted molecules that instruct the architecture of the intestinal epithelia, making it impossible to study solely epithelial autonomous alterations [136–138]. *In vitro* intestinal organoid culture systems have emerged as an experimentally tractable tool to study epithelial-autonomous behaviour [42]. Organoids have the three-dimensional (3D) organisation and cellular composition of intestinal epithelia *in vivo*, complete with crypt-like structures (buds) and villus zones. Organoids generated from the polyps of *Apc*$^{Min/+}$ mice, termed tumoroids, are presumed isogenic to organoids, otherwise lacking functional APC, and form cystic structures without crypts [43]. In this section of the thesis, I describe studies comparing small intestinal epithelial organoids from the isolated crypts from wild-type C57BL/6 mice and tumoroids from isolated cells from the polyps of *Apc*$^{Min/+}$ mice.

To validate whether organoids and tumoroids accurately recapitulate the molecular differences between the intestinal epithelia and tumours, *in vivo*, I probed for markers whose localisation was dependent on the cytoskeleton. In agreement with previous studies [121] and my data derived from intestinal epithelial sections (Figure 3.3), F-actin and β4-integrin maintained their apical and basal distributions in organoids and tumoroids (Figure 3.6). In addition, adherens junctions (visualised using antibodies to β-catenin) and the tight junction protein, ZO-1 were indistinguishable from their localisation in intestinal epithelial tissue sections and were similarly localised in organoids and tumoroids (Figures 3.5 and 3.6). These findings show that the *in vitro* organoid system recapitulates what occurs in the *in vivo* setting with the regulation of the actin cytoskeleton intact upon loss of APC.

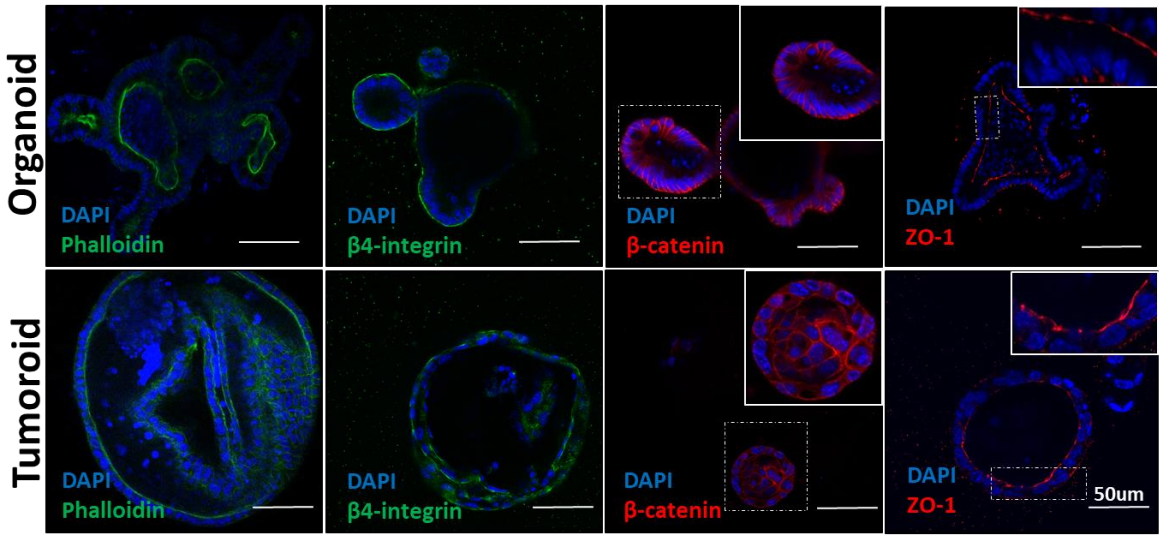

Figure 3. 6: Organoids with inactive APC display intact actin cytoskeleton. Confocal optical sections from immunofluorescent stains of organoids (top panel) and tumoroids (bottom panel). F-actin is marked by phalloidin, adherens junctions by β-catenin and tight junctions by ZO-1. Nuclei are labelled by DAPI.

I then probed the consequence of APC loss in organoids on proteins associated with the microtubule cytoskeleton using antibodies raised against β-tubulin and acetylated α-tubulin. Similar to what I observed in tissue sections of intestinal epithelial cells, I found that organoids demonstrated a similar alignment of microtubules along the AB axis and displayed a concentration of acetylated tubulin apical to the nucleus (Figure 3.7). In contrast, and similar to intestinal epithelial adenoma tissue, tumoroid cells harboured disordered tubulin polymers

compared to organoids, and acetylated tubulin was no longer concentrated at the cell apex (Figure 3.7).

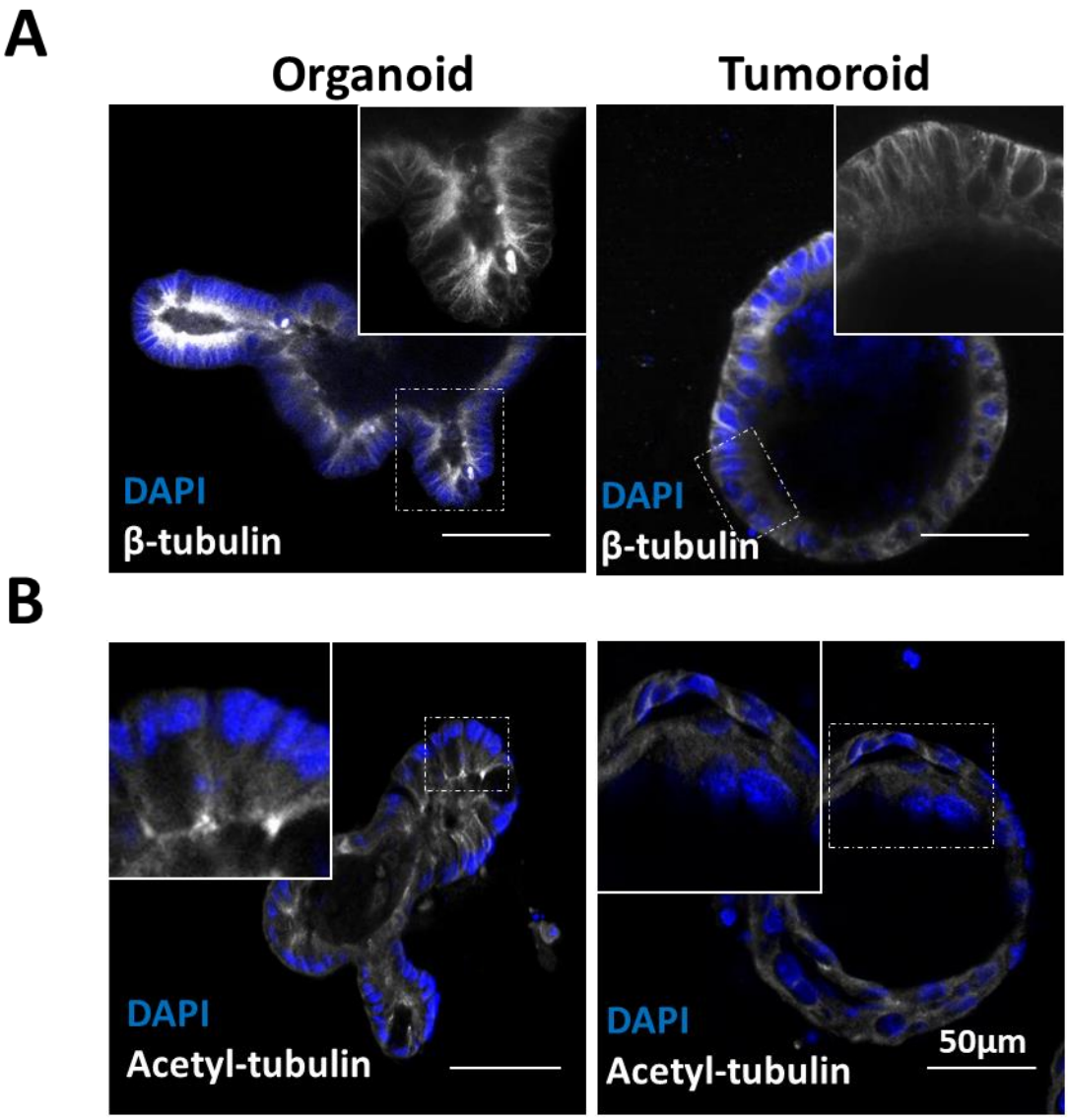

Figure 3. 7: Organoids with inactive APC display altered microtubule cytoskeleton. Confocal optical sections from immunofluorescent stains of organoids (left panel) and tumoroids (right panel). β-tubulin marking microtubules in white (A) Acetyl-tubulin labelling acetylated α-tubulin in white (B). Nuclei are labelled by DAPI.

I quantified the incidence of Golgi and centrosome mislocalisation in organoids and tumoroids. Whereas organoids demonstrated proper positioning of the organelles in 100 % of the cells examined, in around 55 % of the tumoroid cells, the Golgi complex was fragmented and appeared as dispersed stacks throughout the cell body. Similarly, in around 40 % of

tumoroid cells, I observed mislocalisation of the centrosome (Figure 3.8). Taken together, tumoroids recapitulate the defects in microtubule-dependent cellular organisation observed in adenoma tissue. These findings further reiterate the fact that APC inactivation leads to the molecular hallmarks of compromised microtubule cytoskeleton regulation.

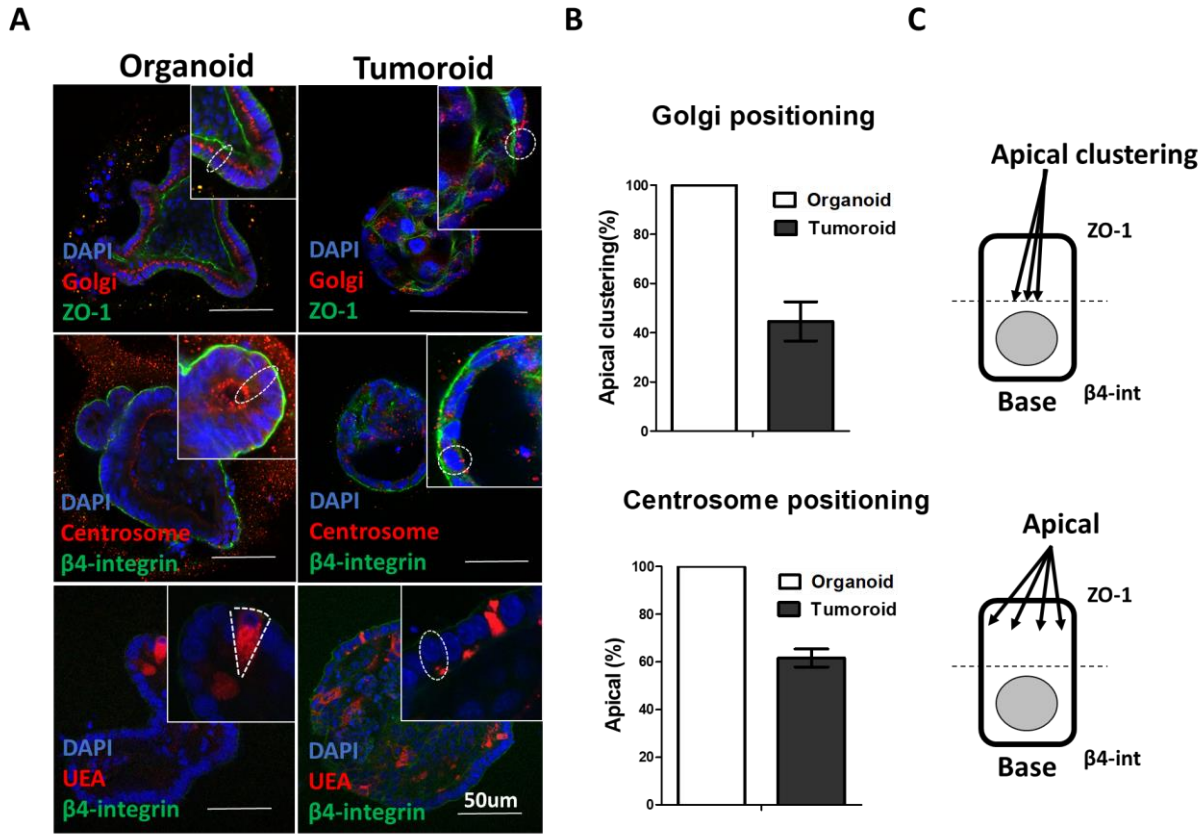

Figure 3. 8: APC inactivation in organoids results in mispositioning of the Golgi complex, the centrosome and Paneth cell vesicles. Representative images of confocal optical sections from immunofluorescent stains of organoids (left panel) and tumoroids (right panel). Nuclei are labelled by DAPI (A). Quantification of the positioning of the Golgi complex and the centrosome. A cumulative of >200 cells from three independent stainings were analysed manually to determine the positioning of either organelle. Error bars: ± SD (B). Criteria for the manual scoring of organelle positioning. ZO-1 that labels tight junctions or β4-integrin was used to mark the apical or basal domains of cells, respectively. Arrow heads represent the positioning of the organelle scored as apical (centrosome) or apically clustered (Golgi complex) (C).

A recent study found that in human colon cancer cell lines APC truncation leads to Golgi fragmentation [99]. The authors of the paper determined that the mechanism was due to the interaction of the N-terminal domain of truncated APC with the APC-stimulated guanine nucleotide-exchange factor (Asef) leading to the activation of the Asef-ROCK-MLC2 pathway. The key experiment in this study was to demonstrate that treatment of the cell lines with the small molecule inhibitor against ROCK (Y27632) prevents Golgi fragmentation (Figure 3.9 A). However, when I repeated the experiment, treating tumoroids (expressing truncated APC) with Y27632, I it did not observe any intact Golgi structure (Figure 3.9 B).

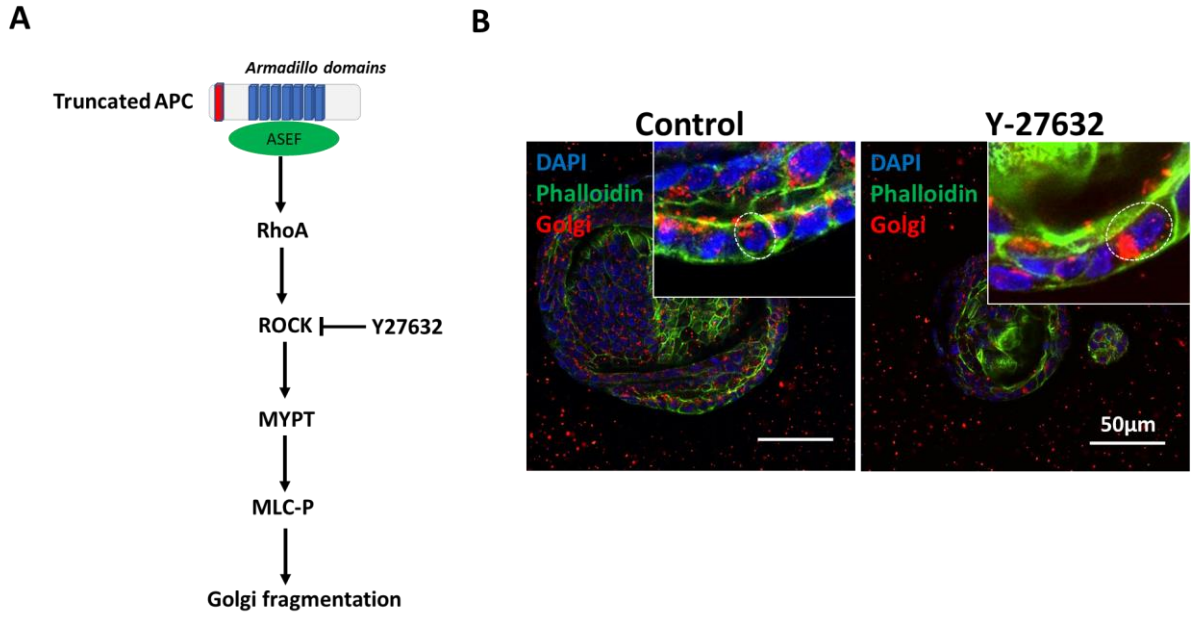

Figure 3. 9: Golgi fragmentation is not rescued by blocking ROCK in organoids with truncated APC. The proposed mechanism of Golgi fragmentation by Kim *et al.* [99] (A). Representative images of confocal optical sections from immunofluorescent stains of tumoroids treated with 0.01 % DMSO (control) or 10 µM ROCK inhibitor (Y-27632) for 72 hours. F-actin is labelled by phalloidin to mark the apical domain. Images are representative of >100 cells analysed (B).

3.3.3 Activated Wnt pathway activity does not lead to compromised cellular organisation

It is well-established that APC loss deregulates the Wnt pathway activity (Figure 1.8) [95,139]. In order to determine whether the observed intracellular disorganisation in tumoroids is due to Wnt target gene expression, I treated organoids with conditioned media containing the Wnt3a ligand. Organoids treated with Wnt3a adopt a cystic morphology, similar to tumoroids. I term these Wnt-oids. Interestingly, I find that the Golgi complex, the centrosome and Paneth cell

vesicles are all normally positioned in Wnt-oids (Figure 3.10). This finding demonstrates that the effect of increased Wnt pathway activity, and perhaps target gene expression, affects organoid epithelial morphology, but has no effect on intracellular organisation as determined via organelle positioning. Future experiments using a repressor for the Wnt target gene transcription, dominant negative TCF [140,141], will further validate this finding.

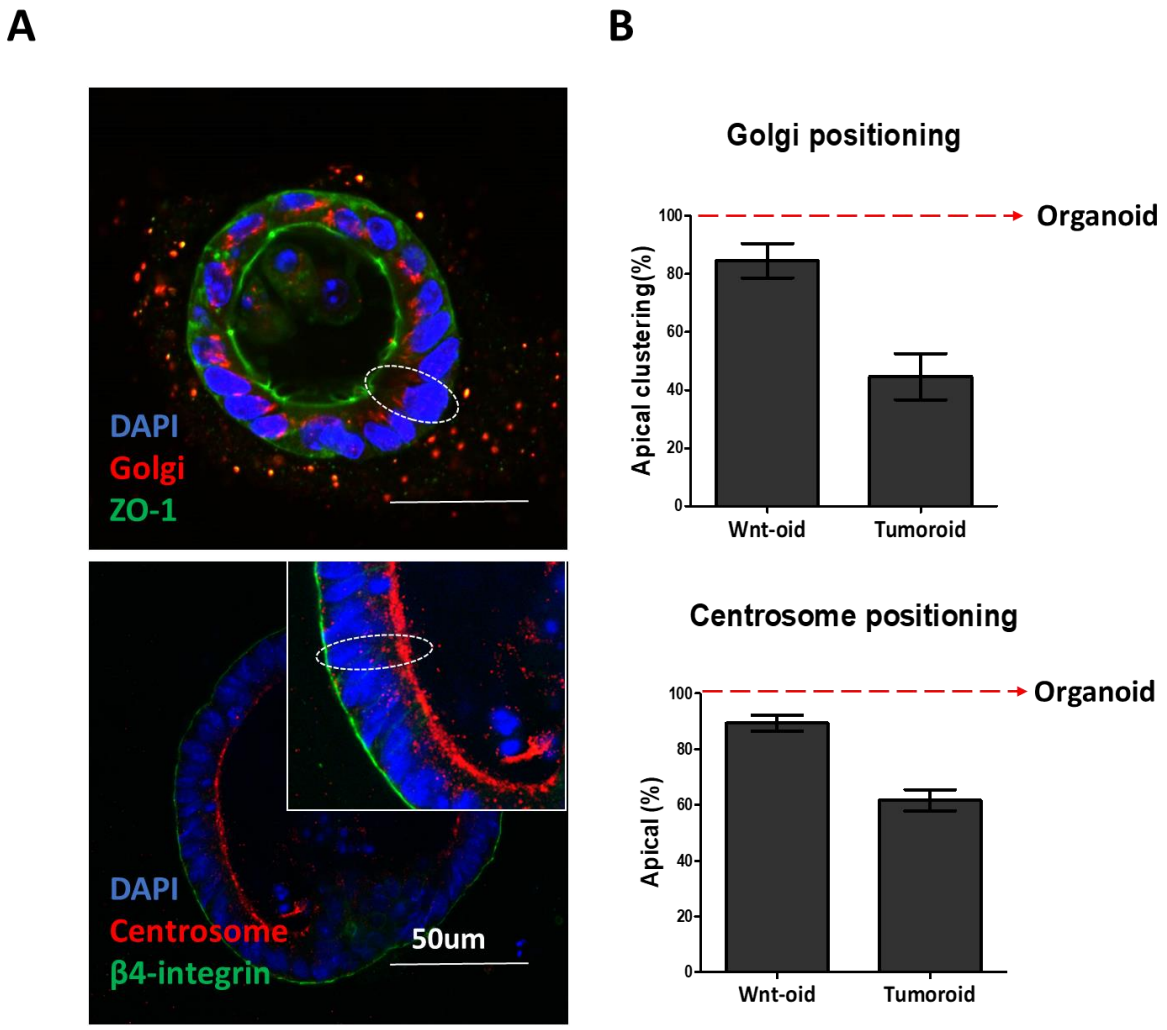

Figure 3. 10: Activated Wnt pathway does not alter the positioning of the Golgi complex and centrosome. Representative images of confocal optical sections from immunofluorescent stains of organoids treated with Wnt3a-conditoned media (WENR) for 72 hours. ZO-1 that labels tight junctions or β4-integrin was used to mark the apical or basal domain of cells, respectively. (A) Quantification of the positioning of the Golgi complex and the centrosome. A cumulative of >200 cells from three independent stainings were analysed manually to determine the positioning of either organelle using criteria described in Figure 3.8 C. Error bars: ± SD (B).

3.3.4 An *in vitro* model of reversible tumorigenesis reveals that cellular disorganisation is the direct consequence of APC inactivation

Based on the comparison of *Apc*$^{Min/+}$ tissue and *Apc*$^{Min/-}$ polyps and organoids and APC deficient tumoroids, I hypothesised that APC inactivation leads to compromised function of the microtubule cytoskeleton. Implicit in this hypothesis is that APC loss is the sole genetic lesion associated with polyps or tumoroids. To determine whether the distinguishing phenotypes in the polyps and tumoroids directly reflect the immediate and direct consequences of APC inactivation, I created a genetically engineered organoid model of APC deficiency using a previously published short-hairpin RNA targeting *Apc* (shApc) [21]. The shApc targets a region at the 5' end of the mRNA (3062-3082bp) and in conditional transgenic mice, potently suppresses *Apc* expression leading to the upregulation of Wnt pathway target genes in the intestine [21].

As a validation step, I used an inducible lentiviral vector to transduce mouse fibroblast cell line NIH/3T3 with shApc. The vector encodes the Tet-ON system for conditional and reversible modulation of *Apc* expression via the tetracycline response element (TRE)-regulated shApc (Figure 3.11 A). Upon cellular treatment of doxycycline (dox), the reverse tet-transactivator (rtTA) is expressed, binds to the TRE leading to *Apc* depletion detectable by RFP expression (Figure 3.11 B). Subsequent doxycycline withdrawal restores endogenous *Apc* expression.

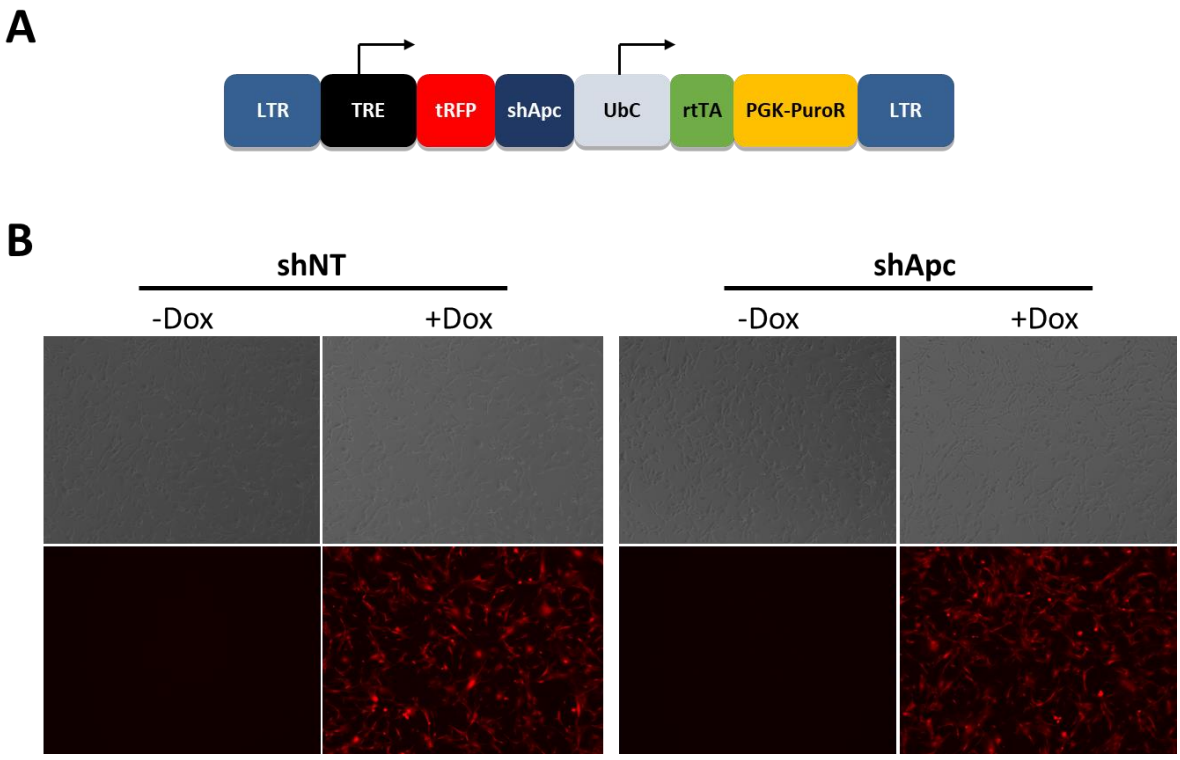

Figure 3. 11: Validation of the inducibility of lentiviral construct expressing shApc. Lentiviral construct expressing doxycycline-inducible shApc (A). NIH/3T3 cells transduced with 2 µg/ml doxycycline for 24 hours showing inducibility of shApc detectable by RFP (B).

Doxycycline treatment of the transduced NIH/3T3 cells led to the gene expression levels of *Apc* to progressively decrease and the Wnt pathway target gene *Axin2* to increase more than 10-fold after 72 hours of doxycycline induction relative to the non-induced control (Figure 3.12 A). Moreover, *Apc* depletion led to an increase in the levels of phosphorylated β-catenin (Figure 3.12 B), another measure of increased pathway activity (Figure 1.8) [87]. These data demonstrate that the shApc functionally increases the Wnt pathway activity through the silencing of *Apc*.

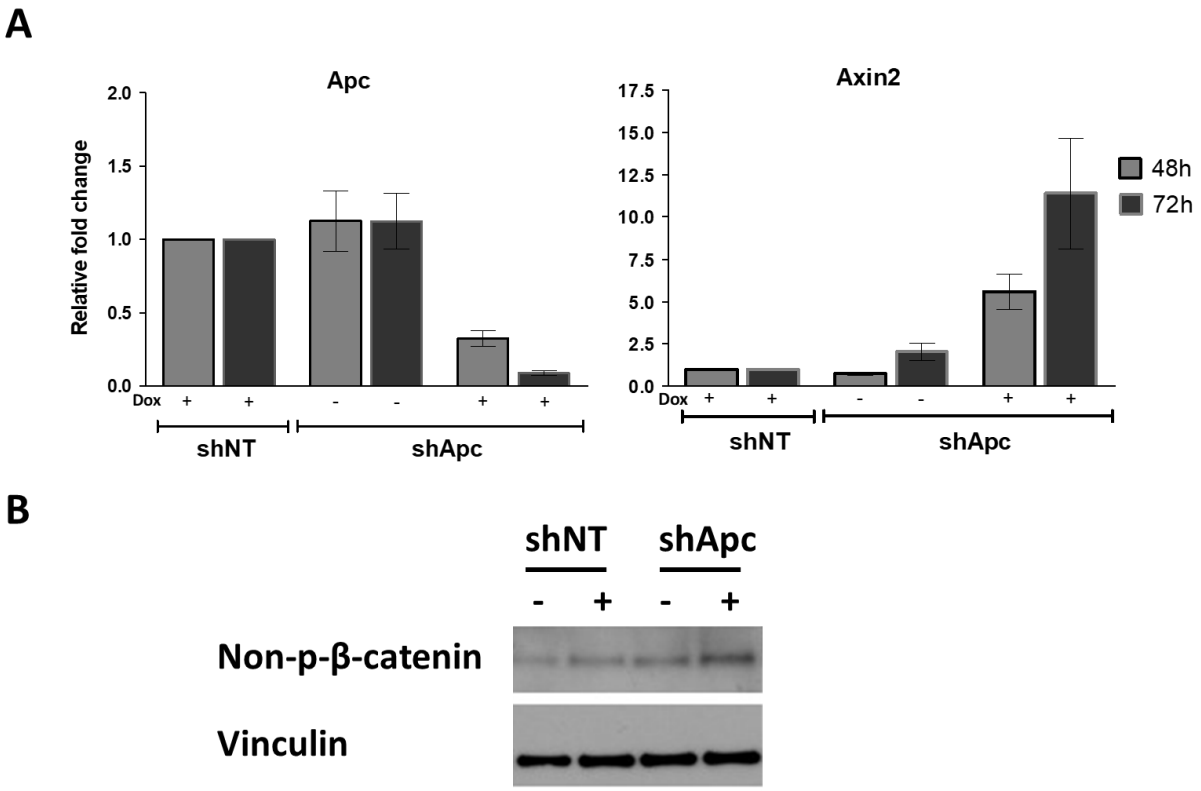

Figure 3. 12: Lentivirally expressed shApc increases Wnt pathway activity. RT-qPCR analysis of gene expression of Apc and Axin2 in transduced NIH/3T3 cells induced with 2 µg/ml doxycycline for 48 or 72 hours. Fold change shown as relative to doxycycline-induced NIH/3T3 cells transduced with a lentivirus expressing shNT (non-targeting). Gapdh was used as a housekeeping gene; data is represented as mean of two independent experiments (±SD) (A). Western blot for APC and non-phosphorylated β-catenin (non-p- β-catenin) in transduced NIH/3T3 cells induced with 2 µg/ml doxycycline for 24 hours. Vinculin was used as loading control (B).

In order to introduce the inducible shApc expression system into organoids, I used the piggyBac (pB) transposon-based expression vector system due to its reported stable and high integration efficiency (Bon-Kyoung Koo, personal communication) [118,142]. The pB transposon is a mobile genetic element that uses the pB transposase enzyme to recognise the inverted terminal repeats (ITRs) located at both ends of the transposon vector and integrate them into TTAA chromosomal sites. I utilised a three-plasmid pB expression system: one plasmid encodes a TRE-driven shApc, followed by an IRES and the coding sequence for mCherry; the second plasmid contains the CAG promoter for constitutive expression for rtTA: and a transposase-encoding plasmid (Figure 3.13).

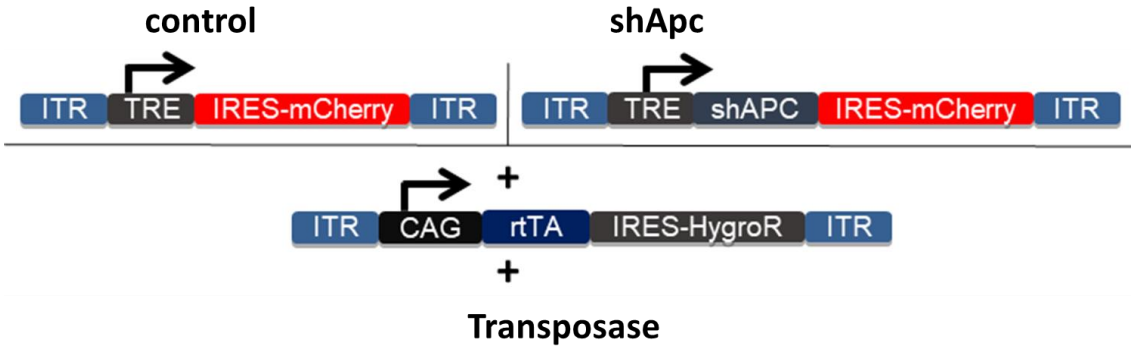

Figure 3. 13: PiggyBac transposon system for inducible shApc expression in organoids. The system is composed of three constructs; it is doxycyline inducible and shApc expression is detectable by mCherry.

I introduced the plasmids into disaggregated organoid cells by electroporation followed by 7 days of antibiotic selection (150 µg/ml Hygromycin B) (Chapter 2). Following the selection, organoids treated with doxycyline for 10 days demonstrated a decrease in *Apc* expression and high levels of *mCherry* expression (Figure 3.14 A). At 6 days of organoid culture post-removal of doxycyline I observed restoration of *Apc* expression and near complete loss of *mCherry* expression. Moreover, organoids re-expressing shApc showed increased levels of canonical Wnt target gene *c-Myc* (Figure 3.14 B). Differences in the expression of these genes demonstrates the reversibility of the system.

A

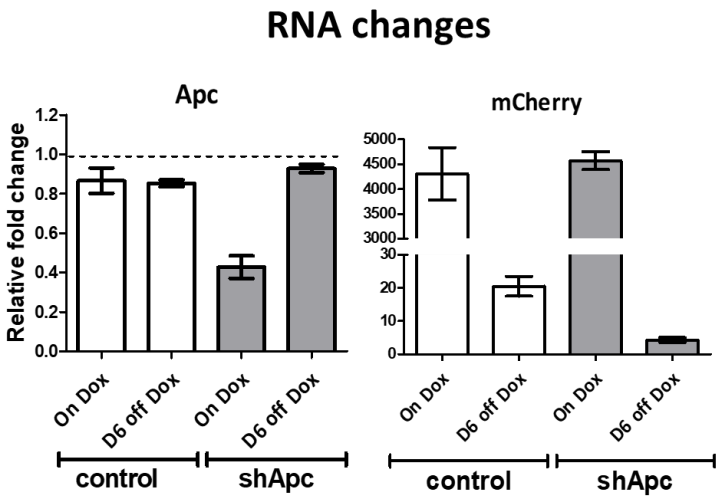

B

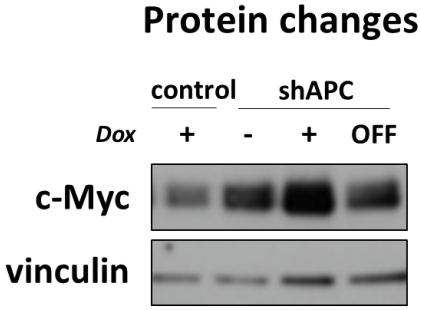

Figure 3. 14: Validation of the reversable organoid-induced tumoroid system. RT-qPCR analysis of gene expression of *Apc* and *mCherry* in organoids expressing pB-control or pB-shApc. Organoids were treated with 2 µg/ml doxycycline for 10 days (On Dox) or analysed 6 days post removal of doxycycline (D6 off Dox). Fold change shown as relative to non-induced electroporated organoids. *B2m* was used as a housekeeping gene; data is represented as mean of two independent experiments (±SD) (A). Western blot for c-MYC of organoids treated with 2 µg/ml doxycycline for 10 days (+) or 6 days post removal of doxycycline (off). Vinculin was used as loading control (B).

Morphologically, doxycycline treatment of the organoids for 10 days led to the transition to hyperproliferative spheroids, reminiscent of tumoroids. Conversely, removal of doxycycline restored normal *Apc* expression and led to the conversion back to the organoid morphology (Figure 3.15). Approximately 70 % of spheroids had formed back into budding organoids 6 days after dox removal. Taken together, the molecular and morphological characterisation of

the organoid-induced tumoroid system (OITS) indicates it is a model of inducible tumorigenesis and tumour regression.

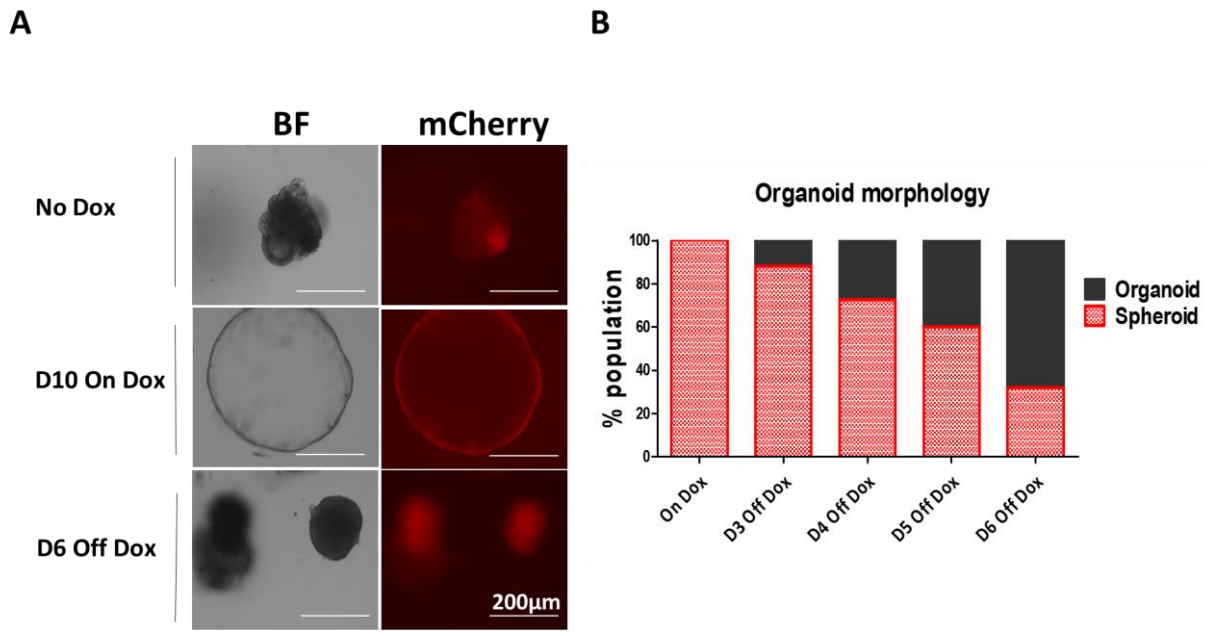

Figure 3. 15: Organoid-induced tumoroid system as a model for inducible tumorigenesis and tumour regression. Representative images of organoids expressing pb-shApc. Organoids were grown in culture for 5 days post split without treatment (No Dox), treated with doxycycline for 10 days (D10 On Dox), followed by removal of doxycyline for 6 days (D6 Off Dox). Organoids were imaged in brightfield (BF) or RFP channel (mCherry) using the EVOS imaging system (A). Quantification of the morphology of pB-shApc organoids treated with doxycyline for 10 days (On Dox) or after removal of doxycyline for up to 6 days. Morphology was scored as "spheroid" when no buds were apparent; organoid with ≥1 bud was scored as "organoid". Graph represents >100 organoids analysed per group from two independent experiments (B).

I used the OITS to analyse the direct effects of *Apc* depletion on cellular organisation, dynamically. In line with my previous results with $Apc^{Min/+}$ intestinal epithelial sections and tumoroids (Figures 3.5 and 3.8), induced *Apc* depletion (via induction of shApc expression) in organoids led to fragmentation of the Golgi complex and dispersed positioning of the centrosome and Paneth cell secretory vesicles (Figure 3.16). All of these hallmarks of compromised cellular organisation were restored upon removal of doxycyline from the spheroids and re-expression of *Apc*. β4-integrin remained localised to the base of the cells upon induction of shApc, identical to that seen in $Apc^{Min/-}$ polyps and tumoroids, indicating

this localisation is not altered with APC loss. Importantly, these results demonstrate that the hallmarks of intracellular organisation associated with the microtubule cytoskeleton I observe are the immediate and direct consequence of functional APC loss.

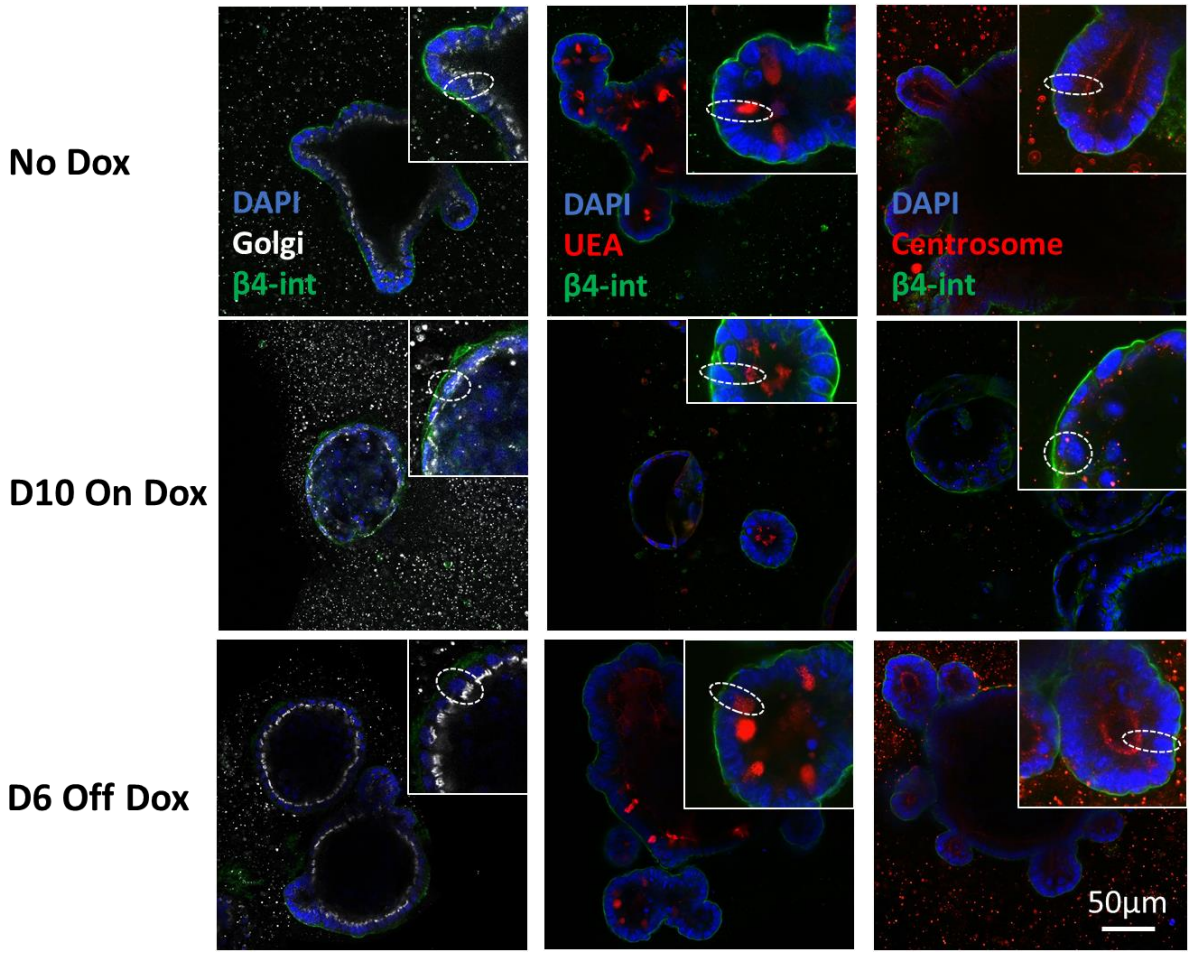

Figure 3. 16: Organoid-induced tumoroid model demonstrates that compromised cellular organisation is a direct consequence of APC inactivation. Representative images of confocal optical sections from immunofluorescent stains of pB-shApc organoids grown without treatment (No Dox), treated with doxycyline for 10 days (On Dox) or after removal of doxycyline for 6 days (D6 Off Dox). UEA marks Paneth cells and DAPI labels the nuclei.

3.3.5 Inhibition of microtubule polymerisation in organoids phenocopies APC deficiency

Microtubules are formed of tubulin subunits and exhibit dynamic instability whereby they can switch between stably growing and rapidly shrinking (termed dynamic instability). This polymerisation and depolymerisation control allows them to reorganize quickly, as required for cellular functions [48]. Molecules that compromise microtubule dynamic instability have

proven to be excellent research tools for understanding microtubule-dependent processes. Nocodazole is a small molecule that inhibits tubulin polymerisation, thereby compromising microtubule functions [143].

I hypothesised that I could phenocopy the consequence of APC inactivation on cellular organisation by affecting microtubule functions with nocodazole treatment. I treated organoids with 0-1000 nM of nocodazole in order to determine the optimal concentration for uncoupling direct effects on microtubules from toxic cellular side-effects. I chose a 48-hour treatment period as it is sufficient for the conversion of organoids to Wnt-oids with Wnt3A treatment (Figure 3.17). This time-point allows for the detection of any tissue morphology effects occurring when disrupting the microtubule cytoskeleton. Organoids treated with 100nM nocodazole showed no change in tissue morphology, however, cells displayed the characteristic Golgi fragmentation of APC deficiency (Figure 3.17). Similarly, nocodazole treatment of Wnt-oids also led to the fragmentation of the Golgi complex. Importantly, nocodazole withdrawal led to the re-localisation of the Golgi complex to the apical domain after 24 hours, supporting the notion that disruption of organelle positioning is a direct effect of deregulating microtubule dynamics. As a control, nocodazole-treated tumoroids maintained the fragmented, mislocalised Golgi complex. Taken together, targeted deregulation of microtubule organisation phenocopies the consequence of APC deficiency.

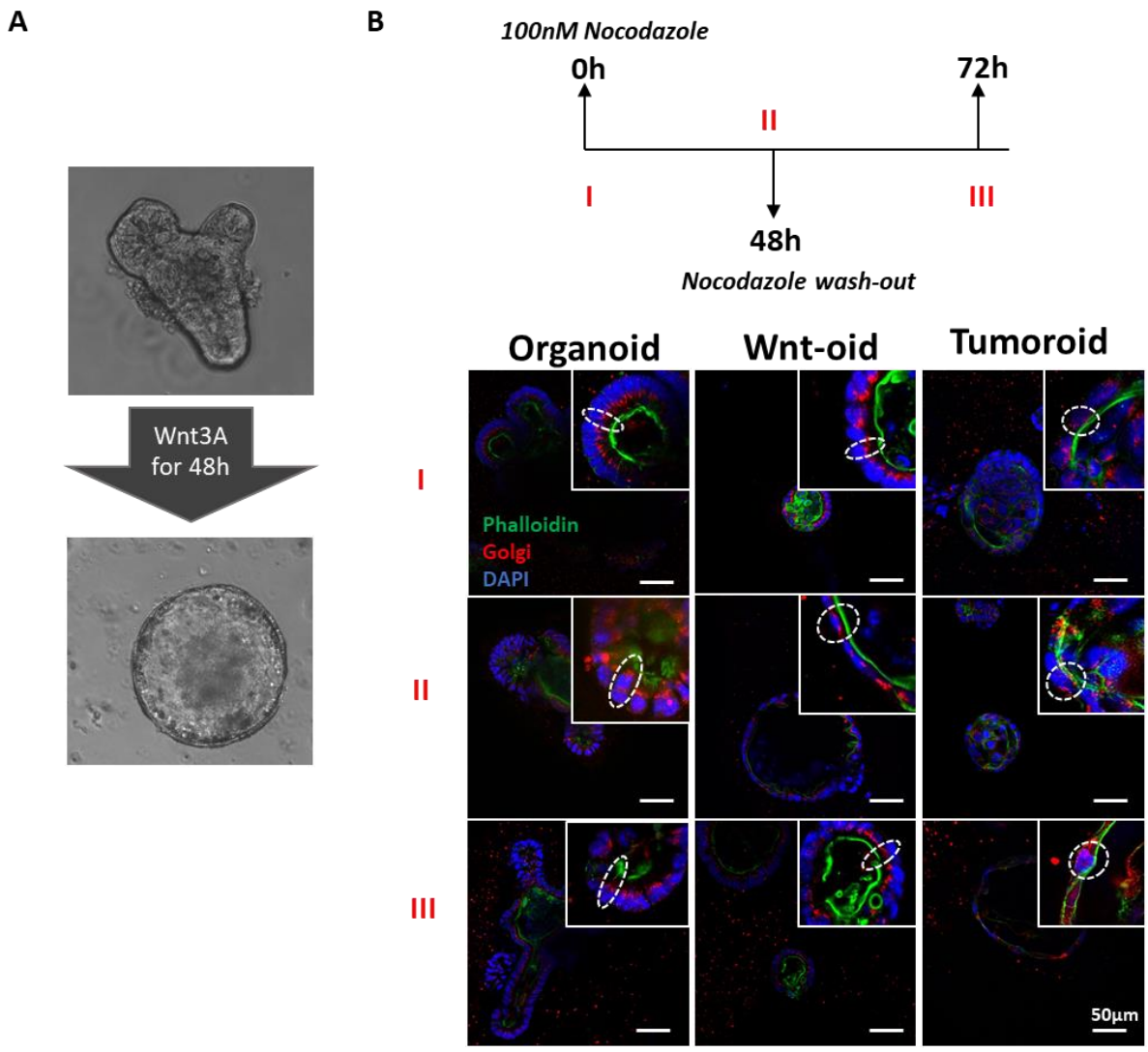

Figure 3. 17: Microtubule destabilisation by nocodazole phenocopies APC deficiency. Organoids cultured in Wnt-conditioned media (WENR) for 48 hours convert into a spheroid morphology (A). Confocal optical sections from immunofluorescent stains of organoids, Wnt-oids and tumoroids. Organoids, Wnt-oids and tumoroids were fixed (I), treated with 100nM nocodazole for 48 hours and fixed (II) or treated with 100nM nocodazole for 48 hours followed by removal of the drug from media for 24 hours and fixed (III). Images are representative of total of 50 organoids per condition per organoid line analysed from two independent experiments. F-actin is labelled by Phalloidin, DAPI marks nuclei (B).

3.4 Discussion

Somatic inactivating mutations in the *APC* gene that result in a truncated protein are widely regarded as the initiating event of most sporadic colorectal tumours. Truncation of APC is known to lead to deregulated Wnt pathway activity, and this has been directly linked to the onset of tumorigenesis in the intestinal epithelia, requiring expression of the Wnt target gene *c-Myc* [41,96]. However, the cellular effects of the inactivation of the protein have not been studied in detail. Using tissue and organoids generated from *Apc*$^{Min/+}$ mice, I show that mutational inactivation of APC leads to compromised microtubule-dependent intracellular disorganisation with mispositioning of vesicles, the Golgi complex and the centrosome. Owing to the generation of an organoid model of controlled APC deficiency I developed, I can demonstrate that microtubule related cellular effects I observe in tumour tissue sections and tumoroids are the immediate and direct consequence of loss of functional APC. Destabilisation of the microtubule cytoskeleton phenocopied APC deficiency, supporting the notion that APC's interaction with the microtubule cytoskeleton controls intracellular organisation.

3.4.1 Advantages of the use of organoids to study cellular organisation

Histological studies of mouse models with germline *Apc* mutations and models of APC deficiency have established that APC inactivation leads to intestinal adenomas and the loss of normal crypt-villus architecture [21,30,34,41]. It is therefore evident that tissue morphology is altered in APC inactivation. However, I have determined that intracellular disorganisation of the microtubule cytoskeleton and associated organelles that accompany APC loss are a novel phenotype. The use of 3D intestinal organoids allows for detection of cellular structures dynamically with better resolution than with tissue sections. I probed for the localisation of F-actin, β4-integrin, β-catenin, ZO-1, secretory vesicles, the Golgi complex and the centrosome in organoids and tumoroids and validated that the organoid system faithfully recapitulates what is present in the corresponding tissue. Moreover, in agreement with previous studies, I find that organoids contain crypt-like structures whereas tumoroids grow as round cysts, devoid of any characteristic morphologies of the intestinal epithelial monolayer [43]. This suggests that the cystic appearance of tumoroids represents the compromised intestinal epithelial morphology observed in APC deficient tumours. In addition, the organoid-induced tumoroid system I developed portray the potential use of organoids for genetic studies. The model can be used to introduce further changes into genes responsible for adenocarcinoma

development, ie oncogene *Kras* and tumour suppressor genes *Smad4* and *Tp53*, to determine the status of cellular organisation in cancer as well as be used for drug screening [144].

3.4.2 Alterations on microtubule cytoskeleton in intestinal cells with APC deficiency

A previous study compared wild-type organoids to organoids isolated from *Apc*$^{fl/fl}$/Cre mice to demonstrate that while tissue morphology is altered, the loss of APC does not lead to changes in the AB cell polarity [121]. I have confirmed the basic premise of this study in tumoroids, where actin-based cytoskeleton stays intact upon APC loss. However, a novel finding is that APC inactivation or depletion alters the microtubule structure in microtubule arrays and leads to a modification in their post-translational acetylation.

Within the intestinal epithelia from both the *Apc*$^{Min/+}$ and *Apc*$^{fl/fl}$/Cre mouse lines , APC is expressed as a truncated version of the protein, lacking protein interaction domains that bind to components of the Wnt pathway and the microtubule cytoskeleton [60,101]. Specifically, the loss of the C-terminal domain does not eliminate the binding of APC to microtubules, but decreases its capacity to stabilise the microtubule ends [101,107]. Probing for β-tubulin shows that the microtubules in the microtubule arrays are more disorganised in adenomas and tumoroids compared to the haplosufficient tissue and wild-type organoids, suggestive of more dynamic microtubules [54]. In addition, acetylation of α-tubulin is evidently affected in cells with inactive APC showing changes in signal location of this post-translational modification. While the direct cellular function of acetylation of tubulin is still unclear, studies have suggested acetylation to be a marker for stable, long-lived microtubules as well as regulator of microtubule functions [65,66,145]. These functions include regulation of cell motility, cell cycle, differentiation as well as intracellular trafficking and signalling [145]. The number of microtubules is significantly reduced within the microtubule arrays of polarised epithelial cells from the inner ear of *Apc*$^{Min/+}$ mouse [53]. However, the present study is the first to demonstrate direct alterations on microtubule cytoskeleton in intestinal cells upon APC deficiency.

3.4.3 Fragmentation of Golgi complex in APC deficiency

Microtubules play a vital role in the control of cell shape and function. Importantly, they provide tracks along which organelles are positioned. In highly polarised cells, such as intestinal epithelial cells, proper spatial arrangement of organelles is critical for their function

[146]. My results indicate that the Golgi complex is fragmented and mispositioned with APC loss. Key roles of the Golgi complex are to modify, and sort proteins derived from the endoplasmic reticulum (ER). The structure of the Golgi complex is vital to ensure proper protein trafficking and defects in this organelle have been observed in many diseases, including Alzheimer's disease, Parkinson's disease and amyotrophic lateral sclerosis (AML) [147]. Intact microtubules are required for the normal structure and function of the Golgi complex. Interestingly, previous studies have used anti-microtubular drugs to drive Golgi fragmentation and found that it only moderately affects protein secretion, suggesting that fragmented Golgi complex retains functionality [63]. Moreover, in agreement with my data, a recent study has shown that in human colon cancer cell lines, truncating mutations of APC (similar to those found in colon cancer) lead to Golgi fragmentation [99]. The mechanism was found to involve the N-terminal domain of truncated APC interacting with Asef and activating the Asef-ROCK-MLC2 pathway leading to Golgi fragmentation. However, in my system, this is not the case; Golgi fragmentation is also the consequence of *Apc* depletion. Moreover, treatment of tumoroids with a ROCK inhibitor does not restore intact Golgi structure. The discrepancy in these findings may be attributed to differences in the experimental systems—the previous study used colon cancer cell lines that harbour the many mutations acquired during carcinogenesis, whereas I used intestinal organoids. In addition, the dependence on the actin cytoskeleton regulation by Asef versus microtubule cytoskeleton may differ between growth in 2D versus 3D [71,148].

A fragmented Golgi complex has been previously observed in colon cancer cell lines and has been termed onco-Golgi – the authors of these studies speculated that onco-Golgi drives cancer progression by modulating the activity of proapoptotic kinases[149,150]. Whether Golgi fragmentation is a cause or consequence of cancer progression is yet to be determined. Here I show that the Golgi complex is fragmented as a direct consequence of APC inactivation and is therefore an early event in malignant transformation.

3.4.4 Centrosome mispositioning in APC deficiency

In epithelial cells, the centrosome is located apically where it provides an organising centre for apical microtubules. However, the majority of microtubules are non-centrosomal and it is not fully understood where these microtubules are anchored [133,151]. Correct centrosomal positioning is important for cell shape and polarity in mammalian cells [146,152]. Centrosome

positioning is thought to be determined by intrinsic cues, such as signalling by the Par complex proteins and planar cell polarity, but also by extrinsic cues which can be both molecular as well as mechanical such as forces exerted by the actin and microtubule cytoskeleton [153].

I show that proper positioning of the centrosome is compromised with depletion or inactivation of APC. Centrosomal aberrations have been described before in tumour-derived cell lines, tumour models as well as primary and metastatic human tumours [154–156]. The abnormalities include changes in centrosome numbers, size as well as compositional changes in the pericentriolar material [154,155,157]. Intriguingly, centrosome amplification has been shown to have the potential to initiate tumorigenesis in flies [158]. Because centrosomes play a major role in the formation of the mitotic-spindle, studies have shown correlative evidence between supernumerary centrosomes and chromosomal instability [154,159]. Chromosomal instability is a hallmark of many colorectal cancers and importantly the loss of the C-terminal domain of APC has been shown to directly contribute to chromosomal instability in cell culture models [160,161]. While in this study I do not address centrosome numbers nor size, I have found that the centrosome is not restrained to the apical position in cells with depleted or mutationally inactive APC. In agreement with my findings, multipolar mitotic-spindles that are characterised by centrosomes positioned at different angles have been shown to be present in organoids made from *Apc*$^{Min/+}$ polyps [162]. In addition to defects in mitoses and stability of the genome, centrosomal aberrations can cause alterations in cellular and tissue architecture [154].

Given the multitude of roles of the centrosome in the cell and the functional alterations its aberrations cause, it will be interesting to study how the loss of APC results in centrosomal mispositioning. Based on the results of this study, I hypothesise that the loss of the microtubule interaction domain in APC truncation or deficiency contributes to the positioning of the centrosome.

3.4.5 Paneth cell vesicle mispositioning in APC deficiency

Paneth cells are specialised secretory cells found in the small intestine that defend against pathogens by releasing antimicrobial proteins, including lysozyme, into the lumen of the crypt (for a detailed description of Paneth cells and their function, see Chapter 5) [13]. One class of

these vesicles contains lysozyme and can be visualised by the fluorescent agglutinin UEA. I have determined that the normal localisation of the apically-disposed UEA positive secretory vesicles in Paneth cells is dramatically altered upon depletion or mutational inactivation of APC. While still apically located, the vesicles are instead held in a compact position confined to the apical membrane in APC deficient Paneth cells. Another consequence of APC loss in Paneth cells is the loss of their normally rigid pyramidal shape.

Vesicular trafficking to the apical membrane is a key step in the release of antimicrobials from Paneth cells [163]. Microtubules and the kinesin and dynein motor proteins are essential for proper intracellular transport and positioning of these vesicles [164]. However, defects in microtubule positioning prevents proper vesicle trafficking, and my work supports the model that the loss of APC's interactions with the microtubule cytoskeleton, either by mutational inactivation or through depletion, disrupts vesicle transport in tumour Paneth cells. It is important to note, however, that one cannot exclude the possibility that the altered vesicle positioning is due to changes in Paneth cell vesicle numbers. The antimicrobial granules are released upon bacterial attack on Paneth cells as shown *in vivo* and in isolated crypts [165,166]. However, a study carried out on organoids has shown that degranulation *in vitro* in the organoid system is only achieved via IFN-γ or by muscarinergic stimulation, while insensitive to a range of microbes [167]. Therefore, it is unlikely that the alteration in vesicle positioning seen in tumoroids and the pB-shApc organoid model reflects an increase in degranulation due to potential undetectable bacterial contamination of culture.

Proper vesicular trafficking is vital for the communication between the cell and its environment. The results of this study demonstrate that the loss of APC results in defective vesicular transport, suggesting that this could result in altered homeostasis in the intestine, potentially contributing to the formation of a malignant phenotype.

3.4.6 Implications of findings

In this chapter, I detail how I have determined that mutational inactivation of APC is directly linked to compromised cellular organisation, revealing a vulnerability in APC-deficient cells with potential therapeutic implications. Except for familial adenomatous polyposis (FAP) patients, where individuals with germline mutation in *APC* develop tumours throughout the

intestinal epithelia, individuals with colon cancer develop tumour predominantly in the colon. The experiments which have been carried out in my study used tissue and organoids derived from the small intestine. Further studies investigating the cellular effects of loss of APC in the colon will reveal if the phenotypic findings seen in the small intestine, are also present in the colon. Defects in cellular organisation could be used as a biomarker for detection of early colorectal tumorigenesis. Current results show correlation between inactive APC, compromised cellular organisation and defective microtubule cytoskeleton. Future experiments into understanding if the relationships are also causative will tell if therapeutic interventions into restoring cellular organisation could be a novel avenue to treat early tumorigenesis of the intestine.

Chapter 4:

Distinct protein interaction domains of APC control intestinal epithelial tissue morphology and intracellular organisation

4.1 Introduction

In Chapter 3, I have established that mutational inactivation or induced depletion of *Apc* leads to changes in intestinal epithelial morphology and compromises hallmarks of microtubule-regulated intracellular organisation, including altered localisation of nuclei, the Golgi complex, centrosome and secretory vesicles in Paneth cells. In this chapter, I investigate the molecular basis by which APC effector pathways regulate epithelial morphology and intracellular organisation. My strategy is to express deletion constructs of APC that dissect out sufficiency for regulation of its respective effector pathways and phenotypic outputs.

4.2 Chapter methods

A detailed description of methods and materials used in this chapter is covered in depth in Chapter 2. Below is a brief overview of Materials and Methods specific to this chapter.

4.2.1 Sample processing for immunofluorescence and imaging

Organoids were derived from the ileum of *Apc*$^{fl/fl}$ *LSL tdTo*m mice (Winton laboratory) and *Myc-335*$^{-/-}$ and *Myc*$^{\Delta 2\text{-}540/\Delta 2\text{-}540}$ mice (Taipale laboratory). For the quantification of organelle positioning within tumoroids, more than 150 cells were counted manually, using the scoring criteria for apical and basal localisation shown in Figure 3.8 C.

4.2.2 Cloning and transfection for APC sufficiency

Full- length human APC and APC mutants lacking the microtubule binding domain (APC$^{\Delta MT}$) and the binding domain for Wnt effectors (APC$^{\Delta Wnt}$) were cloned into the piggyBac vector as described in Chapter 2. SW480 cells were transfected with the constructs, sorted based on mCherry expression using FACS and selected in 400 µg/ml Hygromycin B for 7 days. Tumoroids were electroporated with pB-APC, pB-APC$^{\Delta MT}$ and pB-APC$^{\Delta Wnt}$ as described in Chapter 2. Electroporated tumoroids were selected for integration of constructs using 100 µg/ml Hygromycin B for 7 days followed by sorting based on mCherry expression using FACS. Cre and Cre-ER^{T2} sequences were cloned into the piggyBac vector and electroporated into *Apc*$^{fl/fl}$ *LSL tdTom* organoids as described in Chapter 2.

4.2.3 RT-qPCR

RT-qPCR for *Apc* levels was detected using primer pair *Apc 2* that recognizes the human and mouse sequence.

4.2.4 Treatment of organoids with chemicals and Wnt3a conditioned media

In all the experiments, doxycycline was used at 2 µg/ml, unless otherwise stated, and 4-hydroxytamoxifen (4-OHT) was used at 1 µM. Organoids were treated with Wnt3a conditioned media diluted with ENR+ 10 % FBS to achieve the desired concentrations (0-100 %).

4.3 Results

4.3.1 Independent protein interaction domains in APC specify different effector functions

APC is comprised of several protein interaction domains (see Figure 1.8). To precisely determine APC sufficiency in regulating microtubule-dependent cellular organisation and epithelial morphology, I generated domain-specific deletions of APC. I removed, individually, the central domain of APC involved in regulating Wnt signalling and the C-terminal microtubule interaction domain (Figure 4.1).

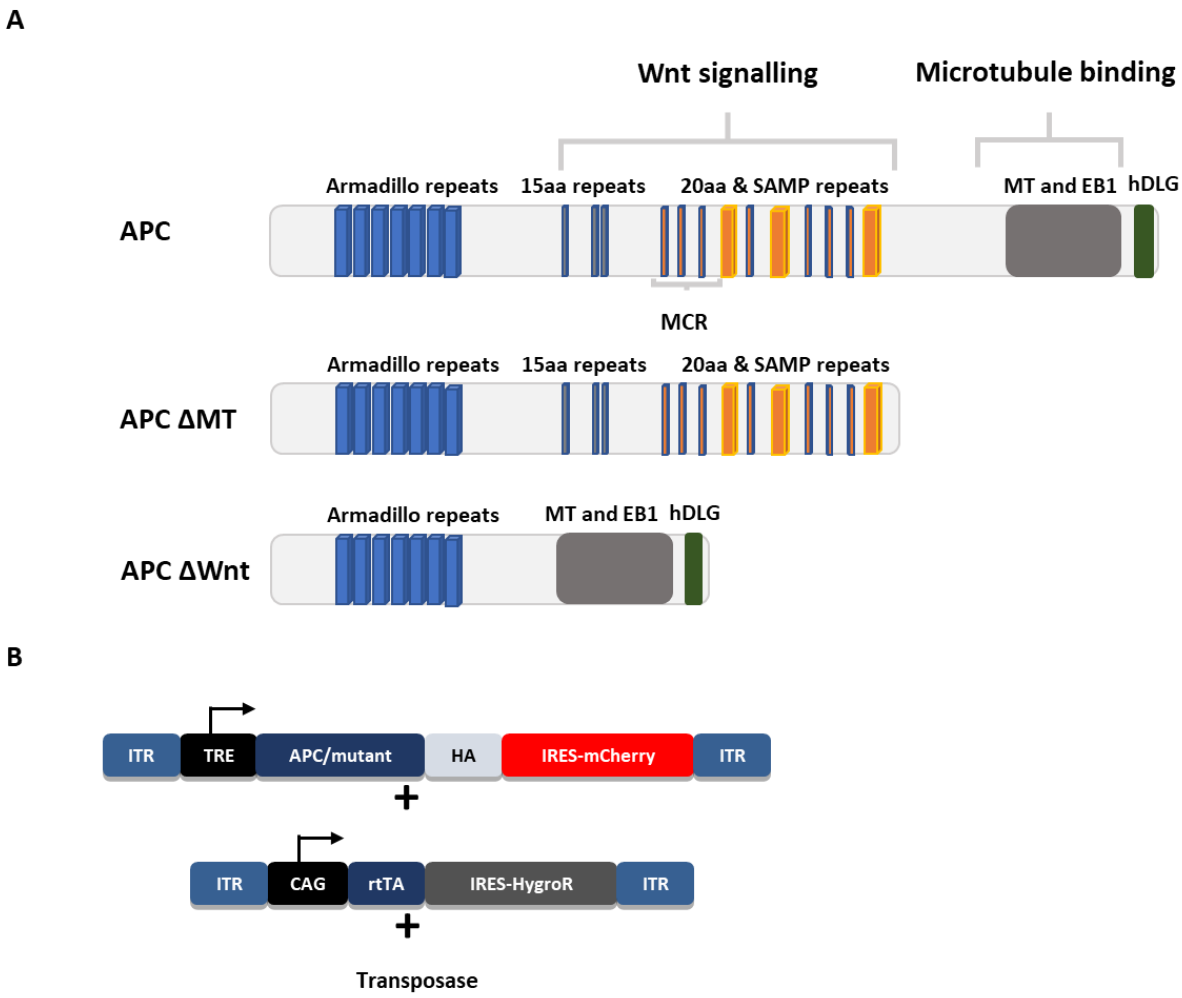

Figure 4. 1: PiggyBac expression system for full length APC, APC$^{\Delta MT}$ and APC$^{\Delta Wnt}$. Protein domains present in the full-length APC, APC lacking the microtubule binding domain (APC$^{\Delta MT}$) and APC lacking the domain for interactions with Wnt pathway effectors (APC$^{\Delta Wnt}$) (A). APC and mutants are expressed in a piggyBac system composed of three constructs. The system is doxycycline inducible, APC/mutants are tagged with HA at the C-terminal domain and the expression of constructs is detectable by mCherry (B).

4.3.1.1 Validation of APC interaction domains in a cell line lacking functional APC

Whilst nocodazole treatment showed that targeted depolymerisation of microtubules results in changes in the positioning of organelles, the direct links between the APC's C-terminal domains to effects on microtubule-dependent processes remain to be established. To probe for sufficiency of protein interaction domains of APC on effector functions, I created a piggyBac transposon-based expression vector system for stable and inducible expression of human APC and two deletion constructs—one omitting the C-terminal microtubule and EB1

binding domains ($APC^{\Delta MT}$), and the second omitting the central β-catenin and Axin binding domains ($APC^{\Delta Wnt}$) (Figure 4.1 A).

To validate the inducible expression system, I used the human colon adenocarcinoma cell line SW480, that expresses truncated APC [168], for stable integration of the deletion constructs. Due to the lack of reliable antibodies against APC, I tagged the APC constructs with a haemagglutinin (HA) epitope tag in the C-terminus and inserted mCherry as a fluorescent probe for transgene expression (Figure 4.1 B). Doxycycline (dox) treatment of transfected SW480 cells showed mCherry expression that was strongest in cells expressing $APC^{\Delta Wnt}$ and empty control (Figure 4.2). There were no obvious morphological alterations apparent for any of the expressed APC constructs after 48 hours of doxycycline treatment. Transfected cells were sorted in order to isolate the population of integrants.

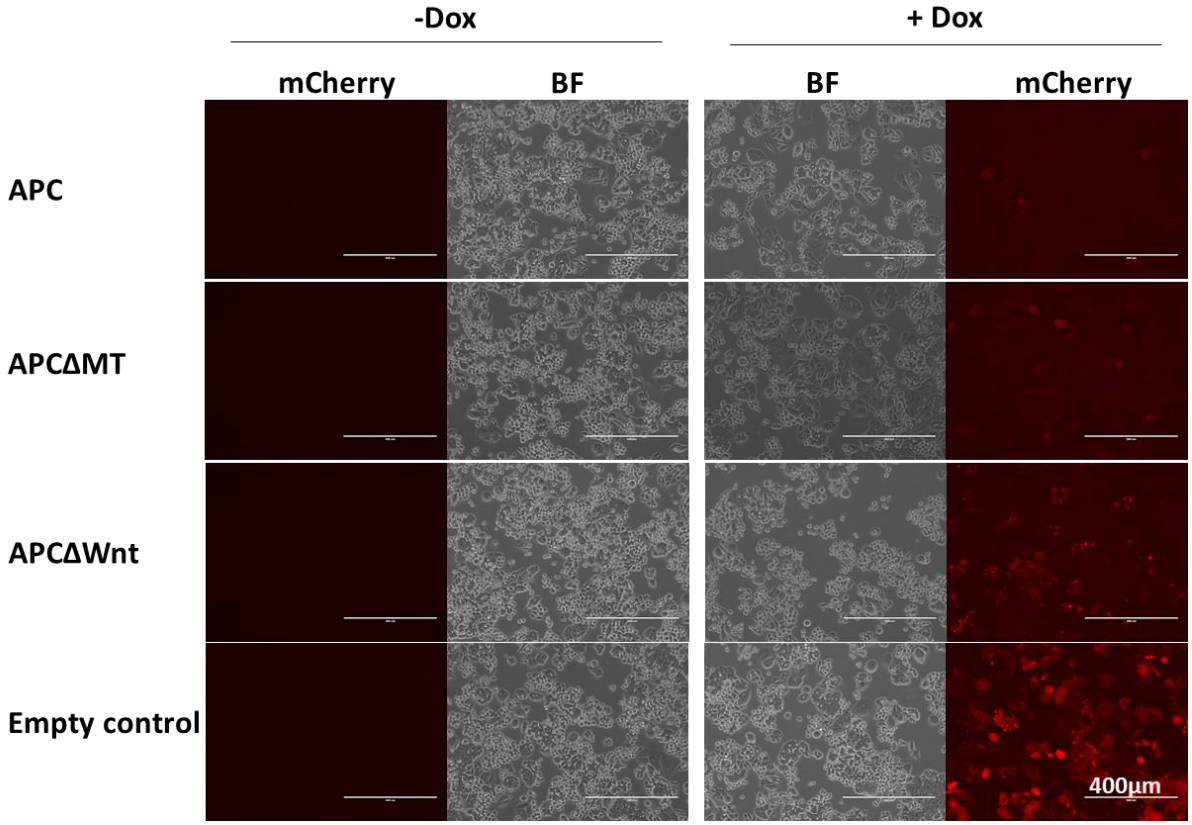

Figure 4. 2: SW480 cells expressing full length APC, $APC^{\Delta MT}$ and $APC^{\Delta Wnt}$. SW480 cells were transfected with piggyBac (pB) constructs: pB-APC, pB-$APC^{\Delta MT}$, pB-$APC^{\Delta Wnt}$ or empty construct expressing no APC/mutant transgene (empty control). Cells were induced for 48 hours with 2 µg/ml doxycycline. Cells were imaged in brightfield (BF) or RFP channel (mCherry) using the EVOS imaging system.

Probing for HA showed that the cells were expressing the different APC constructs at their correct size (Figure 4.3 B). Western blot analysis of the Wnt target genes *AXIN2* and *c-MYC* demonstrated a decrease in protein expression with induction of full-length APC and $APC^{\Delta MT}$, whereas levels of the proteins remained unchanged with expression of the $APC^{\Delta Wnt}$ construct (Figure 4.3 B). Additionally, I used the TOP-Flash assay, a validated, widely-used luciferase-based reporter system of β-catenin-mediated transcriptional activation to measure Wnt signalling. Cells expressing the full-length APC and $APC^{\Delta MT}$ upon doxycycline treatment showed 4-5-fold reduction in Wnt pathway activity (Figure 4.3 C). As expected, the Wnt pathway activity in SW480 cells expressing $APC^{\Delta Wnt}$ was unchanged. These results validate the full-length and the mutant APC constructs functionally from the Wnt pathway regulatory role.

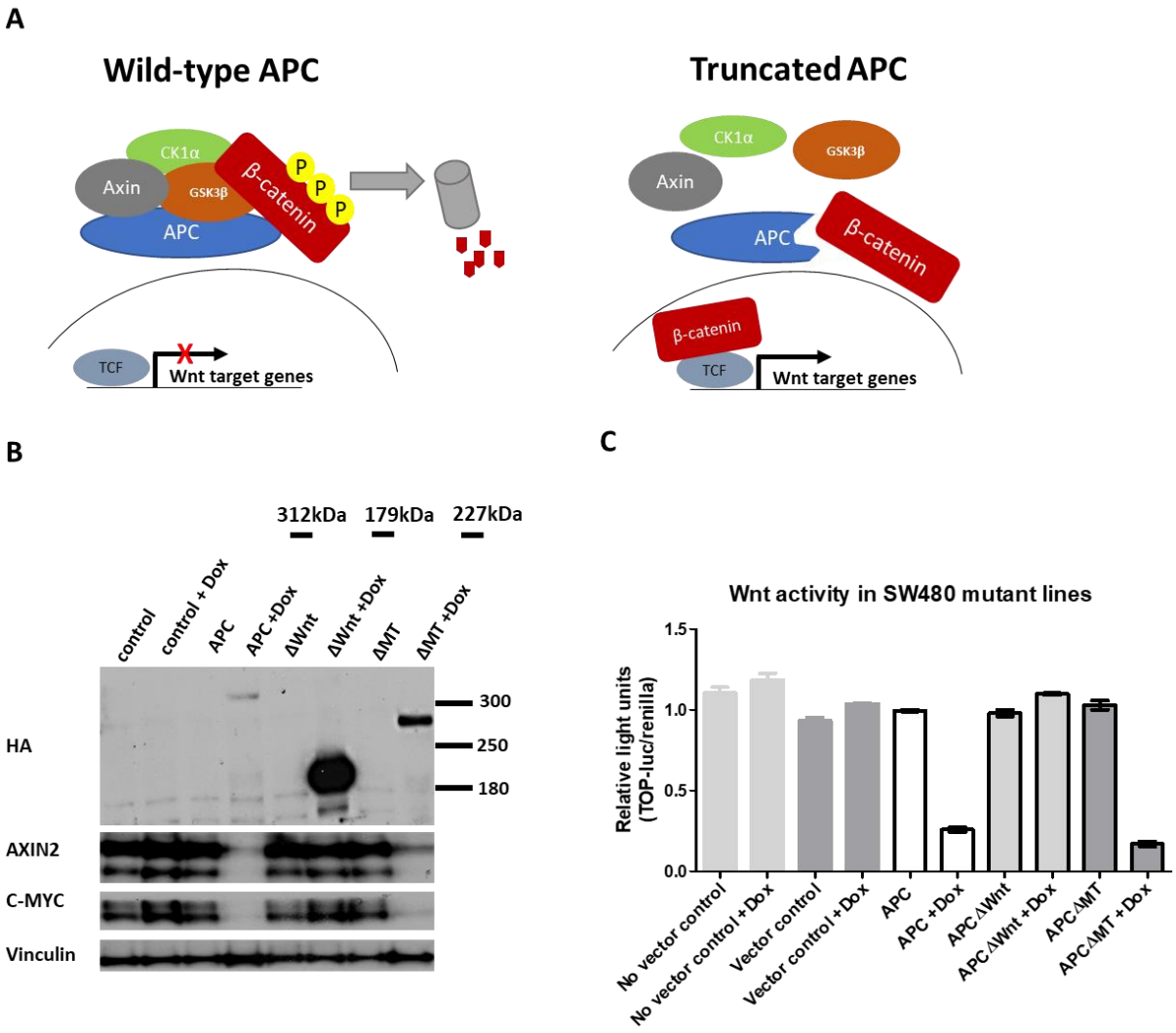

Figure 4. 3: Validation of APC, APC$^{\Delta MT}$ and APC$^{\Delta Wnt}$ constructs in Wnt pathway regulation. Illustration depicting the role of APC in marking β-catenin for degradation. Truncated APC is unable to label β-catenin for degradation leading to unregulated Wnt pathway activity (A). Western blot for HA, AXIN2 and c-MYC in SW480 cells expressing pB-APC, pB-APC$^{\Delta MT}$, pB-APC$^{\Delta Wnt}$ and empty construct (control). Cells were induced for 72 hours with 2 µg/ml doxycycline. Vinculin was used as a loading control (B). The TOP-Flash assay of SW480 cells expressing the constructs induced for 48 hours with 2 µg/ml dox. Data is represented as mean of two independent experiments (±SD) (C).

4.3.1.2 Expression of APC$^{\Delta MT}$ in tumoroids partially restores epithelial morphology but does not rescue cellular disorganisation

In order to study the domain specific functions of APC, I integrated the validated full-length APC, APC$^{\Delta MT}$ and APC$^{\Delta Wnt}$ into tumoroids for sufficiency experiments. As with the SW480 cell

lines I created (section 4.3.1.1), mCherry expression is a marker of successful integration of the constructs (Figure 4.1 B). I electroporated the constructs into tumoroids, followed by selection with 100 µg/ml Hygromycin B for 7 days and then checked for mCherry expression after 48 hours of doxycycline treatment. The transfected tumoroids were expressing mCherry to variable levels, with tumoroids electroporated with the full-length APC showing barely detectable fluorescence. The low mCherry expression in APC-tumoroids could be due to the length of APC upstream from the internal ribosome entry site (IRES) that regulates downstream mCherry expression (Figure 4.1 B). I therefore sorted the tumoroids, collecting all the mCherry positive cells using fluorescence activated cell sorting (FACS) and expanded the surviving clones (Figure 4.4). APC-tumoroids expressed mCherry, but at much lower levels compared to $APC^{\Delta MT}$- and $APC^{\Delta Wnt}$ -expressing tumoroids.

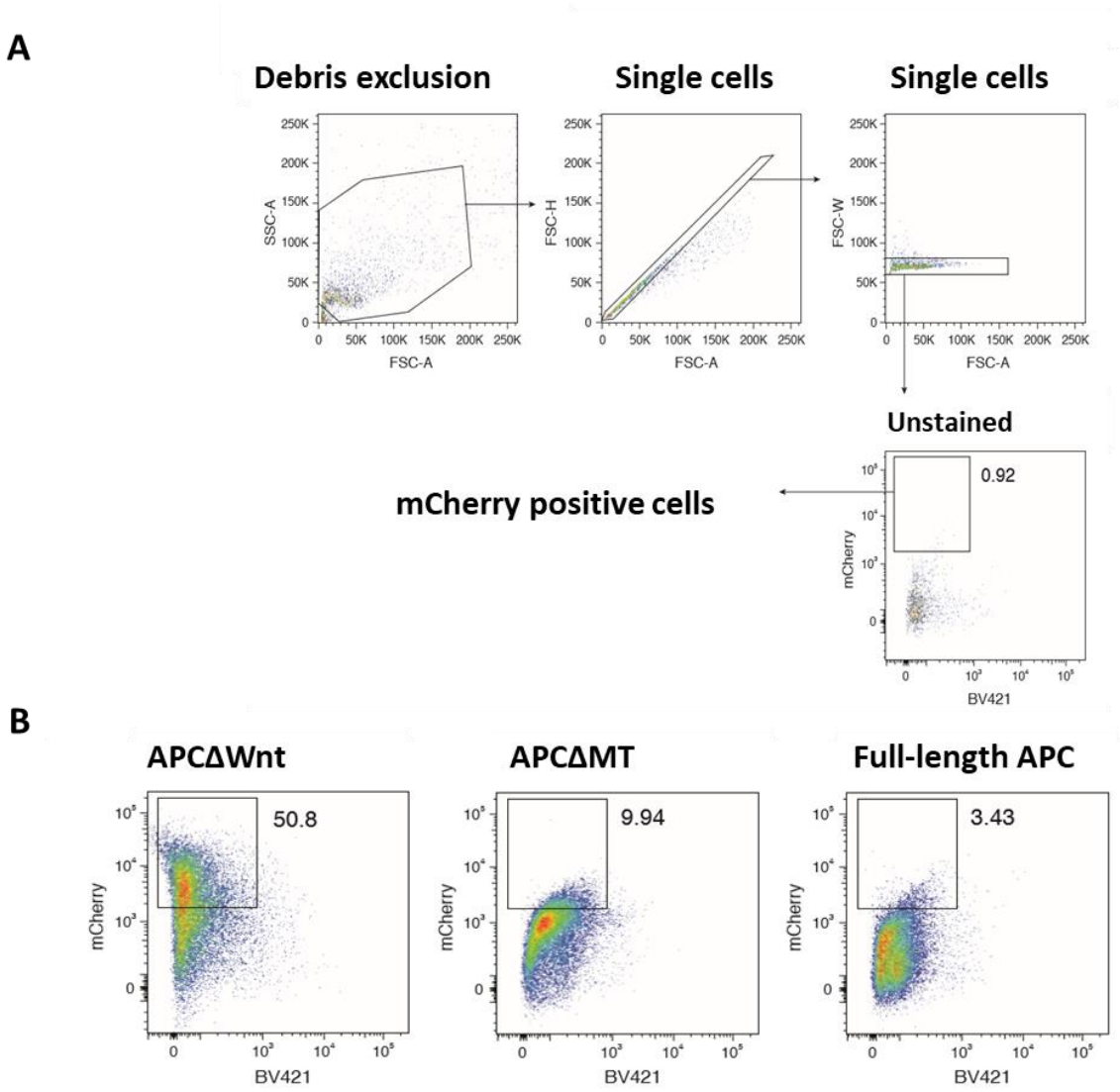

Figure 4. 4: Sorting strategy for tumoroids transfected with APC, APC$^{\Delta MT}$ and APC$^{\Delta Wnt}$ constructs. Gating strategy (A). mCherry positive tumoroid cells sorted for expansion (B).

Morphologically, full-length APC and APC$^{\Delta Wnt}$ -expressing tumoroids looked identical to non-doxycycline treated controls (Figure 4.5 A). Tumoroids expressing APC$^{\Delta MT}$ were heterogeneous in morphology with most displaying spherical shape. However around 15 % showed a morphology closer to that of a budding organoid (Figure 4.5 A). Due to the small size of these budding-like tumoroids, I was not able to isolate them by picking. Titration of concentrations of doxycycline from 2-0 µg/ml led to progressively fewer budding-like tumoroids, suggesting that the morphological changes I observe is a function of APC$^{\Delta MT}$-expression (Figure 4.5 B).

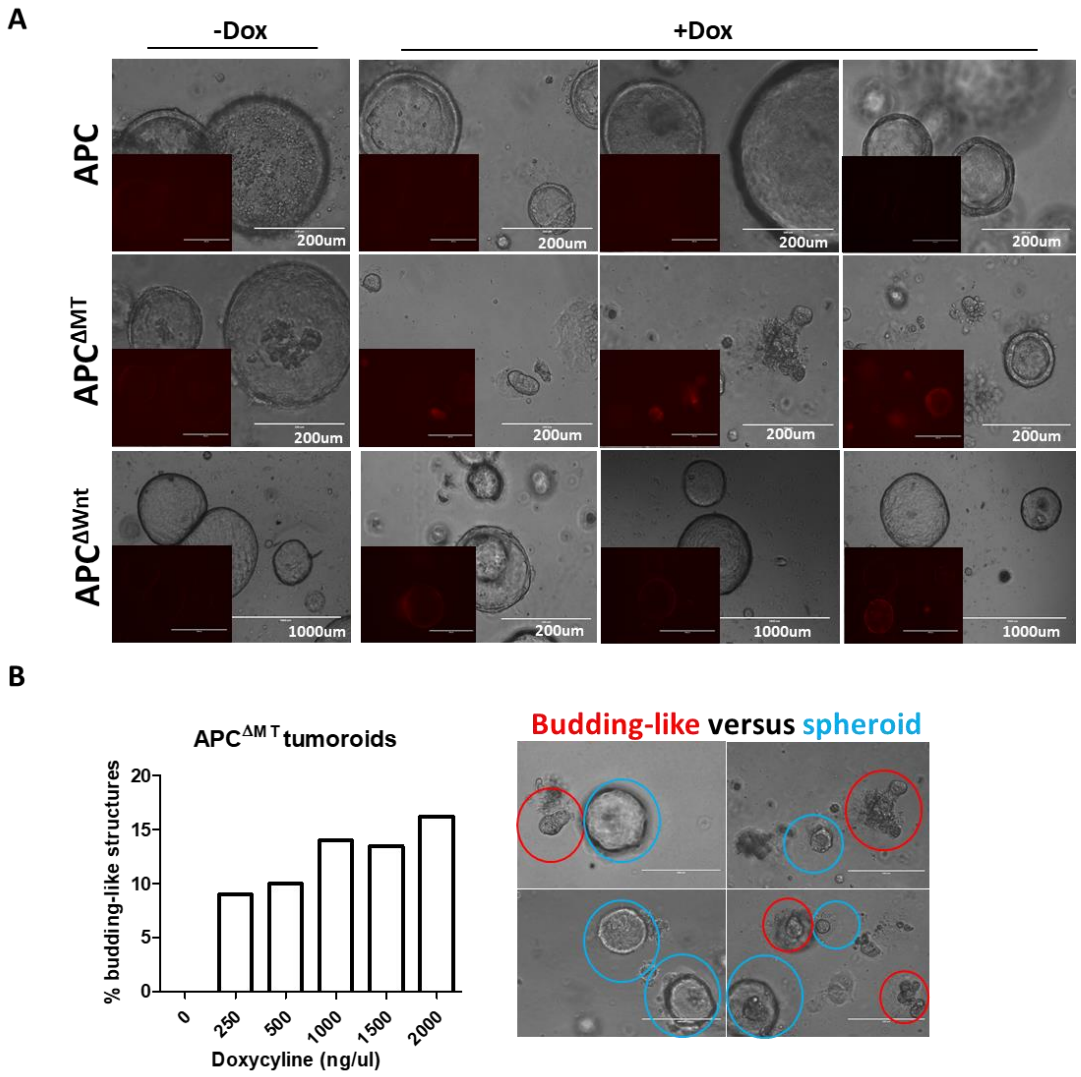

Figure 4. 5: Morphology of tumoroids expressing APC, APC$^{\Delta MT}$ and APC$^{\Delta Wnt}$. Representative images of tumoroids expressing APC, APC$^{\Delta MT}$ or APC$^{\Delta Wnt}$ induced with 2 µg/ml doxycycline for 5 days. Tumoroids were imaged in brightfield or RFP channel (mCherry; inset) using the EVOS imaging system (A). Quantification of budding-like structures in APC$^{\Delta MT}$-tumoroids induced with doxycycline for 5 days. Data represents >30 tumoroids per condition. Scoring criteria for budding-like structures (red) and spheroids (blue) is depicted in the illustrative image (B).

Using quantitative RT-qPCR (RT-qPCR) to determine expression levels of the constructs demonstrated detectable *mCherry* levels in all the tumoroid lines expressing the different APC constructs. However, tumoroids expressing the full-length APC showed much lower *mCherry* levels compared to APC$^{\Delta MT}$- and APC$^{\Delta Wnt}$ -expressing tumoroids which correlated with the fluorescence signal viewed by fluorescence microscope (Figure 4.6). In addition, tumoroids expressing full-length APC had no increased levels of *Apc* compared to the non-doxycycline treated control (Figure 4.6). The pool of APC$^{\Delta MT}$- expressing tumoroids showed more than 8-

fold increase in *Apc*, while APC$^{\Delta Wnt}$ -expressing tumoroids had over 4-fold increase *Apc* expression.

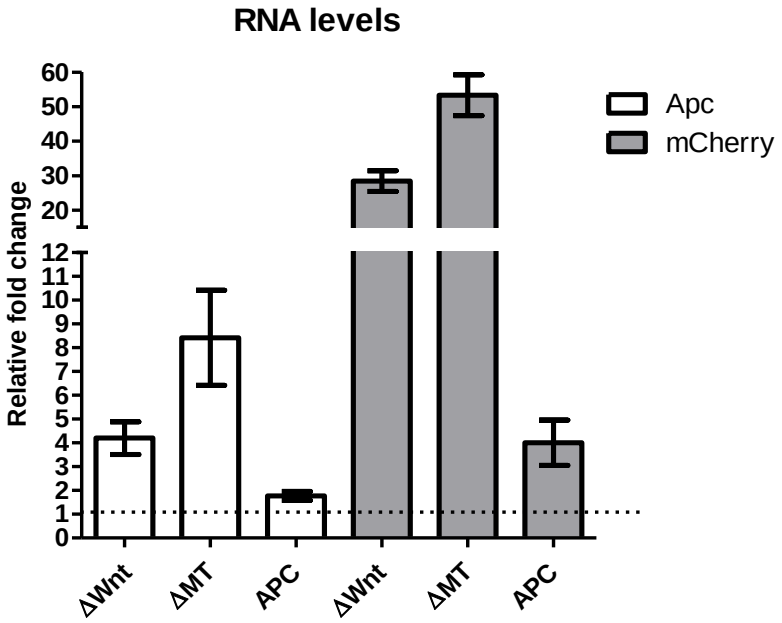

Figure 4. 6: Integration of APC, APC$^{\Delta MT}$ and APC$^{\Delta Wnt}$ constructs in tumoroids. RT-qPCR analysis of gene expression of *Apc* and *mCherry* in tumoroids expressing APC/mutants induced with 2 µg/ml doxycycline for 5 days. Data is normalised to non-induced expressing tumoroids. *B2m* was used as a housekeeping gene. Data is represented as mean of two independent experiments (±SD).

My results indicate that the expression of APC$^{\Delta MT}$ in tumoroids is at sufficient levels to induce a partial rescue of organoid morphology, whereas induction of APC expression either does not rescue morphology, or is expressed at insufficient levels to do so. APC$^{\Delta Wnt}$ protein is expressed at comparable levels to APC$^{\Delta MT}$ but has no effect on epithelial morphology.

To determine if intracellular organisation was restored in tumoroids expressing the various deletion constructs I examined the localisation of the Golgi complex and the centrosome in the expressing tumoroid lines. The expression of APC, APC$^{\Delta MT}$ and APC$^{\Delta Wnt}$ in tumoroids did not rescue the positioning of either the Golgi complex or the centrosome (Figure 4.7). The analysis of the 15 % of APC$^{\Delta MT}$-tumoroids that displayed a morphology change showed that while the tissue morphology was transformed to a more organoid-like, the Golgi complex and centrosome remained mislocalised (Figure 4.7).

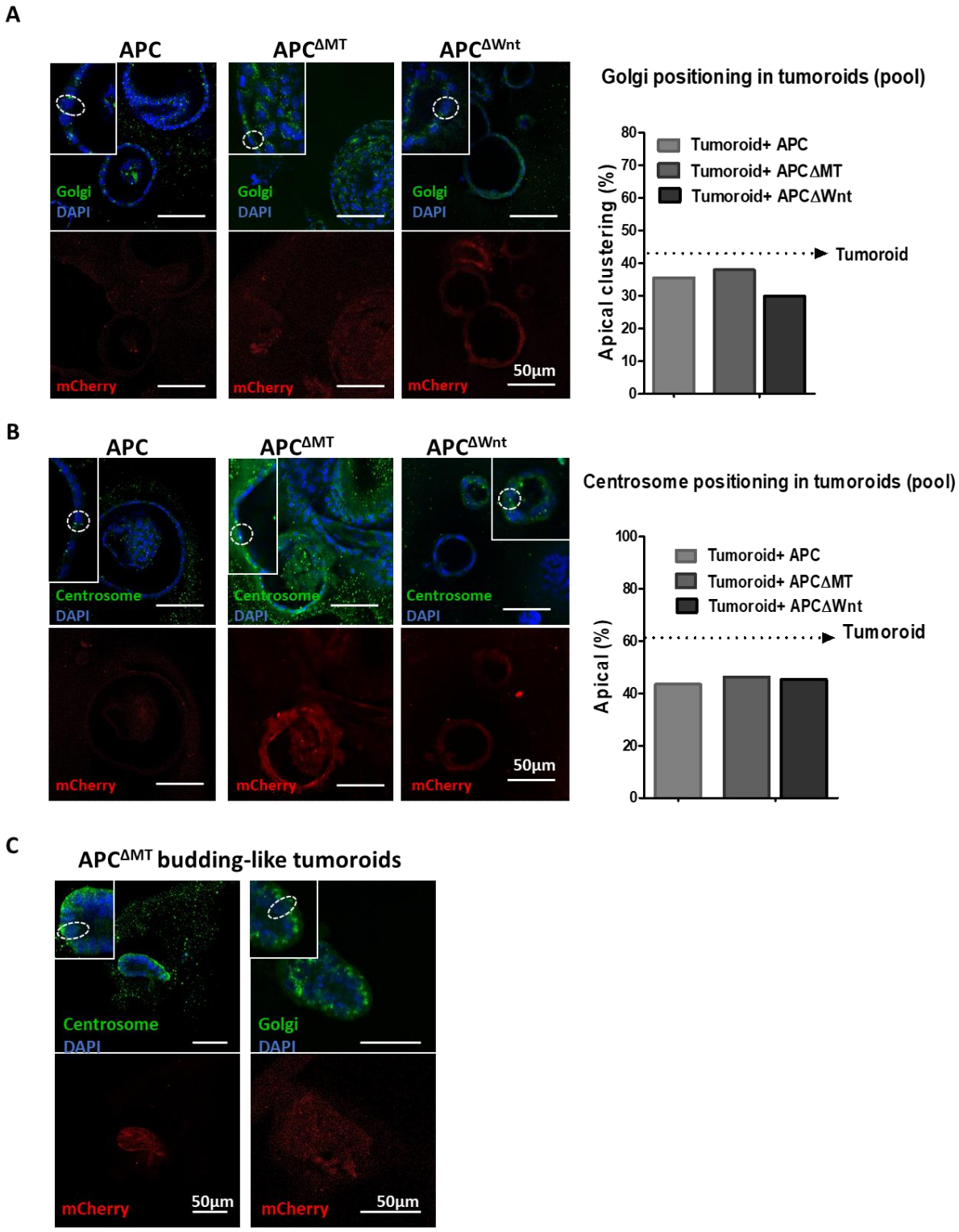

Figure 4. 7: The positioning of Golgi complex and centrosome in tumoroids expressing APC, APC$^{\Delta MT}$ and APC$^{\Delta Wnt}$. Representative images of confocal optical sections from immunofluorescent stains of tumoroids expressing APC, APC$^{\Delta MT}$ or APC$^{\Delta Wnt}$ induced with 2 µg/ml doxycycline for 5 days. >150 cells per tumoroid line were analysed using criteria described in Figure 3.8C (A and B). Confocal optical sections from immunofluorescent stains of tumoroids expressing APC$^{\Delta MT}$ induced with 2 µg/ml doxycycline for 5 days that demonstrated a budding-like structure (C) DAPI labels nuclei.

4.3.1.3 Model of full APC deficiency: Apc$^{fl/fl}$ /pB-Cre-ER^{T2} organoids

Studying the role of specific APC interaction domains in tumoroids has unfortunately several caveats. Firstly, at least one truncated *Apc* allele is always expressed in the mutational signature of tumoroids allowing for some control over effectors that interact with the N-terminus of APC [32,130]. A second consideration is the provenance of the tumoroids—these were derived from the small intestinal epithelia of 110-day old mice. I am unable to determine whether other mutations have incurred in the tumour cells that could influence the sufficiency experiments. To circumvent these issues, I decided to create a system that probed APC function upon immediate inactivation of both *Apc* alleles simultaneously in an organoid. The underlying reason for choosing an *Apc* deletion system rather than the previously developed *Apc* silencing model (pB-shApc, see Chapter 3) was to assure complete loss of functional APC.

I derived organoids from *Apc*$^{fl/fl}$ *LSL tdTom* mice (the mouse intestine was a kind gift from the Winton laboratory [41]). The mouse is homozygous for lox-flanked exon 14 of *Apc* and Cre recombinase expression induces a frameshift mutation at codon 580 leading to the expression of truncated APC. The lox-STOP-lox (LSL)-tdTomato at the Rosa26 locus serves as a reporter for recombination (Figure 4.8).

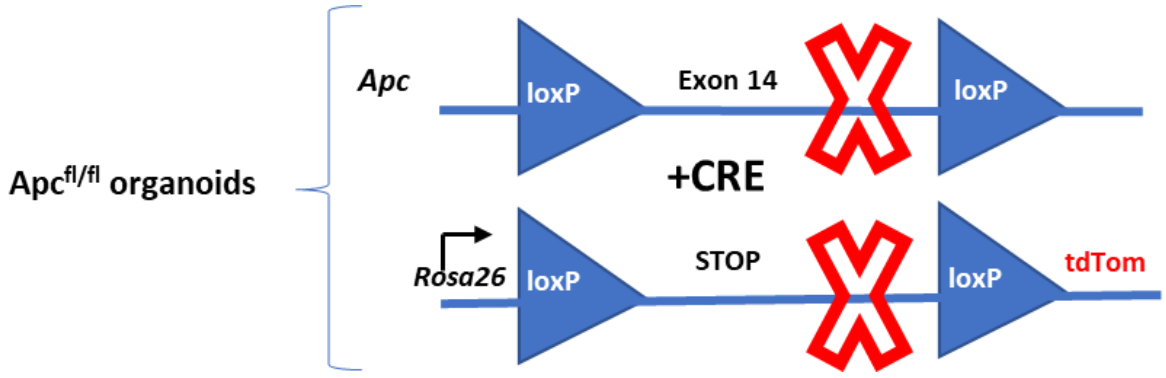

Figure 4. 8: Organoids from *Apc*$^{fl/fl}$ *LSL tdTom* mouse model. Illustration showing the genotype of *Apc*$^{fl/fl}$ *LSL tdTom* mouse with homozygous loxP sites flanking exon 14 of *Apc* and lox-STOP-lox *tdTomato* inserted into Rosa26 locus.

I cloned the Cre recombinase transgene into the piggyBac transposon-based expression vector system for inducible expression, marked with expression of GFP. I transfected *Apc*$^{fl/fl}$ *LSL tdTom* organoids with pB-Cre-GFP via electroporation to create the Apc$^{fl/fl}$ /pB-Cre organoid

line. However, organoids expressed both GFP and tdTomato 48 hours after electroporation without the addition of doxycycline (Figure 4.9 A) indicating that Cre recombinase expression was leaky and constitutive. To circumvent this problem, I generated a 'double-lock' system by using a transgenic fusion of the modified, tamoxifen-inducible estrogen receptor and Cre recombinase [169] (Cre-ER^{T2} recombinase) under the control of the *Tet* operator (Figure 4.10 B). The transgene expression system (pB-Cre-ERT2) enables tight control of Cre recombinase activity requiring combined treatment of doxycycline and 4-hydroxytamoxifen (4-OHT). pB-Cre-ER^{T2} transfected *Apc$^{fl/fl}$ LSL dTom* (Apc$^{fl/fl}$ /pB-Cre-ER^{T2}) organoids did not show any GFP expression without treatment (Figure 4.9 B). The addition of doxycycline and 4-OHT led to GFP and tdTomato expression, detectable 48 hours after treatment. As with tumoroids, floxed organoids were hyperproliferative and spherical in morphology. Therefore, Apc$^{fl/fl}$ /pB-Cre-ER^{T2} organoids are a reliable organoid model for inducible depletion of APC. Ongoing experiments with the expression of the different APC interaction domains in the Apc$^{fl/fl}$ /pB-Cre-ER^{T2} organoids will elucidate the contributions of the specific domains of APC on its effector roles.

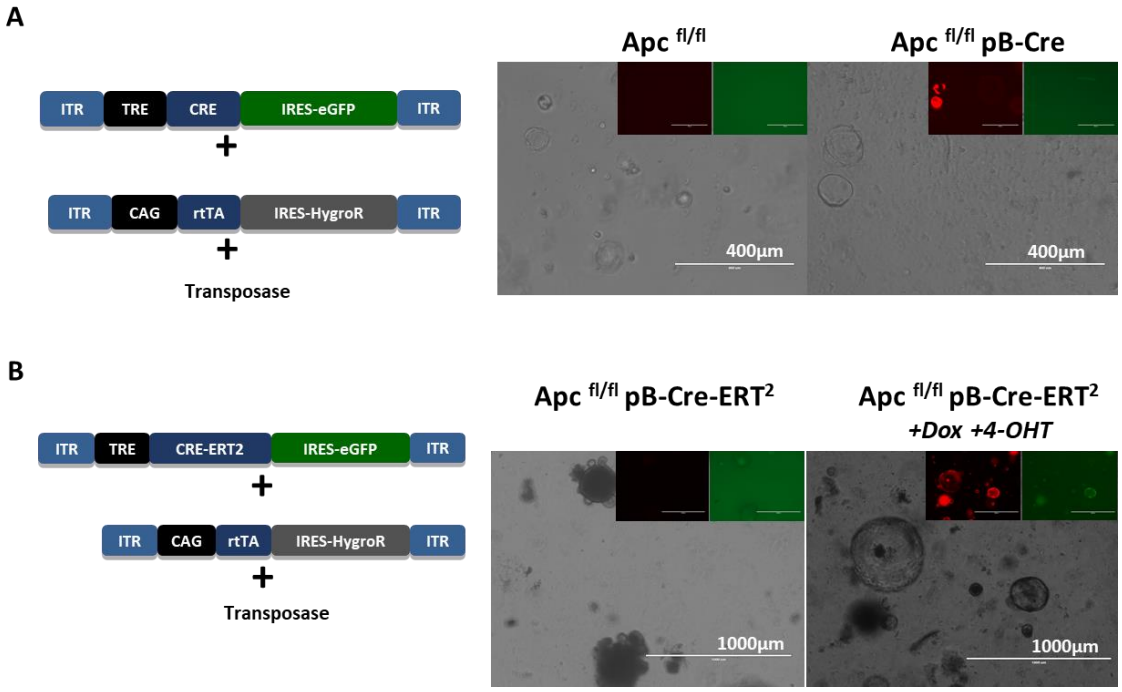

Figure 4. 9: Apc$^{fl/fl}$ /pB-Cre-ER^{T2} organoids as a reliable organoid model for inducible *Apc* depletion. Cre in piggyBac (pB) transposon-based expression system expressed in *Apc$^{fl/fl}$ LSL tdTom* organoids without doxycycline treatment shows leakiness of the system (A). pB construct with Cre-ER^{T2} shows expression only when doxycycline (2 µg/ml) and 4-OHT (1 µM) are added to the media (B). Organoids were imaged in brightfield, RFP channel (tdTomato; inset) or GFP channel (inset) using the EVOS imaging system.

4.3.2 The Wnt pathway target gene *c-Myc* does not mediate the regulation of epithelial morphology

The floxing of *Apc* led to a tissue morphology change whereby a budding organoid was converted into a spheroid, demonstrating that APC regulates epithelial morphology. Moreover, the expression of $APC^{\Delta MT}$ in tumoroids showed that selectively rescuing the interaction domain of APC with Wnt effectors had the potential to alter epithelial morphology from a spheroid to a more organoid-like structure, while not rescuing compromised intracellular organisation. These findings suggest that the regulation of epithelial morphology by APC is via the Wnt pathway and target gene expression. The output of the Wnt pathway is carried out by its target genes. Based on its well-defined roles in mediating the malignant transformation of the intestinal epithelia *in vivo* [96,129], an obvious candidate controlling epithelial morphology is the proto oncogene *Myc*.

To study the role of *Myc* in regulating epithelial morphology, I derived organoids from a mouse line deficient in a putative *MYC* regulatory element that decreases *Myc* expression to Wnt pathway activation by lacking a major Tcf7l2 binding site (*Myc-335*$^{-/-}$; the mouse intestine was a kind gift from the Taipale laboratory) [170]. Validation of the mouse line has been previously carried out by the Taipale laboratory—recombination with the *Apc*$^{Min/+}$ allele (*Apc*$^{Min/+}$; *Myc-335*$^{-/-}$) led to a mouse line that demonstrated a greatly reduced incidence of polyps in the intestine, indicating the requirement of this *MYC* regulatory element for APC-inactivation-driven tumorigenesis [170]. In order to determine whether *Myc* mediates the control of intestinal epithelial morphology by APC, I treated the *Myc-335*$^{-/-}$ organoids with increasing concentrations of Wnt3a ligand for 7 days and monitored the formation of Wnt-oids.

Interestingly, there was no change in the spheroid-formation potential between wild-type and Myc-335$^{-/-}$ organoids (Figure 4. 10). After 7 days of 100 % Wnt3a conditioned media, around 80 % of wild-type organoids had become spherical Wnt-oids, with *Myc-335*$^{-/-}$ organoids showing identical behaviour. I conclude from this result that organoids with reduced responsiveness of *Myc* to Wnt pathway activation are still capable of epithelial morphology change, suggesting that *Myc* in the increased Wnt pathway context is not essential for the tissue morphology change in intestinal tumorigenesis.

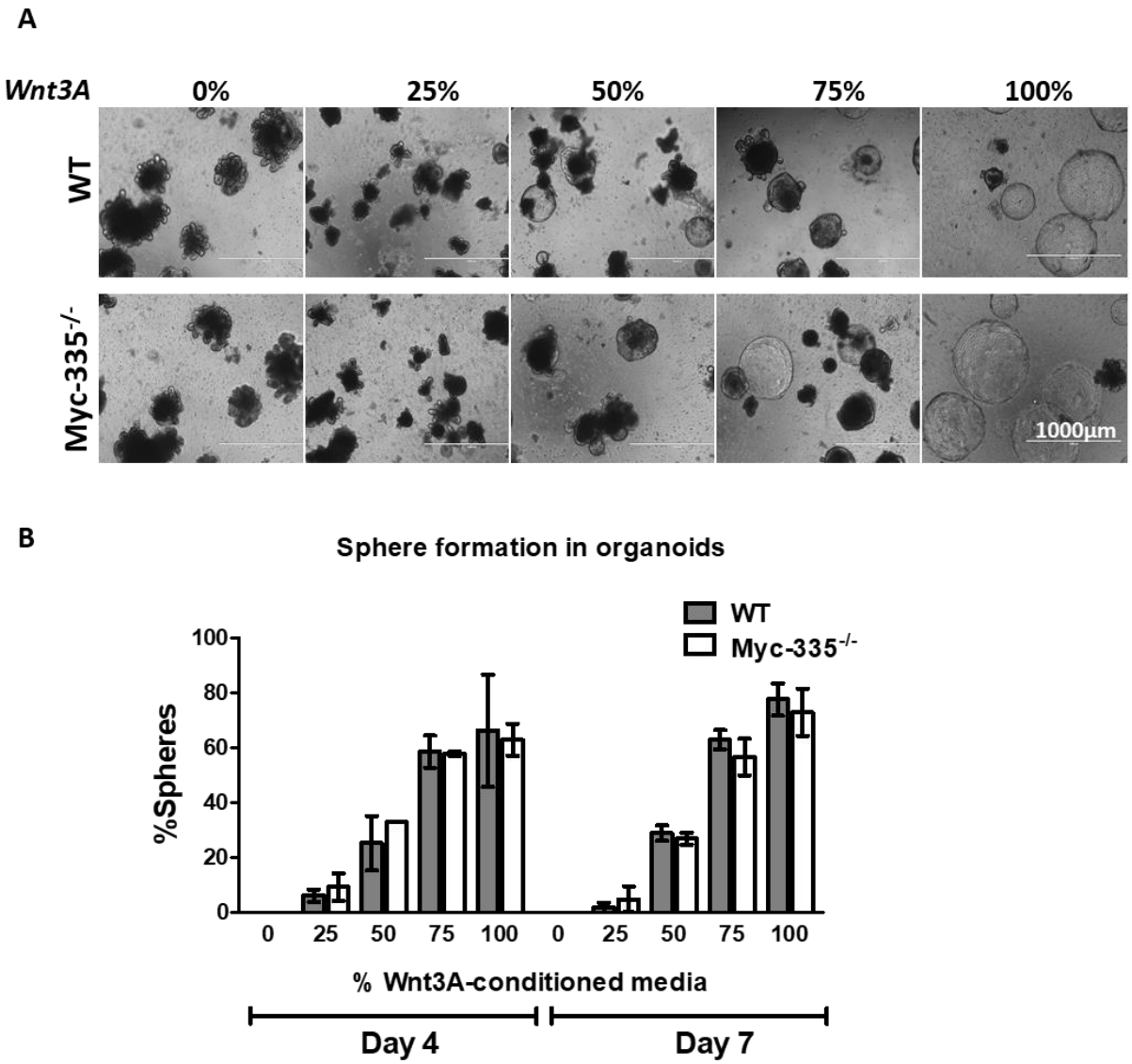

Figure 4. 10: *Myc* is not the main regulator of epithelial morphology. Representable images of wild-type and *Myc-335*$^{-/-}$ organoids grown in different ratios of Wnt3a conditioned media for 7 days (A). Quantification of wild-type and *Myc-335*$^{-/-}$ organoids grown in different ratios of Wnt3a conditioned media for 4 and 7 days. Data is represented as a mean of two independent experiments (±SD) (B).

I probed the wild-type and *Myc-335*$^{-/-}$ organoids for Golgi complex to study whether cellular organisation was compromised. Golgi complex was localised apically for both organoid lines (Figure 4. 11), showing that decreased responsiveness to the Wnt pathway regulator *Myc* does not affect cellular organisation.

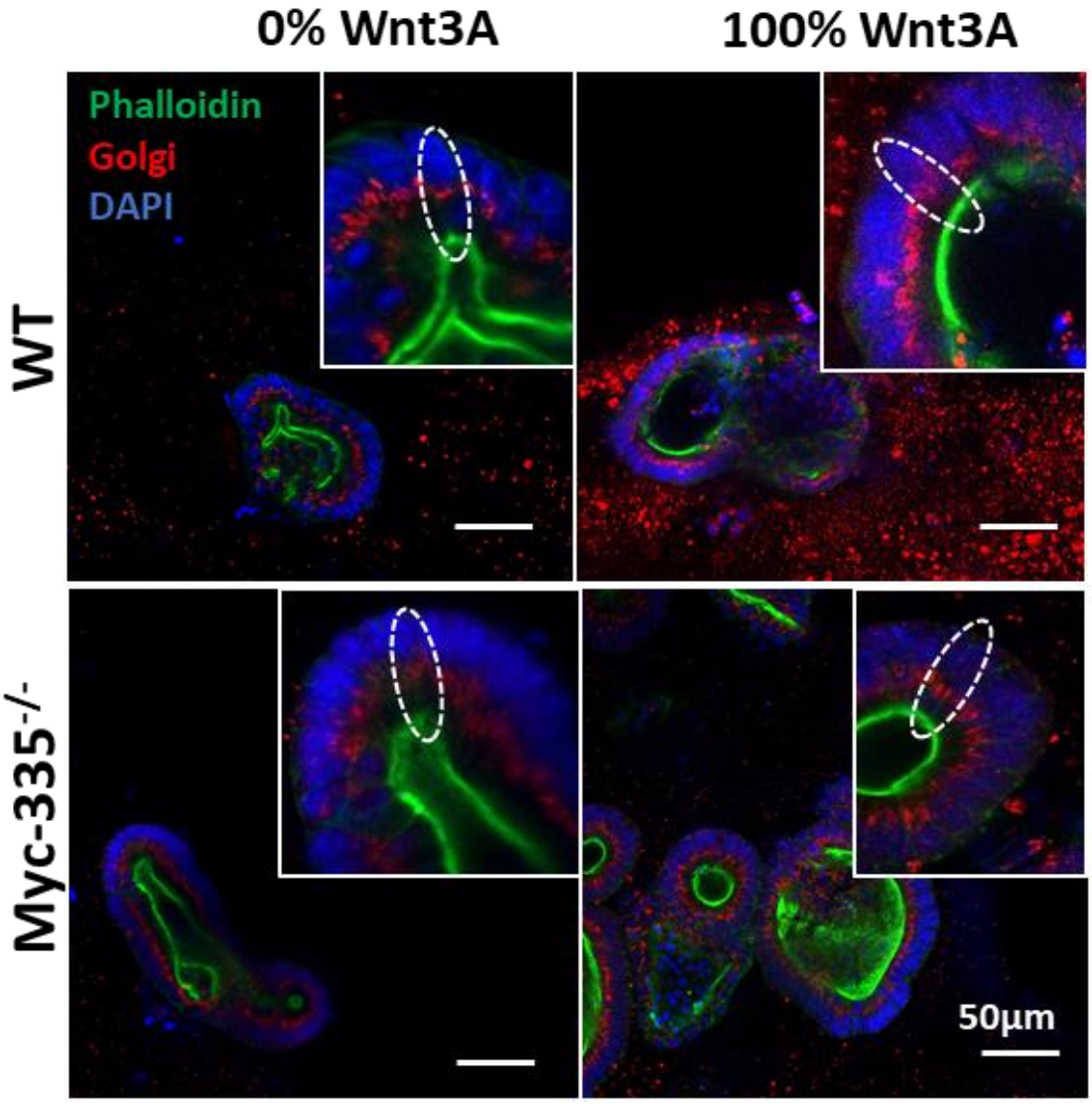

Figure 4. 11: Decreased responsiveness to *Myc* does not affect cellular organisation. Confocal optical sections from immunofluorescent stains of wild-type and Myc-335$^{-/-}$ organoids grown in ENR (0 % Wnt3A) or 100 % Wnt3a conditioned media for 7 days. Phalloidin labels F-actin, DAPI label nuclei.

Given that *Myc-335*$^{-/-}$ organoids represent a decreased response to Wnt pathway activity rather than complete ablation, I tested whether a stronger suppression of Wnt pathway-dependant *Myc* activation would result in a difference in morphology change as a response to the Wnt pathway stimulation. I therefore decided to make organoids from a mouse line deficient in the so called Myc "super-enhancer region" that decreases *c-Myc* expression in tissues and lowers polyp numbers even more than *Myc-335*$^{-/-}$ in *Apc*$^{Min/+}$ background

(*Myc*$^{\Delta 2\text{-}540/\Delta 2\text{-}540}$; the mouse intestine was a kind gift from Taipale lab) [171]. Unfortunately, crypts isolated from this mouse line did not grow in normal organoid culture conditions and I was unable to test the hypothesis (Figure 4. 12). The failure to grow organoids from *Myc*$^{\Delta 2\text{-}540/\Delta 2\text{-}540}$ intestines could be due to the fact that the levels of *Myc*, a known global regulator, were too low, and/or the media components could not support the growth of these organoids in culture.

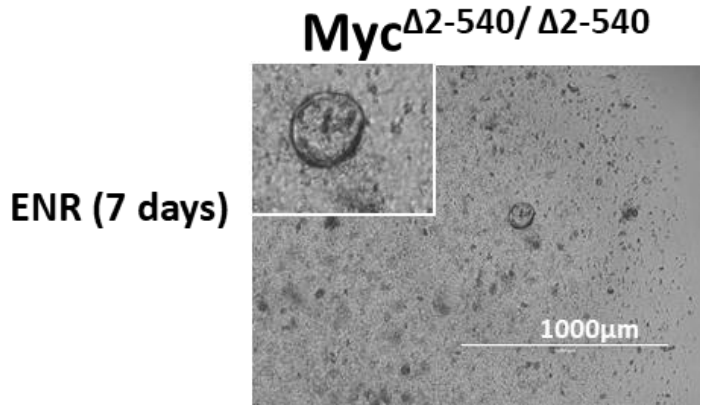

Figure 4. 12: Organoids lacking Myc super-enhancer region do not grow in vitro. Image of a Myc$^{\Delta 2\text{-}540/\Delta 2\text{-}540}$ organoid not growing beyond a few cells after 7 days in culture.

4.4 Discussion

APC is a crucial signalling node controlling homeostasis in the intestinal epithelial tissue. The various interaction domains in APC are responsible for the diverse biological functions of this protein [83]. In Chapter 3, I established that truncation or induced depletion of *Apc* unleashes control over intestinal epithelial morphology and intracellular organisation. To determine APC's domain-specific sufficiency for the regulation of these phenotypic outputs, I expressed different deletion constructs of APC in tumoroids. I show that the expression of APC lacking the C-terminal domain (APC$^{\Delta MT}$) can rescue epithelial morphology but not intracellular organisation, suggesting that the interaction domain of APC with Wnt pathway effectors regulates tissue morphology. Further, my findings suggest that the regulation of tissue morphology is not mediated solely via the Wnt target gene *Myc*.

4.4.1 APC restoration in intestinal tumorigenesis

Acute loss of *Apc* in the murine small intestinal epithelium has been shown to activate Wnt signalling and alter intestinal cell differentiation, proliferation, migration and crypt architecture [41,172]. Doxycycline-inducible shRNA-mediated *Apc* suppression *in vivo* demonstrated that *Apc* depletion phenocopies *Apc* loss [21]. Importantly, it was shown that the restoration of endogenous *Apc* by removal of shApc expression recovers normal intestinal epithelial tissue morphology and function [21]. I attempted to express APC in tumoroids, in order to restore normal intestinal epithelial morphology and intracellular organisation. However, I was unsuccessful, likely due to the inability to express APC to sufficient levels (Figure 4.6 and 4.7). Achieving stable physiological levels of this potent cell regulator is vital to study the cellular role of APC. Of note, the restoration of APC with exogenous expression of the protein has only been successfully carried out in colon cancer cell lines [173,174]. One of the studies showed that transient expression of full-length APC in colon carcinoma cell line HT29 results in inhibition of cell growth leading to cells undergoing apoptosis [173]. However, in another study, the authors showed that stable expression of full-length APC in human colon carcinoma cell line SW480 does not lead to an increase in apoptosis but results in a decrease in proliferation [174]. Notably, the authors showed that the relatively low expression levels of full-length APC result in tighter cell-cell adhesion with consequent changes in cell morphology. These results show that the effect of ectopic APC is dependent on the level of expression, whereby the concentration of APC in a cell defines its response. The failure to express full-length APC in tumoroids can be because of either too low levels of the transgene integration, or toxicity associated with too high levels of APC expression.

4.4.2 APC domain-specific sufficiency for effector roles in the intestinal epithelia

Truncating mutations in APC result in the loss of the central and C-terminal domain regulating the Wnt pathway activity and interacting with the microtubule cytoskeleton. The contributions of these domains to specific effector functions of APC and whether there is a functional link between them remains largely unknown [175]. The pool of APC associated with the β-catenin destruction complex is distinct from the pool that binds to microtubules [176]. Further, the phosphorylation of APC by GSK3β inhibits the interaction of APC with microtubules, a finding opposite to the effect on APC binding to β-catenin, suggesting that the binding of APC to microtubules and β-catenin is mutually exclusive [101]. In addition to the

different pools of APC, whether there is an influence on an effector function by several domains within APC, is to be determined.

4.4.2.1 Intracellular organisation

In Chapter 3, I show that the destabilisation of microtubules by nocodazole phenocopies APC truncation leading to an alteration in intracellular organisation with fragmentation of the Golgi complex. Importantly, nocodazole treatment did not alter tissue morphology, suggesting that the destabilisation of microtubules only affects cellular organisation. APC is known to bind to and stabilise microtubules [60,77,101]. I therefore hypothesised that the loss of the C-terminal microtubule binding domain in truncated APC contributes to the compromised intracellular organisation in APC inactivation. However, I show that the expression of APC containing the microtubule binding domain ($APC^{\Delta Wnt}$) does not restore the positioning of the Golgi complex or the centrosome. In addition, the expression of APC lacking the microtubule binding domain ($APC^{\Delta MT}$) does not rescue altered cellular organisation, but can restore tissue morphology. These results suggest that the loss of the C-terminal domain of APC is not the sole cause of compromised intracellular organisation, while the interaction of APC with Wnt pathway effectors is sufficient to regulate tissue morphology. The regulation of intracellular organisation could involve synergy between the roles of APC in Wnt signalling and microtubule regulation. Successful expression of full-length APC in tumoroids would allow me to test this possibility. Alternatively, the lack of response of $APC^{\Delta Wnt}$ could be due to the level of expression of the exogenous APC, a criteria not tested in this experiment. In addition, expression of $APC^{\Delta Wnt}$ in an *Apc* depletion model (*Apc*$^{fl/fl}$ *LSL tdTom* organoids) removes the uncertainty of whether other mutations or the truncated APC present in tumoroids confounded the results.

The role of the microtubule-binding domain of APC has been previously studied *in vivo.* Two independent mouse models (*Apc*$^{\Delta SAMP/+}$ and *Apc*$^{1638T/1638T}$) (Figure 1.10) demonstrated that the C-terminal domain of APC does not influence the intestinal adenoma development or progression [113,114]. The *Apc*$^{\Delta SAMP/+}$ model also showed that the expression of the C-terminus of APC had no effect on the localisation of APC and EB1 on microtubules [114]. The subcellular localisation of EB1 was also found unchanged in the *Apc*$^{1638T/1638T}$ mouse model. Using *Apc*$^{1638T/1638T}$ mouse embryonic fibroblasts, the authors further showed, that β-tubulin

distribution remains unchanged when the C-terminal domain of APC is missing [113]. The binding of EB1 to microtubules independent of APC has been reported previously [61]. In addition, it has been shown that APC can bind to microtubules upon the deletion of its microtubule binding domain, but this decreases its ability to stabilise the microtubules [101]. In Chapter 3, I show differences in microtubule organisation in *Apc*$^{Min/+}$ polyps and tumoroids compared to the haplosufficient tissue and wild-type organoids. Elucidating results from probing for microtubules in *Apc*$^{1638T/1638T}$ fibroblasts needs to be interpreted cautiously owing to the fact that there is a difference in the dependence on actin and microtubule cytoskeleton between 2D fibroblasts and 3D intestinal epithelial cells [177,178]. Further, a previous study revealed numerical and structural chromosomal aberrations in *Apc*$^{1638T/1638T}$ embryonic stem (ES) cells [108]. Intriguingly, the authors of another study noted that tumours from *Apc*$^{1322T/-}$ mice (lacking β-catenin and C-terminal domains; Figure 1.10) and *Apc*$^{\Delta SAMP/+}$ mice had no chromosomal aberrations indicative of CIN, arguing that the discrepancy in findings is due to blocking apoptosis to avoid the clearance of highly unstable ES cells in the *Apc*$^{1638T/1638T}$ model [114]. The authors therefore concluded that the loss of the C-terminal domain of APC could increase the tendency to CIN, but is not sufficient to cause it.

Taken together, the role of the microtubule binding domain of APC in the intestinal epithelia remains to be fully elucidated. Further experiments with full-length APC and APC$^{\Delta Wnt}$ expression with controlled levels in *Apc*$^{fl/fl}$ *LSL tdTom* organoids will be required to determine the contribution of the microtubule binding domain to the internal organisation of the intestinal epithelial cell.

4.4.2.2 Tissue morphology

My results and previous reports establish that APC regulates intestinal epithelial morphology—inactivation of the protein or its depletion is sufficient to compromise tissue morphology leading to a tumour, or in the case of organoids, into a spheroid [21,41]. I show that the expression of APC lacking the microtubule binding domain, but with an intact Wnt regulatory domain (APC$^{\Delta MT}$), in tumoroids is sufficient to convert a spheroid into a budding-like structure. Not all the tumoroids expressing APC$^{\Delta MT}$ demonstrated a change in tissue morphology, potentially due to the variability in expression levels and/or heterogeneity in the expression levels within cells in a tumoroid.

The finding that organoids treated with Wnt3a demonstrate compromised epithelial tissue morphology and not intracellular organisation suggests a specific role for Wnt pathway target gene expression in tissue morphology change. Importantly, I determined that the control of tissue morphology was unlikely to be mediated by the Wnt pathway target gene *Myc*. Although the identity of the responsible gene(s) is unknown, I have identified some promising candidates. One of these genes is epithelial membrane protein 2 gene (*Emp2*) that encodes for a protein regulating cell membrane composition. Interestingly, an *in vitro* study on polarised Madin-Darby Canine Kidney (MDCK) cells showed that APC regulates spheroid size through EMP2 [179], suggesting that *Emp2* could be a candidate gene for epithelial morphology regulation. Further, the Hippo pathway has been shown to be involved in the regulation of tissue morphology and there is growing evidence for crosstalk between Hippo and Wnt/β-catenin signalling [180].

In conclusion, my findings demonstrate that APC regulates tissue morphology via its Wnt regulatory domain, most probably involving Wnt pathway activity. Future work will focus on identifying the Wnt pathway target gene(s) regulating intestinal epithelial morphology.

4.4.3 Implications of findings

APC is commonly mutated in colon cancer, leading to the loss of the central and C-terminal domains, regulating the Wnt pathway activity and interacting with the microtubule cytoskeleton. As a result, deregulated Wnt pathway promotes uncontrolled proliferation and malignant transformation of intestinal epithelia [95], accompanied by altered tissue morphology. Defects in the regulation of microtubules by APC may contribute to mitotic spindle abnormalities leading to CIN, and potentially fuelling the development of adenocarcinoma [108,109,111,112,114,160]. I demonstrate here that the compromised intracellular organisation present in early intestinal tumorigenesis is potentially caused by the loss of both the central and the C-terminal domain of APC. The disruption of the diverse functions of APC may therefore synergistically contribute to tumour progression. Future studies determining the relative contributions of APC-Wnt effectors and APC-microtubule interactions to the alterations manifested in intestinal tumorigenesis will further unravel the extent to which APC's interaction with the microtubule cytoskeleton acts as a barrier to malignant transformation of intestinal epithelia.

Chapter 5:

Paneth cells in intestinal tumorigenesis

5.1 Introduction

Paneth cells of the small intestinal epithelia reside at the base of crypts in intimate contact with stem cells. They are distinguished by their pyramidal shape with the apex pointing into the lumen of the gut. Within the apical compartment of Paneth cells, vesicles are poised for secretion of their contents into the gut lumen. The vesicles are filled with antimicrobials that function in host-defence [13]. Antibodies raised against lysozyme or fluorescently labelled agglutinin (UEA) that binds to the fucose residues on the vesicles, can be used for visualisation of these granules by fluorescent microscopy. In Chapters 3 and 4, I show that APC inactivation compromises microtubule-regulated cellular organisation; APC deficient Paneth cells lose their characteristic pyramidal shape and UEA positive vesicles, normally restricted apically, are mislocalised (Figure 3.2). In addition, APC inactivation results in altered tissue morphology with loss of the distinct crypt-villus structure in adenoma and tumoroids (Figures 3.1 and 3.6). Paneth cells are rigid cells, important for supporting and maintaining stem cells at the stem cell niche at the bottom of the crypt [17]. It is tempting to speculate that changes to the intracellular structure of Paneth cells could alter their intimate interaction with stem cells and disrupt crypt homeostasis leading to changes in tissue morphology. There have been limited studies addressing the potential for adenomas originating from non-stem cells [29]. Given changes in the shape and vesicle location in adenoma Paneth cells and their importance in maintaining the stem cell niche [15], I hypothesise that APC-dependent maintenance of Paneth cell organisation is a barrier to tumorigenesis.

5.2 Chapter methods

A detailed description of methods and materials used in this chapter is covered in depth in Chapter 2. Below is a brief overview of Materials and Methods specific to this chapter.

5.2.1 Transduction and transfection of organoids

Organoids transduced or transfected by electroporation with Paneth cell specific shApc constructs were selected with 2 μg/ml puromycin for 7 days or with 150 μg/ml Hygromycin B for 7 days, respectively.

5.2.2 Live imaging of organoids

Live imaging of organoids was carried out within AstraZeneca facilities using the YOKOGAWA Cell Voyager CV8000 spinning disc confocal microscope in collaboration with Samantha Peel and Yinhai Wang.

5.2.3 Compounds

In all the experiments, doxycycline was used at 2 µg/ml, unless stated otherwise, and 4-hydroxytamoxifen (4-OHT) was used at 1 µM.

5.3 Results

5.3.1 Adenoma Paneth cells show defects in cellular organisation

In addition to labelling the Paneth cell vesicles, Ulex europeus agglutinin-1 (UEA), also stains the fucose residues present on the vesicles of goblet cells [181]. In order to validate that the disruptions in vesicles upon APC loss were specific to Paneth cell granules, I labelled organoids and ApcMin/+ tissue for lysozyme that is secreted exclusively by Paneth cells in the intestine [14]. Lysozyme staining of wild-type organoids and normal epithelia displayed the apically located vesicles that filled the cytoplasm of a pyramidally shaped cell (Figure 5.1). In tumoroids and adenoma tissue, lysozyme staining displayed vesicles that had lost their shape and normal positioning in a non-pyramidally-shaped cell (Figure 5. 1). Therefore, the lysozyme staining reiterated the pattern seen when UEA-labelling was used, suggesting that APC inactivation results in Paneth cell specific loss of shape and altered localisation of vesicles.

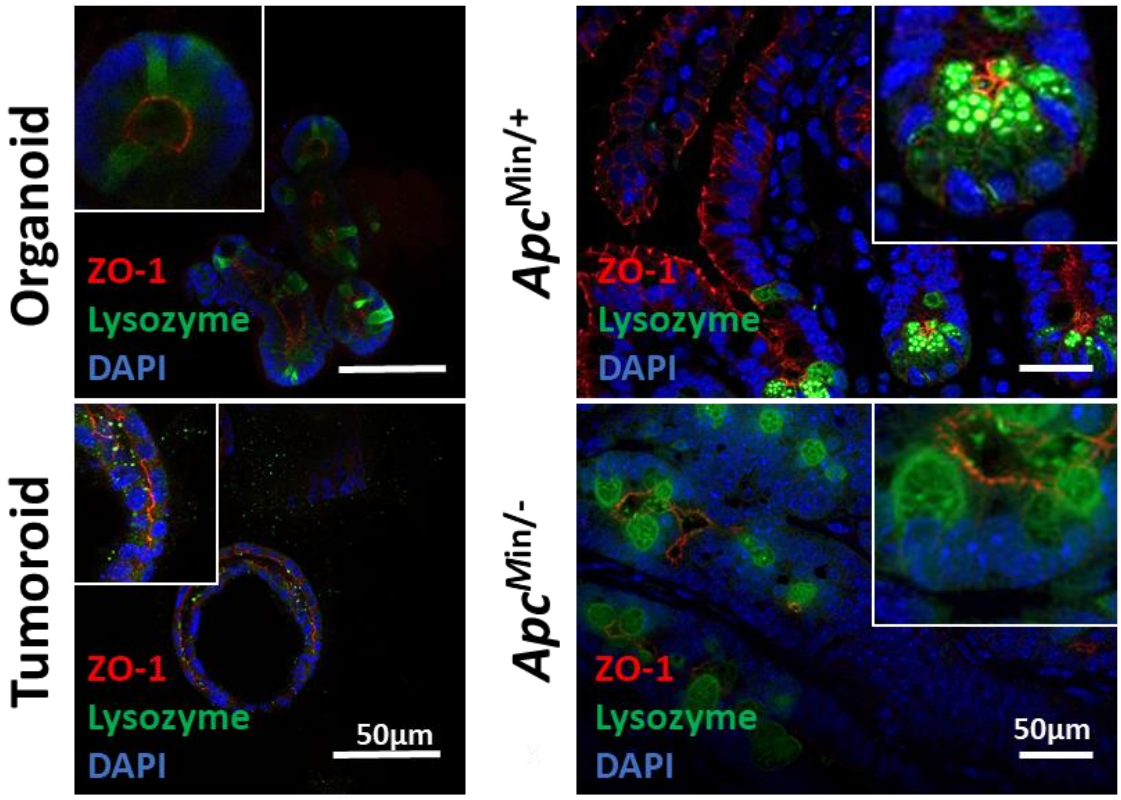

Figure 5. 1: Dispersed positioning of Paneth cell vesicles in APC inactivation. Confocal optical sections from immunofluorescent stains of organoids and tumoroids and the small intestinal tissue from *Apc*$^{Min/+}$ mouse displaying haplosufficient tissue (*Apc*$^{Min/+}$; upper panel) and polyps (*Apc*$^{Min/-}$; lower panel). Paneth cell vesicles are marked with lysozyme, tight junctions are labelled by ZO-1 and DAPI labels nuclei.

5.3.2 Human alpha defensin 5 (DEFA5) expression is exclusive to Paneth cells

To test my hypothesis that APC-dependent maintenance of Paneth cell organisation is tumour suppressive, I required a system that allows for controlled transgene expression specific to Paneth cells. The 1402 proximal bases of the human defensin 5 gene (DEFA5) [182] has previously demonstrated activity in the intestinal epithelium specific to Paneth cells. Thus, I generated an inducible lentiviral Tet-On system that is under the control of the DEFA5 promoter (pLV-DEFA5-GFP) (Figure 5.2 A). In order to determine whether the construct is inducible, I transduced human embryonic kidney cells (HEK293T cells) with the Paneth cell specific lentiviral construct (pLV-DEFA5-GFP). A low level of GFP expression in doxycycline (dox) induced HEK293T cells showed a low activity of the DEFA5 promoter in these cells (Figure 5.2 B). I therefore carried out a control experiment in which HEK293T cells were transduced with both the pLV-DEFA5-GFP construct, as well as a doxycycline-inducible lentiviral construct

where the expression of reverse tetracycline-controlled transactivator (rtTA) is under the control of the ubiquitously expressed ubiquitin C promoter (pLV-UbC-RFP). UbC driven rtTA can thus act on the tetracycline response element (TRE) of the pLV-DEFA5-GFP construct. I observed high levels of GFP expression (over 10-fold higher than for pLV-DEFA5-GFP on its own) in cells transduced with both viruses upon doxycycline treatment, demonstrating the inducibility of the pLV-DEFA5-GFP construct (Figure 5. 2B).

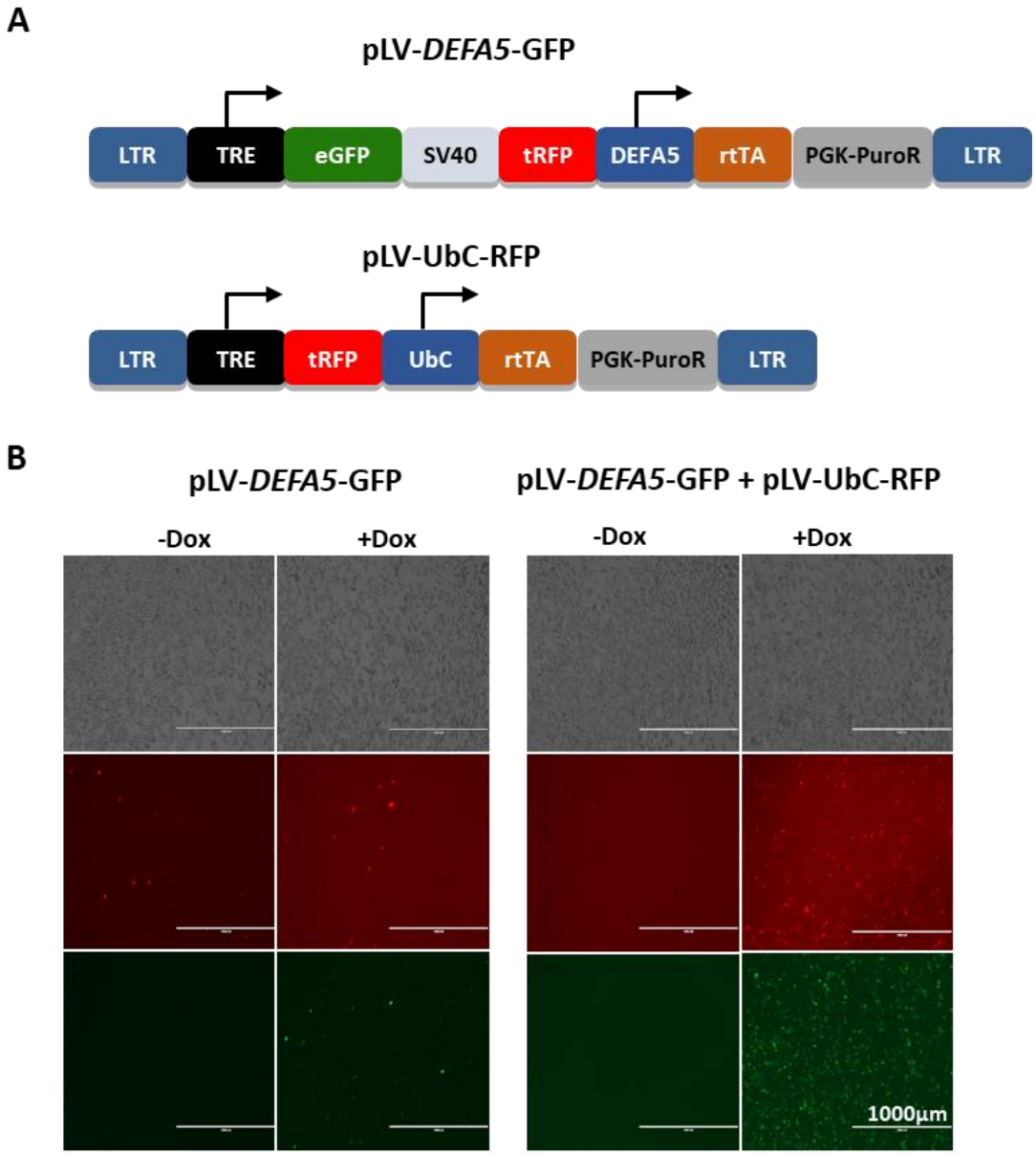

Figure 5. 2: Inducibility of the pLV-*DEFA5*-GFP construct. Paneth cell specific inducible lentiviral construct (pLV-*DEFA5*-GFP) and an inducible construct expressed ubiquitously (pLV-UbC-RFP) used as a control (A). Transduced HEK293T cells were induced with 2 µg/ml of doxycycline for 72 hours (B).

Next, to validate the DEFA5 promoter specificity in Paneth cells, I transduced organoids with pLV-DEFA5-GFP construct and established a stable line using 2 µg/ml puromycin selection for 7 days. At 48 hours post doxycycline treatment, organoids displayed GFP expression confirming the inducibility of the construct and activity of the human DEFA5 promoter in murine-derived organoids (Figure 5.3). To determine DEFA5 promoter specificity, I probed the transduced organoids for lysozyme. All GFP positive cells in the organoid crypt were lysozyme positive suggesting DEFA5 activity solely in Paneth cells (Figure 5.3).

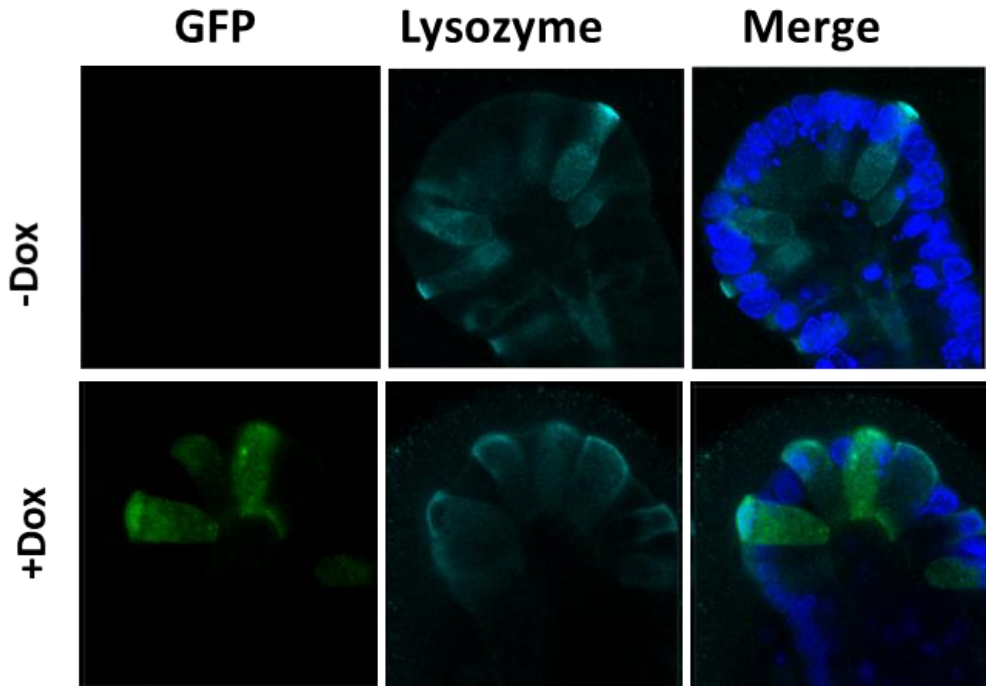

Figure 5. 3: *DEFA5* promoter shows specificity to Paneth cells. Confocal optical sections from immunofluorescent stains of pLV-*DEFA5*-GFP organoids. The images are zoomed into the bud domain of the organoid.

5.3.3 Paneth cell specific silencing of APC does not trigger a tumoroid

5.3.3.1 pLV-*DEFA5*-shAPC

To determine whether APC-dependent maintenance of Paneth cell organisation is a barrier to tumorigenesis, I inserted the functionally-validated shApc sequence (see Chapter 3, Figures 3.14 and 3.15) into the dox inducible lentiviral pLV-DEFA5-GFP vector, where GFP is a marker of shApc expression (pLV-DEFA5-shApc) (Figure 5.5). In a parallel experiment, I cloned the

same shApc into an inducible lentiviral vector where the shRNA is under the control of a ubiquitously expressed promoter (UbC), detectable by RFP expression (pLV-UbC-shApc) (Figure 5.5). Ubiquitous depletion of Apc in organoids converts organoids to tumoroids (see Chapter 3, Figure 3.15). I transduced wild-type organoids with the lentiviral constructs, followed by antibiotic selection with 2 µg/ml puromycin for 7 days to generate stable lines.

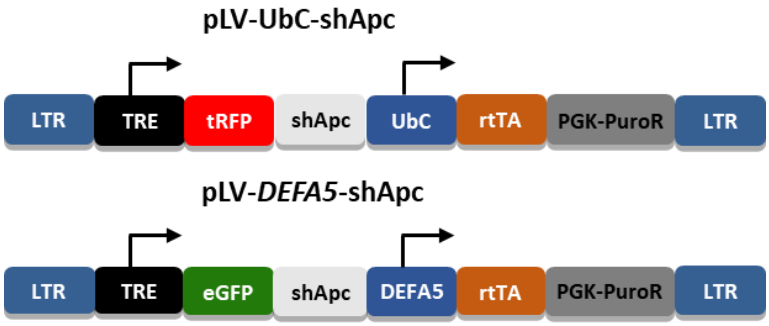

Figure 5. 4: Lentiviral system for inducible Paneth cell specific *Apc* silencing. Doxycyline-inducible lentiviral construct for ubiquitous (pLV-UbC-shApc) and Paneth cell specific (pLV-*DEFA5*-shApc) *Apc* silencing.

Doxycycline treatment of organoids stably expressing pLV-UbC-shApc resulted in organoids expressing RFP, confirming successful construct integration (Figure 5.5 A). However, the expression of RFP was heterogeneous and not all cells expressed RFP within the same organoid. In addition, the doxycycline treated pLV-UbC-shApc expressing organoids maintained their budding structure. The finding that the ubiquitous silencing of Apc did not generate a tumoroid suggests that either the lentiviral delivery of shApc did not lead to high enough levels of silencing of *Apc*, or that the heterogeneous shApc expression affected the organoid response. To note, the heterogeneous expression was not inherent to shApc induction, as transduction with an empty lentiviral construct lacking shApc (pLV-UbC-RFP) also led to organoids with mosaic expression of RFP (Figure 5.5 B). In addition, I tried fluorescence activated cell sorting (FACS) to derive ubiquitously expressing organoid lines. However, the sorting procedure resulted in low survival of cells and no organoid growth after one week.

Doxycyline treatment of organoids stably expressing pLV-DEFA5-shApc resulted in the expression of shApc detectable by GFP. The GFP expressing cells fully overlapped with UEA+ cells, demonstrating that the induced shApc was expressed solely in Paneth cells (Figure 5.5 A). Morphologically, the loss of APC only in Paneth cells did not alter the budding organoid

structure. However, owing to the lack of discernible phenotype with ubiquitous expression of shApc, the results of the Paneth cell specific silencing cannot be reliably interpreted.

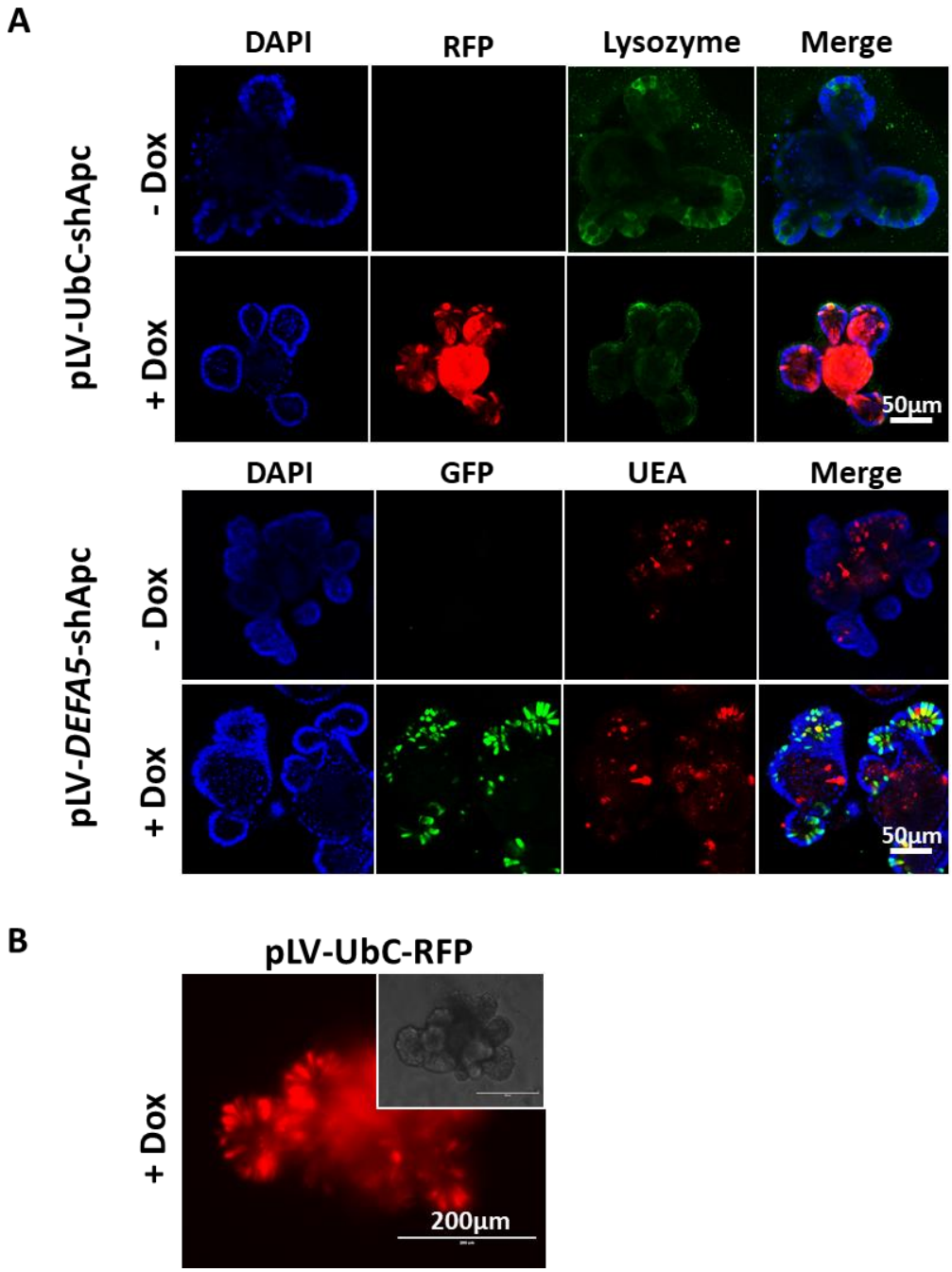

Figure 5. 5: Paneth cell specific silencing of *Apc* using a lentiviral expression system. Confocal optical sections from immunofluorescent stains of organoids transduced with pLV-UbC-shApc or pLV-*DEFA5*-shApc and induced with doxycycline for 10 days. UEA and lysozyme label Paneth cell vesicles. GFP and RFP signal is detected from endogenously expressed protein (A). Organoids transduced with pLV-UbC-RFP show heterogeneous RFP expression upon doxycycline addition (2 µg/ml). Organoids were imaged in brightfield (inset) or RFP channel using the EVOS imaging system (B).

5.3.3.2 pB-*DEFA5*-shAPC

Based on my previous success with shApc expression using the piggyBac constructs (Figures 3.14 and 3.15; pB-shApc, hereafter pB-CAG-shApc), I decided to opt for this system to drive Paneth cell specific loss of APC. In this system, the silencing of *Apc* efficiently leads to a tumoroid formation. The pB-*DEFA5*-shApc construct was designed for constitutive GFP expression in all transfected cells, and mCherry expression as a reporter of induced shApc expression in Paneth cells (Figure 5.6).

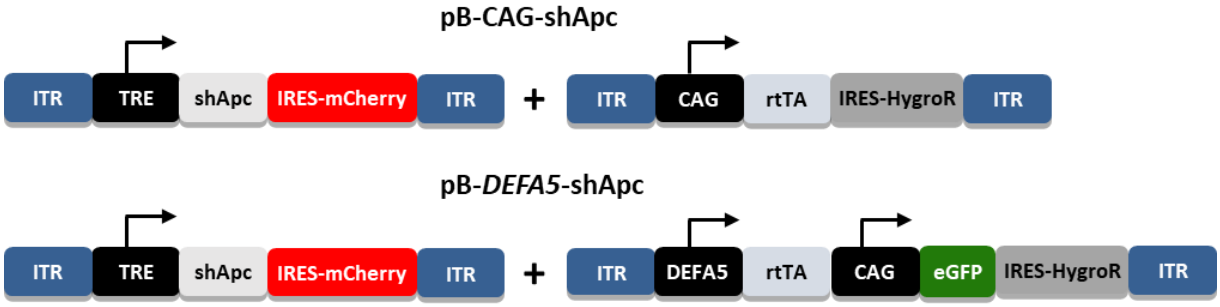

Figure 5. 6: PiggyBac transposon system for inducible Paneth cell specific *Apc* silencing. The system is composed of three constructs (transposase not shown). Doxycyline addition induces shApc expression in all cells (pB-CAG-shApc) or solely in Paneth cells (pB-*DEFA5*-shApc), detectable by mCherry. In addition, pB-*DEFA5*-shApc construct expresses ubiquitously expressed constitutive GFP.

Organoids integrated with pB-CAG-shApc formed spheres upon doxycycline treatment, reminiscent of tumoroids (Figure 5.7). In contrast, Paneth cell specific loss of APC in organoids integrated with pB-DEFA5-shApc did not alter their morphology upon shApc expression. These organoids continued to grow as budding structures upon doxycycline treatment over the course of 30 days and 4 passages.

Intriguingly, while expression of mCherry was detectable after 30 days of dox induction in control pB-DEFA5-mCherry organoids, organoids transfected with pB-DEFA5-shApc lost the expression of mCherry in lysozyme+ cells (Figure 5.8). I conclude that while Paneth cell specific loss of APC does not immediately lead to a tumoroid formation, my results suggest that in the longer term Apc depletion in Paneth cells is detrimental to organoid growth, and is selected against.

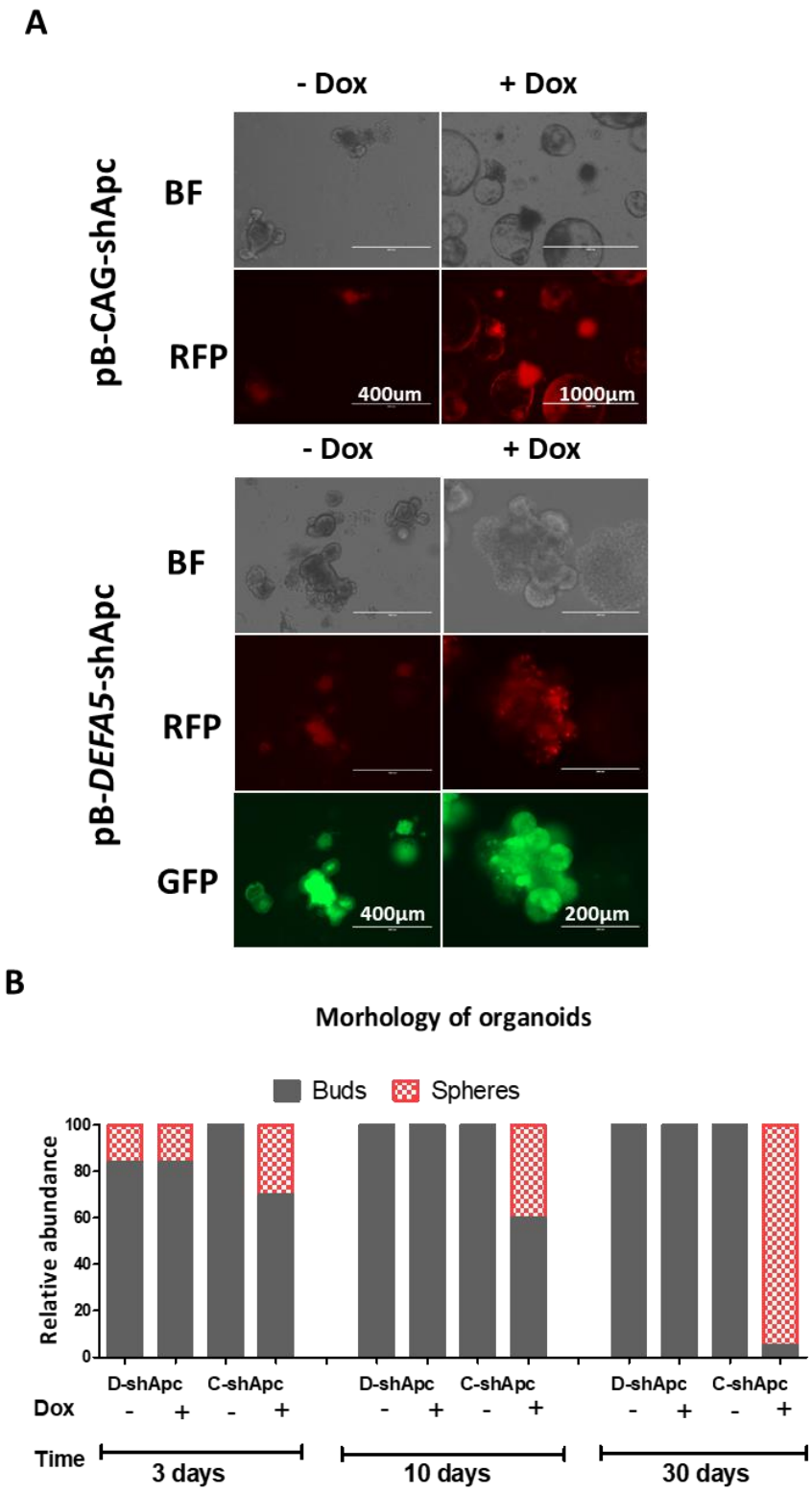

Figure 5. 7. Paneth cells specific silencing of *Apc* does not alter tissue morphology. Representable images of organoids expressing pB-CAG-shApc or pB-*DEFA5*-shApc induced for 10 days with doxycycline (2 µg/ml). Organoids were imaged in brightfield, GFP and RFP (mCherry) channel using the EVOS imaging system (A). Quantification of organoid morphology. Morphology was scored as "spheres" when no buds were apparent; organoid with ≥1 bud was scored as "buds". Graph represents >60 organoids analysed per condition per day (B).

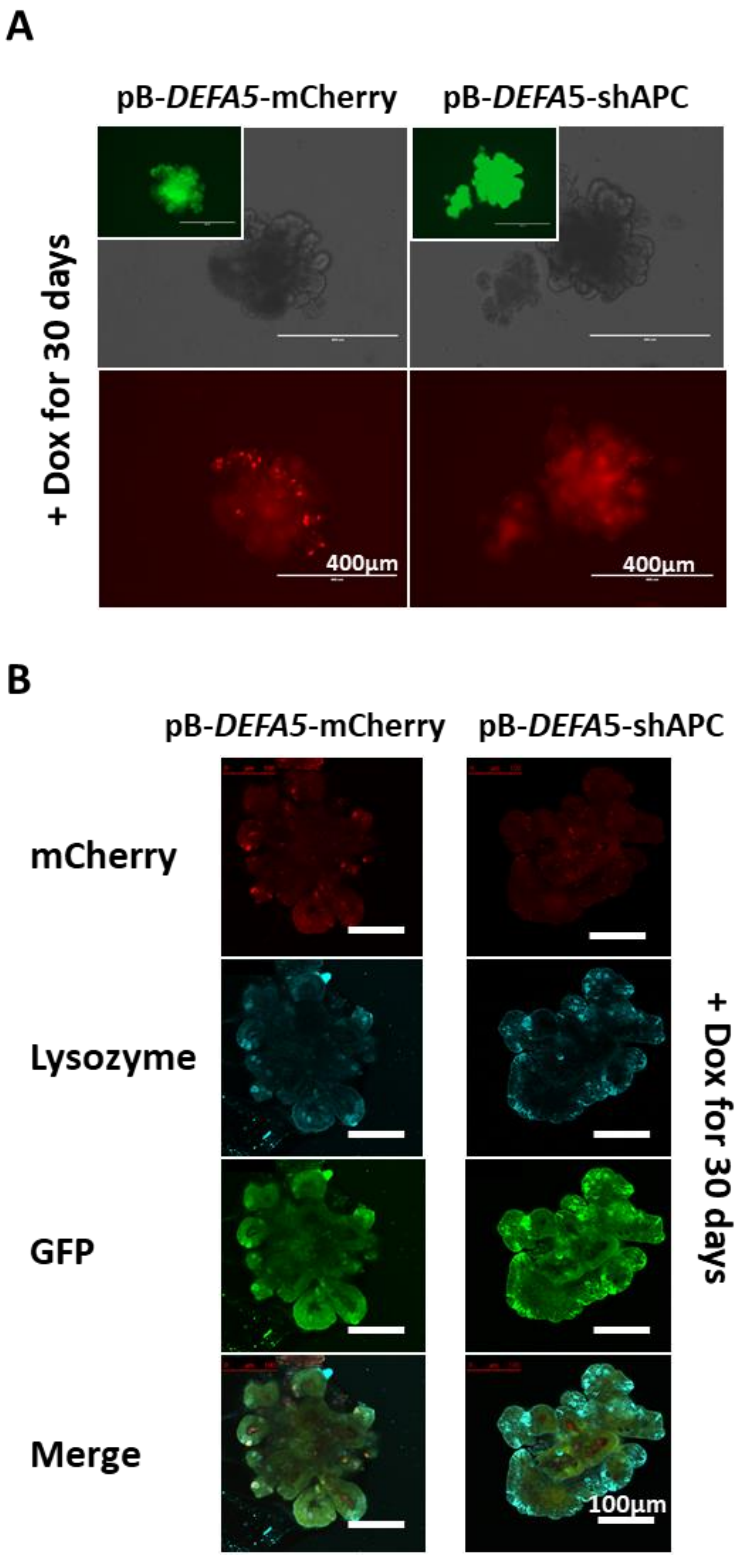

Figure 5. 8: Long-term *Apc* silencing is not tolerated in Paneth cells. Representable images of organoids expressing pB-*DEFA5*-mCherry or pB-*DEFA5*-shApc induced for 30 days with doxycycline (2 µg/ml). Organoids were imaged in brightfield, GFP (inset) and RFP (mCherry) channel using the EVOS imaging system (A). Confocal optical sections from immunofluorescent stains of the organoids expressing pB-*DEFA5*-mCherry or pB-*DEFA5*-shApc induced for 30 days with doxycycline (2 µg/ml). Lysozyme labels Paneth cell vesicles. GFP and mCherry signal is detected from endogenously expressed protein (B).

5.3.3.3 Apc$^{fl/fl}$ -*DEFA5*-rtTA

Because shApc expression in Paneth cells was unstable, I designed a system to delete *Apc* specifically in Paneth cells. I used organoids derived from *Apc$^{fl/fl}$ LSL tdTom* mice that also contain the tdTomato fluorescent marker of Cre recombinase activity (Chapter 4, Figure 4.9). I created a Paneth cells specific expression system for Cre-ERT2 (pB-*DEFA5*-Cre-ER^{T2}) and integrated it into the *Apc$^{fl/fl}$ LSL tdTom* organoids (Figure 5.9). I also integrated a construct for ubiquitous Cre-ER^{T2} expression (Chapter 4, Figure 4.10, pB-Cre-ER^{T2}-GFP- hereafter pB-CAG-Cre-ER^{T2}) into the *Apc$^{fl/fl}$ LSL tdTom* organoids (Figure 5.9).

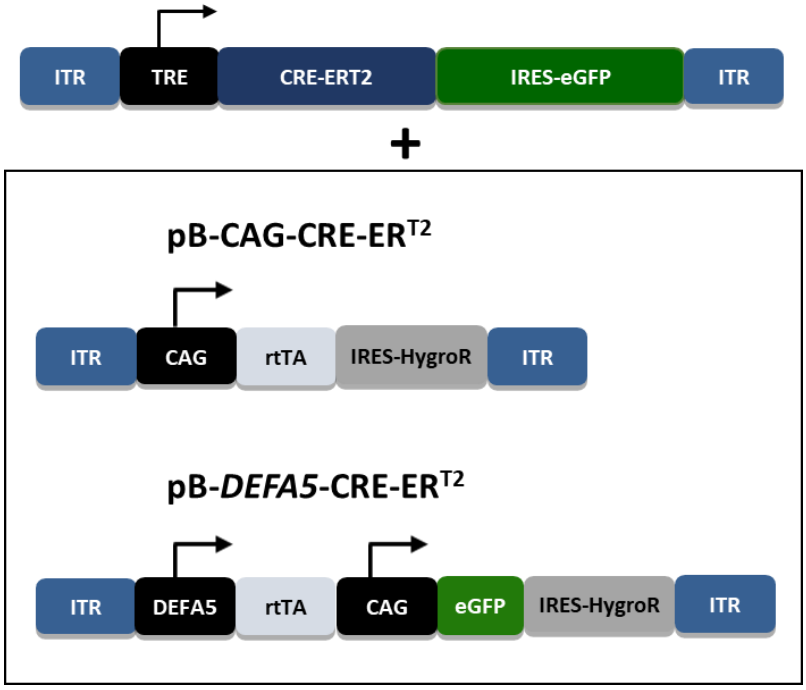

Figure 5. 9: Inducible Paneth cell specific *Apc* depletion. PiggyBac constructs designed where the rtTA is driving Paneth cell specific *Apc* depletion (pB-*DEFA5*-Cre-ER^{T2}), or depletion of *Apc* in all cells (pB-CAG-Cre-ER^{T2}) in *Apc$^{fl/fl}$ LSL tdTom* organoids.

As expected, doxycycline and 4-hydroxytamoxifen (4-OHT) treatment of Apcfl/fl /pB-CAG-Cre-ERT2 organoids led to the formation of spheroids with dispersed lysozyme vesicles, identical to tumoroids, validating the system (Figure 5.10) (Chapter 4, Figure 4.10). The treatment of Apcfl/fl /pB-DEFA5-Cre-ERT2 organoids with doxycycline and 4-OHT showed Paneth cell specific depletion of APC with tdTomato expression overlapping with lysozyme staining. However, after 5 days of treatment there was no change in organoid morphology in

Apcfl/fl /pB-DEFA5-Cre-ERT2 organoids (Figure 5.10). Interestingly, the lysozyme vesicles in tdTomato+ Paneth cells looked similar to wild-type. These results indicate that APC inactivation in Paneth cells does not lead to the formation of a tumoroid. However, I cannot conclude that Paneth cells can tolerate APC loss, owing to the appearance of apically localised vesicles, a hallmark of functional APC (Chapter 3).

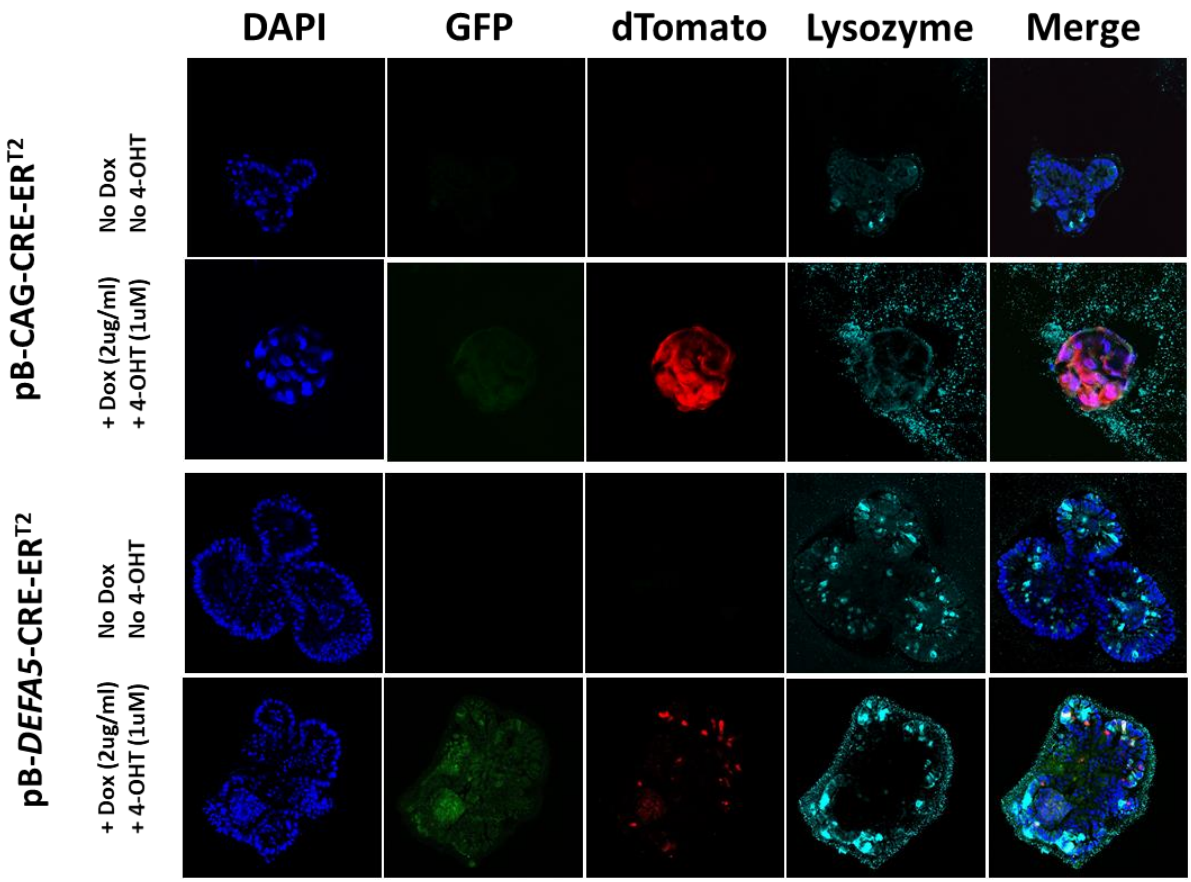

Figure 5. 10: Paneth cell specific depletion of *Apc* does not alter tissue morphology. Representable images of confocal optical sections from immunofluorescent stains of Apc$^{fl/fl}$ /pB-CAG-Cre-ER^{T2} and Apc$^{fl/fl}$ /pB-*DEFA5*-Cre-ER^{T2} organoids treated for 5 days with 2 µg/ml doxycycline and 1 µM 4-OHT. Lysozyme labels Paneth cell vesicles. DAPI labels nuclei. GFP and tdTomato signal is detected from endogenously expressed protein.

5.3.4 Dynamic imaging of Paneth cells to model epithelial organisation

In addition to examining the tumour suppressive role of Paneth cells, the Paneth cell specific expression system I developed enables studying the formation of the crypt in an organoid.

Crypt formation or budding has been shown to initiate in regions with high Paneth cell density and Paneth cells are thought to be structurally important for crypt morphology [17,131,183]. Paneth cell specific expression of GFP allows live tracking of morphological changes such as crypt formation or the conversion of organoids to tumoroids. In addition, Paneth cell tracking can be used to screen for small molecules or inhibitory RNAs that modulate organoid or tumoroid morphologies.

I transduced organoids with the pLV-*DEFA5*-GFP lentiviral construct that led to constitutive GFP expression in Paneth cells. The imaging and analysis of the transduced organoids was carried out in collaboration with AstraZeneca (AZ). In collaboration with Samantha Peel in AZ imaging facility, I used a spinning disk confocal microscope for live-imaging of organoids for 72 hours in a 96-well format and optimised it for detection while minimising light toxicity (Figure 5.11 A). In collaboration with Yinhai Wang from AZ, we were able to demonstrate that a 3-dimensional reconstruction of an organoid at a chosen time point could be used to measure the crypt size and shape by measuring the clustering of GFP^+ Paneth cells (Figure 5.11 A inset). Using the established imaging parameters, we were able to track organoids with three active lasers without fluorescent bleaching nor organoid death (Figure 5.11). In conclusion, the system established a tool for determining the consequence of altering gene expression in, or drug treatment of, organoids and tumoroids using cell shape, organisation and epithelial morphology as quantitative read-outs.

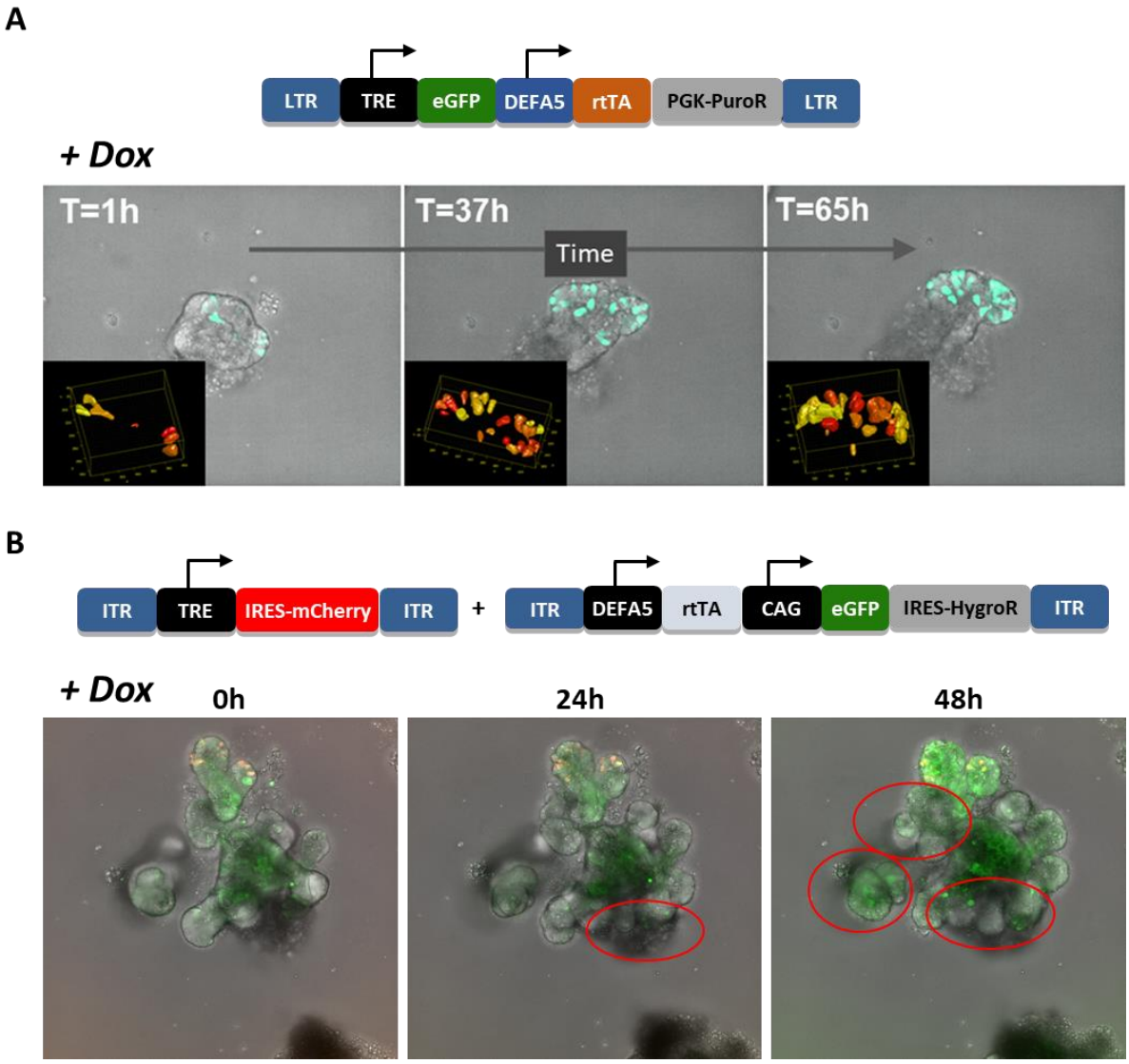

Figure 5. 11: Dynamic imaging of Paneth cells to study epithelial organisation. Snapshots from time-lapse imaging of organoids expressing pLV-*DEFA5*-GFP (A) or pB-*DEFA5*-mCherry-CAG-GFP (B) using a spinning disc confocal microscope. An image was taken every hour for 72 hours with 2 µm Z-stacks through an organoid. Single Paneth cells can be modelled for shape and intensity of fluorescence (A, inset). The formation of new buds in an organoid can be tracked over time (B, red circles).

5.4 Discussion

Mutational inactivation of APC is sufficient to initiate intestinal epithelial tumorigenesis. In Chapter 3, I show that APC loss compromises Paneth cell shape and intracellular organisation. I hypothesised that Paneth cells act as intrinsic organisational centres for the intestinal

epithelia. Based on my results that demonstrated that APC loss alters epithelial morphology, I tested whether Paneth cell specific APC loss was sufficient to initiate intestinal epithelial tumorigenesis. Using the *DEFA5* proximal promoter, I developed a system for Paneth cell specific expression. I show that Paneth cell specific silencing or depletion of *Apc* does not result in tumoroid formation in my experimental systems. This finding suggests that Paneth cells are not capable of tumour initiation upon solely the loss of functional APC. In addition, I show that *DEFA5* promoter can be used as a marker for crypt formation. Since the structure of a crypt is lost when APC is inactivated, dynamic imaging of *DEFA5*-GFP^{+} organoids can be used in the future for targeted drug screens and genetic studies using organoid morphology as a phenotypic read-out.

5.4.1 *DEFA5* as a Paneth cell specific marker

I validate a sequence of the *DEFA5* gene [182] as a promoter specific to mouse Paneth cells *in vitro*. Previous studies have used different mouse knock-in lines to track or manipulate Paneth cells *in vivo* [7,184]. Mouse *Lyz1* locus that encodes a Paneth cell specific lysozyme was used to create a targeted allele replacing the coding region for *Lyz1* with the coding region for Cre recombinase fused to estrogen receptor (ER) to generate the *Lyz1*$^{CreER/+}$; Rosa26-EYFP (enhanced yellow fluorescent protein) mouse [184]. Tamoxifen administration labelled Paneth cells with EYFP and it was shown that 100 % of EYFP^{+} cells were positive for endogenous lysozyme, suggesting the allele was Paneth cell specific. However, the authors reported that Cre activation led to recombination in only 9 % of Paneth cells, as detected by fluorescence, showing control of only a small proportion of Paneth cells. In addition, a mouse Paneth cell specific cryptidin-4 locus, α-Defensin 4 (*Defa4*), was used to create a *Defa4*^{Cre}; Rosa26-tdTom (tandem dimer Tomato) mouse where Paneth cells were labelled with tdTom [7]. The authors showed that tdTom expression co-localised with lysozyme, validating Paneth cell specificity. While the knock-in mouse lines using *Lyz1* and *Defa4* loci for Paneth cell specificity are useful for *in vivo* studies and manipulation, the *DEFA5* promoter sequence I have validated allows for unprecedented Paneth cell specific manipulation of transgene and gene expression *in vitro*.

5.4.2 Paneth cells in the initiation of intestinal tumorigenesis

Transformed intestinal stem cells have long been thought to be the origin of colorectal cancer [28]. However, as more studies are showing plasticity within the intestinal epithelial cells, the paradigm has started to shift towards potentially other sources of tumour initiating cells for origin of initiation of tumorigenesis [29,185]. Paneth cells have long been considered as terminally differentiated [15]; however, recent reports indicate that upon insult like an injury or inflammation, precursors to cells of the secretory lineage and mature Paneth cells can acquire stem-like features [5,7,9,184]. While studies have looked at the potential of adenoma formation upon APC loss in differentiated villus cells and transit amplifying cells [29], no studies had investigated the role of Paneth cells as tumour initiating cells at the beginning of my study. The finding that Paneth cells are not able to initiate tumorigenesis upon solely the loss of APC was recently confirmed by a study using the *Defa4*^{Cre} mouse (see above) for Paneth cell specific inactivation of APC [7]. Using a mouse model of Paneth cell specific biallelic APC inactivation, *Defa4*^{Cre}; *Apc*$^{fl/fl}$, the authors showed that the mice were healthy with no apparent adenomas, and survived beyond 5 months. Intriguingly, the study demonstrated that global activation of Notch signalling in these mice was sufficient for the formation of severely dysplastic crypts and adenomas, concluding that Notch activation had transformed *Defa4*$^{+}$ cells into stem/progenitor-like cells capable of forming an adenoma. The findings from my study and others therefore suggest that solely loss of APC in a Paneth cell is not enough to initiate tumorigenesis, however simultaneous activation of Notch pathway and subsequent de-differentiation of Paneth cells results in adenoma formation. Interestingly, it has been shown that radiation increases Notch pathway activity [184], suggesting that during radiation, when fast-cycling Lgr5^{+} stem cells are eliminated [186], APC deficient Paneth cells contribute to adenoma formation.

While the loss of APC in Paneth cells does not initiate tumorigenesis, my results show that there is a selective advantage of maintaining APC expression in Paneth cells. Organoids expressing shApc exclusively in Paneth cells detectable by mCherry expression show a loss of mCherry expression within 30 days in culture. This finding is not the result of loss of stably expressing organoid clones, as constitutively expressed GFP in these organoids was still evident. In addition, organoids expressing a control construct lacking shApc maintained mCherry expression after 30 days in culture. Therefore, there appears to be a selective

disadvantage of activating the Wnt pathway with APC loss in Paneth cells. This is not without precedent, as a recent study has found that Paneth cell specific constitutive expression of β-catenin leads to loss of fluorescence that marks the Paneth cells [184]. The authors used the *Lyz1* locus for Paneth cell specificity and created a knock-in mouse line where β-catenin becomes constitutively active upon tamoxifen addition solely in Paneth cells detectable by tdTom (*Lyz1*$^{CreER/+}$; Rosa26-tdTom; β-catenin $^{ex3fl/fl}$). It was shown that while there was no detectable epithelial hyperplasia or adenoma, 3 months after tamoxifen administration there were no remaining tdTom^{+} Paneth cells in the mouse intestine. Together, the data indicates that Paneth cells cannot tolerate high levels of Wnt pathway activity and more moderate levels are critical for the normal functioning of Paneth cells. Future studies, titrating levels of *Apc* depletion by shApc will determine why high levels of Wnt pathway activity specifically ablate Paneth cells.

5.4.3 Use of *DEFA5* promoter to track organoid budding as a phenotypic read-out

It is believed that Paneth cells are responsible for establishing a crypt. Organoid budding (crypt formation) has been modelled computationally and demonstrates that crypts form in areas rich in Paneth cells [131,183]. Paneth cells are thought to be more stiff compared to neighbouring stem cells and therefore are suggested to be responsible for determining the site of the crypt formation [17]. A recent study found that transient cell-to-cell variable intrinsic YAP1 expression and subsequent Notch signalling drives the localised formation of a Paneth cell leading to crypt formation [187]. The crypt structure is lost in APC inactivation as seen in tumoroids lacking crypt-like structures (buds) and in adenoma tissue. Therefore, variables around crypt formation (eg the time of formation; number, width and length of the crypt) can be used as a phenotypic read-out to test compounds that target intestinal tumorigenesis. I have developed assay parameters to track budding of organoids with fluorescently labelled Paneth cells to mark the crypt. The system builds on a previous study that used time-lapse imaging of organoids treated with various pharmacological inhibitors [188]. In this study, resolution was limited to perturbation in the epithelial monolayer and individual cells or crypt structure were not reliably identifiable. The established assay can be useful in the future to interrogate a focussed library of compounds that target cytoskeletal components for their ability to attenuate the intraconversion of organoids to tumoroids.

5.4.4 Implications of findings

In this study, I found that, while APC loss in the intestinal epithelia leads to tumoroids replete with APC-deficient Paneth cells, specific APC loss exclusive to Paneth cells is not tolerated. These two results are at odds with each other, and indicate added layers of complexity in the regulation of the intestinal epithelial stem cell niche—likely involving additional signalling pathways and cell-cell crosstalk. It will be important to establish novel ways in which to examine this phenomenon in detail, in order to fully understand intestinal epithelial homeostasis.

Chapter 6:

Conclusion and Future Perspectives

6.1 Conclusion

APC is an important signalling node controlling homeostasis in the intestinal epithelium. The various interaction domains within APC mediate the diverse biological roles of this protein. In my study, I utilised tissue samples and organoids from different mouse models and developed various genetically modified organoid systems to study the consequence of the loss of APC's C-terminal domains in intestinal tumorigenesis. I show that, via its binding domain to Wnt effectors, APC regulates epithelial tissue morphology. Intriguingly, I demonstrate that the Wnt target gene *Myc* is not the main mediator of this effector role of APC. Further, I reveal a novel role of APC in regulating intracellular organisation in the intestinal epithelia. I show that inhibition of microtubule polymerisation phenocopies the compromised intracellular organisation with APC deficiency, indicating a link between defective microtubule cytoskeleton and loss of APC. Future studies into sufficiency of the microtubule binding domain of APC in intracellular organisation will elucidate domain-specific roles of APC further. Finally, I demonstrate that the loss of APC in a stem cell supporting cell, identifiable by a distinct cellular morphology—the Paneth cell—does not compromise tissue morphology, a key characteristic of intestinal epithelial tumorigenesis.

6.2 Future perspectives

While the results of my study have expanded on the previous knowledge about the role of APC in the intestinal epithelial homeostasis, they have also created new questions:

6.2.1 Why is APC loss not tolerated in Paneth cells?

Using organoid to tumoroid intraconversion as a metric, I show that solely the loss of APC exclusively in Paneth cells does not initiate tumorigenesis. However, I demonstrate that over a course of 30 days Paneth cells lose the expression of shApc. Future experiments tracking $Apc^{fl/fl}$ /pB-*DEFA5*-Cre-ER^{T2} organoids over a longer time-point than 5 days currently studied will further validate whether there is a selective disadvantage for Paneth cells lacking APC. Uncovering the specific role(s) of APC in Paneth cells will be a critical first step. Given the findings in Chapter 3 and 4 showing that APC regulates intracellular organisation, it will be important to study the organisation of microtubules and localisation of organelles at early time-points in APC deficient Paneth cells.

6.2.2 What are the relative contributions of the interaction domains of APC to its effector roles in intestinal tumorigenesis?

Most tumorigenic *Apc* mutations simultaneously abrogate the interaction of APC with Wnt effectors and the microtubule binding domain, making it difficult to separate these roles experimentally. I show that mutational inactivation or depletion of *Apc* in the intestine leads to altered tissue morphology and compromised intracellular organisation. My findings from the sufficiency experiments indicate that the interaction domains of APC with Wnt effectors regulate tissue morphology and this is uncoupled from the regulation of intracellular organisation. The failure to express full-length APC in tumoroids makes it difficult to reliably interpret data from the expression of the APC mutant constructs. Moreover, tumoroids may have been derived from cells that have incurred additional mutations that impact epithelial tissue morphology and intracellular organisation. I have therefore opted to make use of conditional *Apc* inactivation using *Apc* flox (*Apc*$^{fl/fl}$ *LSL tdTom*) organoids. The major limitation to this system is that the levels of expressed APC proteins may vary, and this may affect the phenotypic outcome. This limitation may be overcome using a CRISPR /Cas9 technology to precisely modify the *Apc* gene for the expression of the mutant constructs.

6.2.3 What is the role of compromised microtubule cytoskeleton in tumorigenesis?

The results of my study reveal a novel role of APC in the intestine in regulating the positioning of organelles such as the Golgi complex, centrosome and Paneth cell vesicles. Organelle positioning is specifically regulated by microtubules and nocodazole treatment to inhibit microtubule polymerisation results in altered positioning of the Golgi complex. It is therefore tempting to speculate that compromised intracellular organisation is a surrogate for misregulated microtubule cytoskeleton.

My studies do not establish whether the compromised microtubule cytoskeleton is a bystander consequence of APC mutations or whether it contributes to tumorigenesis. Changes in microtubule stability and organisation affect cellular adhesion and migration and could thus promote epithelial-to-mesenchymal transition (EMT) present in many tumours and crucial for metastasis [189]. Microtubules form the mitotic spindle and defects in microtubule regulation may impair chromosome segregation leading to chromosomal instability (CIN). While the role of APC loss in CIN and whether CIN is a cause or consequence of colon cancer remains

controversial [112,190], any alterations in microtubules would predictably lead to defects in the mitotic spindle affecting the normal functioning of the cell. Microtubules are involved in protein trafficking and defects in their stability and organisation could alter the trafficking of proteins involved in pro-survival and pro-apoptotic pathways in a cell. Intriguingly, a study has demonstrated the presence of a primary cilia in colon [191]. Cilia are microtubule-based organelles involved in cell-cell communication, signalling and cell division and loss of cilia has been described in colon tumorigenesis [191,192]. Therefore, given the multitude of roles for microtubules in homeostasis, functional defects in them could provide a cell an ability to survive and proliferate uncontrollably, and potentially invade into other tissues.

In addition, it would be intriguing to examine tumours in other tissues to determine whether altered microtubule cytoskeleton could be a general hallmark of epithelial tumorigenesis. Loss of apical-basal (AB) polarity in early stages of tumour progression in breast tissue has been reported [193]. Given that microtubules play a key role in establishing AB polarity [97], it would be intriguing to examine the status of intracellular organisation in breast tumours. There are several tumour suppressor genes including *RASFF1A* (Ras association domain family 1 isoform A) and *VHL* (Von-Hippel-Lindau) that are associated with the development of various tumour types and have been reported to interact with microtubules [194]. Studying the intracellular organisation of these tumours would further elucidate whether microtubule changes are a general characteristic of epithelial tumours.

6.3 Concluding remarks

The results of my study reveal a novel role for APC in the intestinal epithelia in the maintenance of the microtubule cytoskeleton, intracellular organisation and epithelial tissue morphology. Future experiments will reveal the domain(s) required for APC's regulation of intracellular organisation and demonstrate to what extent the loss of its microtubule-binding domain contributes to the compromised intracellular organisation in intestinal tumorigenesis. Ultimately, it will be useful to determine whether molecular control over these APC functions can be exploited therapeutically or diagnostically to target intestinal epithelial cancers.

References

1. Gehart, H. & Clevers, H. Tales from the crypt: new insights into intestinal stem cells. *Nat. Rev. Gastroenterol. Hepatol.* 16, 19–34 (2019).
2. Näthke, I. S. THE ADENOMATOUS POLYPOSIS COLI PROTEIN: The Achilles Heel of the Gut Epithelium. *Annu. Rev. Cell Dev. Biol.* 20, 337–366 (2004).
3. Barker, N. *et al.* Identification of stem cells in small intestine and colon by marker gene Lgr5. *Nature* 449, 1003–1007 (2007).
4. Potten, C. S., Owen, G. & Booth, D. Intestinal stem cells protect their genome by selective segregation of template DNA strands. *J. Cell Sci.* 115, 2381–2388 (2002).
5. Buczacki, S. J. a *et al.* Intestinal label-retaining cells are secretory precursors expressing Lgr5. *Nature* 495, 65–69 (2013).
6. Snippert, H. J. *et al.* Intestinal crypt homeostasis results from neutral competition between symmetrically dividing Lgr5 stem cells. *Cell* 143, 134–144 (2010).
7. Jones, J. C. *et al.* Cellular Plasticity of Defa4 Cre -Expressing Paneth Cells in Response to Notch Activation and Intestinal Injury. *Cmgh* 7, 533–554 (2019).
8. Westphalen, C. B. *et al.* Long-lived intestinal tuft cells serve as colon cancer – initiating cells. *J. Clin. Invest.* 124, 1283–1295 (2014).
9. Schmitt, M. *et al.* Paneth Cells Respond to Inflammation and Contribute to Tissue Regeneration by Acquiring Stem-like Features through SCF/c-Kit Signaling. *Cell Rep.* 24, 2312-2328.e7 (2018).
10. Parker, A. *et al.* Cell proliferation within small intestinal crypts is the principal driving force for cell migration on villi. *FASEB J.* 31, 636–649 (2017).
11. Krndija, D. *et al.* Active cell migration is critical for steady-state epithelial turnover in the gut. *Science (80-.).* 365, 705–710 (2019).
12. Barker, N., Van Oudenaarden, A. & Clevers, H. Identifying the stem cell of the intestinal crypt: Strategies and pitfalls. *Cell Stem Cell* 11, 452–460 (2012).
13. Clevers, H. C. & Bevins, C. L. Paneth cells: maestros of the small intestinal crypts. *Annu Rev Physiol* 75, 289–311 (2013).
14. Bevins, C. L. & Salzman, N. H. Paneth cells, antimicrobial peptides and maintenance of intestinal homeostasis. *Nat. Rev. Microbiol.* 9, 356–368 (2011).
15. Sato, T. *et al.* Paneth cells constitute the niche for Lgr5 stem cells in intestinal crypts.

Nature 469, 415–8 (2011).

16. Pentinmikko, N. *et al.* Notum produced by Paneth cells attenuates regeneration of aged intestinal epithelium. *Nature* 571, (2019).
17. Langlands, A. J. *et al.* Paneth Cell-Rich Regions Separated by a Cluster of Lgr5+ Cells Initiate Crypt Fission in the Intestinal Stem Cell Niche. *PLoS Biol.* 14, 1–31 (2016).
18. Sasaki, N. *et al.* Reg4 + deep crypt secretory cells function as epithelial niche for Lgr5 + stem cells in colon . *Proc. Natl. Acad. Sci.* 113, E5399–E5407 (2016).
19. Kim, T.-H., Escudero, S. & Shivdasani, R. A. Intact function of Lgr5 receptor-expressing intestinal stem cells in the absence of Paneth cells. *Proc. Natl. Acad. Sci. U. S. A.* 109, 3932–7 (2012).
20. Durand, A. *et al.* Functional intestinal stem cells after Paneth cell ablation induced by the loss of transcription factor Math1 (Atoh1). *Proc. Natl. Acad. Sci. U. S. A.* 109, 8965–70 (2012).
21. Dow, L. E. *et al.* Apc Restoration Promotes Cellular Differentiation and Reestablishes Crypt Homeostasis in Colorectal Cancer. *Cell* 161, 1539–1552 (2015).
22. Volgestein, B. & Fearon, E. A Genetic Model for Colorectal tumorogenesis. *Cell* 61, 759–767 (1990).
23. Groden, J. *et al.* Identification and Characterization of the Familial Adenomatous Polyposis Coli Gene. *Cell* 66, 589–600 (1991).
24. Polakis, P. The adenomatous polyposis coli (apc) tumor suppressor. *Biochim. Biophys. Acta* 12, (1997).
25. Fodde, R., Smits, R. & Clevers, H. APC, Signal transduction and genetic instability in colorectal cancer. *Nat Rev Cancer* 1, 55–67 (2001).
26. Preston, S. L. *et al.* Bottom-up histogenesis of colorectal adenomas: Origin in the monocryptal adenoma and initial expansion by crypt fission. *Cancer Res.* 63, 3819–3825 (2003).
27. Shih, I. *et al.* Top-down morphogenesis of colorectal tumors. *PNAS* 98, 2640–2645 (2001).
28. Barker, N. *et al.* Crypt stem cells as the cells-of-origin of intestinal cancer. *Nature* 457, 608–611 (2009).
29. Huels, D. J. & Sansom, O. J. Stem vs non-stem cell origin of colorectal cancer. *Br. J. Cancer* 113, 1–5 (2015).

30. Zeineldin, M. & Neufeld, K. L. Understanding phenotypic variation in rodent models with germline apc mutations. *Cancer Res.* 73, 2389–2399 (2013).
31. Jackstadt, R. & Sansom, O. J. Mouse models of intestinal cancer. *J. Pathol.* 238, 141–151 (2016).
32. Su, L. K. *et al.* Multiple intestinal neoplasia caused by a mutation in the murine homolog of the APC gene. *Science (80-.).* 256, 668–670 (1992).
33. Moser, A., Dove, W. R., Kevin A. Roth & Jeffrey I. Gordon. The Min (multiple intestinal neoplasia) mutation: Its effect on gut epithelial cell differentiation and interaction with a modifier system. *J. Cell Biol.* 116, 1517–1526 (1992).
34. Moser, A. R., Pitot, H. C. & Dove, W. F. A dominant mutation that predisposes to multiple intestinal neoplasia in the mouse. *Science (80-.).* 247, 322–324 (1990).
35. Moser, A. R. *et al.* ApcMin: A mouse model for intestinal and mammary tumorigenesis. *Eur. J. Cancer* 31, 1061–1064 (1995).
36. Kinzler, K. W. *et al.* Identification of FAP locus genes from chromosome 5q21. a-helical coiled coil homology. *Science (80-.).* 253, 661–664 (1991).
37. De La Roche, M., Ibrahim, A. E. K., Mieszczanek, J. & Bienz, M. LEF1 and B9L shield b-catenin from inactivation by axin, desensitizing colorectal cancer cells to tankyrase inhibitors. *Cancer Res.* 74, 1495–1505 (2014).
38. Shoemaker, A. R., Gould, K. A., Dove, W. F. & Bilger, A. Manipulation of the mouse germline in the study of Min-induced neoplasia. *Semin. Cancer Biol.* 7, 249–260 (1996).
39. Nagy, A. Cre Recombinase : The Universal Reagent for Genome Tailoring. 109, 99–109 (2000).
40. Shibata, H. *et al.* Rapid Colorectal Adenoma Formation Initiated by Conditional Targeting of the Apc Gene Rapid Colorectal Adenoma Formation Initiated by Conditional Targeting of the Apc Gene. *Science (80-.).* 278, 120–123 (1997).
41. Sansom, O. J. *et al.* Loss of Apc in vivo immediately perturbs Wnt signaling, differentiation, and migration. *Genes Dev.* 18, 1385–1390 (2004).
42. Sato, T. *et al.* Single Lgr5 stem cells build crypt-villus structures in vitro without a mesenchymal niche. *Nature* 459, 262–5 (2009).
43. Sato, T. *et al.* Long-term expansion of epithelial organoids from human colon, adenoma, adenocarcinoma, and Barrett's epithelium. *Gastroenterology* 141, 1762–

1772 (2011).

44. Martin-Belmonte, F. & Perez-Moreno, M. Epithelial cell polarity, stem cells and cancer. *Nat. Rev. Cancer* 12, 23–38 (2012).
45. Royer, C. & Lu, X. Epithelial cell polarity: a major gatekeeper against cancer? *Cell Death Differ.* 18, 1470–1477 (2011).
46. Li, R. & Gundersen, G. G. Beyond polymer polarity: How the cytoskeleton builds a polarized cell. *Nat. Rev. Mol. Cell Biol.* 9, 860–873 (2008).
47. Coradini, D., Casarsa, C. & Oriana, S. Epithelial cell polarity and tumorigenesis: new perspectives for cancer detection and treatment. *Acta Pharmacol Sin* 32, 552–564 (2011).
48. Fletcher, D. a & Mullins, R. D. Cell mechanisms and cytoskeleton. *Nature* 463, 485–492 (2010).
49. Alberts, B. *et al. The Molecular Biology of the Cell*. (Garland Science, Taylor and Francis Group, LLC, 2008).
50. Mitchison, T., Kirschner, M. & Mitchison T, K. M. Dynamic instability of microtubule growth. *Nature* 312, 237–42 (1984).
51. Sanchez, A. D. & Feldman, J. L. Microtubule-organizing centers: from the centrosome to non- centrosomal sites Ariana. *Curr. Opin. Cell Biol.* 44, 93–101 (2017).
52. Bellett, G. *et al.* Microtubule plus-end and minus-end capture at adherens junctions is involved in the assembly of apico-basal arrays in polarised epithelial cells. *Cell Motil. Cytoskeleton* 66, 893–908 (2009).
53. Mogensen, M. M., Tucker, J. B., Mackie, J. B., Prescott, A. R. & Näthke, I. S. The adenomatous polyposis coli protein unambiguously localizes to microtubule plus ends and is involved in establishing parallel arrays of microtubule bundles in highly polarized epithelial cells. *J. Cell Biol.* 157, 1041–1048 (2002).
54. Goldspink, D. a *et al.* The microtubule end-binding protein EB2 is a central regulator of microtubule reorganisation in apico-basal epithelial differentiation. *J. Cell Sci.* 126, 4000–14 (2013).
55. Gavilan, M. P. *et al.* The dual role of the centrosome in organizing the microtubule network in interphase. *EMBO Rep.* 19, 1–21 (2018).
56. Noordstra, I. *et al.* Control of apico-basal epithelial polarity by the microtubule minus-end-binding protein CAMSAP3 and spectraplakin ACF7. *J. Cell Sci.* 129, 4278–4288

(2016).

57. Toya, M. *et al.* CAMSAP3 orients the apical-to-basal polarity of microtubule arrays in epithelial cells. *Proc. Natl. Acad. Sci. U. S. A.* 113, 332–337 (2016).
58. Mimori-Kiyosue, Y., Shiina, N. & Tsukita, S. Adenomatous polyposis coli (APC) protein moves along microtubules and concentrates at their growing ends in epithelial cells. *J. Cell Biol.* 148, 505–517 (2000).
59. Morrison, E. E., Wardleworth, B. N., Askham, J. M., Markham, A. F. & Meredith, D. M. EB1, a protein which interacts with the APC tumour suppressor, is associated with the microtubule cytoskeleton throughout the cell cycle. *Oncogene* 17, 3471–3477 (1998).
60. Su, L. *et al.* APC Binds to the Novel Protein EB11. *Cancer Res.* 55, 2972–2977 (1995).
61. Berrueta, L. *et al.* The adenomatous polyposis coli-binding protein EB1 is associated with cytoplasmic and spindle microtubules. *Proc. Natl. Acad. Sci. U. S. A.* 95, 10596–10601 (1998).
62. Cole, N. B. & Lippincott-Schwartz, J. Organization of organelles and membrane traffic by microtubules. *Curr. Opin. Cell Biol.* 7, 55–64 (1995).
63. Thyberg, J. & Moskalewski, S. Role of microtubules in the organization of the golgi complex. 246, 263–279 (1999).
64. Liang, W. H. *et al.* Microtubule Defects Influence Kinesin-Based Transport in Vitro. *Biophys. J.* 110, 2229–2240 (2016).
65. Janke, C. The tubulin code: Molecular components, readout mechanisms, functions. *J. Cell Biol.* 206, 461–472 (2014).
66. Westermann, S. & Weber, K. Post-translational modifications regulate microtubule function. *Nat. Rev. Mol. Cell Biol.* 4, 938–947 (2003).
67. Akhmanova, A. & Steinmetz, M. O. Microtubule +TIPs at a glance. *J. Cell Sci.* 123, 3415–3419 (2010).
68. Akhmanova, A. & Hoogenraad, C. C. Microtubule minus-end-targeting proteins. *Curr. Biol.* 25, R162–R171 (2015).
69. Chang, P. & Walker, J. M. *The Mitotic Spindle: Methods and Protocols. Methods in Molecular Biology*. (2016). doi:10.1016/B978-0-12-394447-4.20062-X
70. Dumontet, C. & Jordan, M. A. Microtubule-binding agents: A dynamic field of cancer therapeutics. *Nat. Rev. Drug Discov.* 9, 790–803 (2010).
71. Kawasaki, Y. *et al.* Asef, a Link Between the Tumor Suppressor APC and G-Protein

Signaling. *Science (80-.).* 289, 1194–1197 (2000).

72. Watanabe, T. *et al.* Interaction with IQGAP1 links APC to Rac1, Cdc42, and actin filaments during cell polarization and migration. *Dev. Cell* 7, 871–883 (2004).
73. Jimbo, T. *et al.* Identification of a link between the tumour suppressor APC and the kinesin superfamily. *Nat. Cell Biol.* 4, 323–327 (2002).
74. Rubinfeld, B. *et al.* Association of the APC gene product with beta-catenin. *Science (80-.).* 262, 1731–1734 (1993).
75. Kohler, E. M., Chandra, S. H. V., Behrens, J. & Schneikert, J. β-Catenin degradation mediated by the CID domain of APC provides a model for the selection of APC mutations in colorectal, desmoid and duodenal tumours. *Hum. Mol. Genet.* 18, 213–226 (2009).
76. Fagotto, F. *et al.* Domains of Axin involved in protein-protein interactions, Wnt pathway inhibition, and intracellular localization. *J. Cell Biol.* 145, 741–756 (1999).
77. Munemitsu, S. *et al.* The APC Gene Product Associates with Microtubules in Vivo and Promotes Their Assembly in Vitro. *Cancer Res.* 3676–3681 (1994).
78. Matsumine, A. *et al.* Binding of APC to the human homolog of the Drosophila discs large tumor suppressor protein. *Science (80-.).* 272, 1020–1023 (1996).
79. Rosin-Arbesfeld, R., Cliffe, A., Brabletz, T. & Bienz, M. Nuclear export of the APC tumour suppressor controls β-catenin function in transcription. *EMBO J.* 22, 1101–1113 (2003).
80. Rosin-Arbesfeld, R., Ihrke, G. & Bienz, M. Actin-dependent membrane association of the APC tumour suppressor in polarized mammalian epithelial cells. *EMBO J.* 20, 5929–5939 (2001).
81. Rosin-Arbesfeld, R., Townsley, F. & Bienz, M. The APC tumour suppressor has a nuclear export function. *Nature* 406, 1009–1012 (2000).
82. Neufeld, K. L. *et al.* Adenomatous polyposis coli protein contains two nuclear export signals and shuttles between the nucleus and cytoplasm. *Proc. Natl. Acad. Sci.* 97, 12085–12090 (2000).
83. Nelson, S. & Näthke, I. S. Interactions and functions of the adenomatous polyposis coli (APC) protein at a glance. *J. Cell Sci.* 126, 873–7 (2013).
84. Li, Z. & Näthke, I. S. Tumor-associated NH2-terminal fragments are the most stable part of the adenomatous polyposis coli protein and can be regulated by interactions

with COOH-terminal domains. *Cancer Res.* 65, 5195–5204 (2005).

85. Li, Z., Kroboth, K., Newton, I. P. & Nathke, I. S. Novel self-association of the APC molecule affects APC clusters and cell migration. *J. Cell Sci.* 121, 1916–1925 (2008).
86. Krausova, M. & Korinek, V. Wnt signaling in adult intestinal stem cells and cancer. *Cell. Signal.* 26, 570–579 (2014).
87. Gao, C., Xiao, G. & Hu, J. Regulation of Wnt/β-catenin signaling by posttranslational modifications. *Cell Biosci.* 4, 13 (2014).
88. Sansom, O. J. *et al.* Loss of Apc in vivo immediately perturbs Wnt signaling, differentiation, and migration. *Genes Dev.* 18, 1385–1390 (2004).
89. Clevers, H. Wnt/Beta Catenin Signaling in Development and Disease. *Cell* 127, 469–480 (2006).
90. Fodde, R. The APC gene in colorectal cancer. *Eur. J. Cancer* 38, 867–871 (2002).
91. Bienz, M. The subcellular destinations of APC proteins. *Nat. Rev. Mol. Cell Biol.* 3, 328–338 (2002).
92. Hart, M. J., de los Santos, R., Albert, I. N., Rubinfeld, B. & Polakis, P. Downregulation of β-catenin by human Axin and its association with the APC tumor suppressor, β-catenin and GSK3β. *Curr. Biol.* 8, 573–581 (2004).
93. Salic, A., Lee, E., Mayer, L. & Kirschner, M. W. Control of β-catenin stability: Reconstitution of the cytoplasmic steps of the Wnt pathway in Xenopus egg extracts. *Mol. Cell* 5, 523–532 (2000).
94. Bienz, M. APC: The plot thickens. *Curr. Opin. Genet. Dev.* 9, 595–603 (1999).
95. Bienz, M. & Clevers, H. Linking Colorectal Cancer to Wnt Signaling. *Cell* 103, 311–320 (2000).
96. Sansom, O. J. *et al.* Myc deletion rescues Apc deficiency in the small intestine. *Nature* 446, 676–679 (2007).
97. Rodriguez-Boulan, E. & Macara, I. G. Organization and execution of the epithelial polarity programme. *Nat. Rev. Mol. Cell Biol.* 15, 225–242 (2014).
98. Takaishi K, Sasaki T, Kotani H, Nishioka H & Takai Y. Regulation of cell-cell adhesion by rac and rho small G proteins in MDCK cells. *J. Cell Biol.* 139, 1047–1059 (1997).
99. Kim, S. B. *et al.* Truncated Adenomatous Polyposis Coli Mutation Induces Asef-Activated Golgi Fragmentation. *Mol. Cell. Biol.* 38, 1–17 (2018).
100. Tirnauer, J. S. A new cytoskeletal connection for APC: Linked to actin through IQGAP.

Dev. Cell 7, 778–780 (2004).

101. Zumbrunn, J., Kinoshita, K., Hyman†, A. A. & Nathke, I. S. Binding of the adenomatous polyposis coli protein to microtubules increases microtubule stability and is regulated by GSK3 phosphorylation. *Curr. Biol.* 11, 44–49 (2001).
102. Barth, A. I. M., Siemers, K. a & Nelson, W. J. Dissecting interactions between EB1, microtubules and APC in cortical clusters at the plasma membrane. *J. Cell Sci.* 115, 1583–1590 (2002).
103. Weiner, A. T., Lanz, M. C., Goetschius, D. J., Hancock, W. O. & Rolls, M. . Kinesin-2 and Apc function at dendrite branch points to resolve microtubule collisions. *Cytoskeleton* 73, 35–44 (2016).
104. Mattie, F. J. *et al.* Directed microtubule growth, +TIPs and kinesin-2 are required for uniform microtubule polarity in dendrites. *Curr. Biol.* 24, 2169–2177 (2010).
105. Lui, C., Ashton, C., Sharma, M., Brocardo, M. G. & Henderson, B. R. APC functions at the centrosome to stimulate microtubule growth. *Int. J. Biochem. Cell Biol.* 70, 39–47 (2016).
106. Näthke, I. S., Adams, C. L., Polakis, P., Sellin, J. H. & Nelson, W. J. The adenomatous polyposis coli tumor suppressor protein localizes to plasma membrane sites involved in active cell migration. *J. Cell Biol.* 134, 165–179 (1996).
107. Karin Kroboth *et al.* Lack of Adenomatous Polyposis Coli Protein Correlates with a Decrease in Cell Migration and Overall Changes in Microtubule Stability. *Mol. Biol. Cell* 75, 910–918 (2007).
108. Fodde, R. *et al.* Mutations in the APC tumour suppressor gene cause chromosomal instability. Nat. Cell Biol. 3, 433–438 (2001).Mutations in the APC tumour suppressor gene cause chromosomal instability. *Nat. Cell Biol.* 3, 433–438 (2001).
109. Dikovskaya, D. *et al.* Loss of APC induces polyploidy as a result of a combination of defects in mitosis and apoptosis. *J. Cell Biol.* 176, 183–195 (2007).
110. Green, R. A. & Kaplan, K. B. Chromosome instability in colorectal tumor cells is associated with defects in microtubule plus-end attachments caused by a dominant mutation in APC. *J. Cell Biol.* 163, 949–961 (2003).
111. Kaplan, K. B. *et al.* A role for the Adenomatous Polyposis Coli protein in chromosome segregation. *Nat. Cell Biol.* 3, 429–432 (2001).
112. Pino, M. S. & Chung, D. C. The Chromosomal Instability Pathway in Colon Cancer.

Gastroenterology 138, 2059–2072 (2010).

113. Smits, R. *et al.* Apc1638T: A mouse model delineating critical domains of the adenomatous polyposis coli protein involved in tumorigenesis and development. *Genes Dev.* 13, 1309–1321 (1999).
114. Lewis, A. *et al.* The C-terminus of Apc does not influence intestinal adenoma development or progression. *J. Pathol.* 226, 73–83 (2012).
115. Darmoul, D. & Ouellette, A. J. Positional specificity of defensin gene expression reveals Paneth cell heterogeneity in mouse small intestine. *Am. J. Physiol.* 271, G68-74 (1996).
116. Haigis, K. M. *et al.* Tumor regionality in the mouse intestine reflects the mechanism of loss of Apc function. *Proc. Natl. Acad. Sci.* 101, 9769–9773 (2004).
117. Urbischek, M. *et al.* Organoid culture media formulated with growth factors of defined cellular activity. *Sci. Rep.* 9, 1–11 (2019).
118. Fujii, M., Matano, M., Nanki, K. & Sato, T. Efficient genetic engineering of human intestinal organoids using electroporation. *Nat. Protoc.* 10, 1474–1485 (2015).
119. Koo, B.-K. *et al.* Controlled gene expression in primary Lgr5 organoid cultures. *Nat. Methods* 9, 81–3 (2012).
120. Schwank, G., Andersson-Rolf, A., Koo, B. K., Sasaki, N. & Clevers, H. Generation of BAC Transgenic Epithelial Organoids. *PLoS One* 8, 6–11 (2013).
121. Fatehullah, A., Appleton, P. L. & Näthke, I. S. Cell and tissue polarity in the intestinal tract during tumourigenesis: cells still know the right way up, but tissue organization is lost. *Philos. Trans. R. Soc. Lond. B. Biol. Sci.* 368, 20130014 (2013).
122. Goldspink, D. A., Matthews, Z. J., Lund, E. K., Wileman, T. & Mogensen, M. M. Immuno-fluorescent Labeling of Microtubules and Centrosomal Proteins in Ex Vivo Intestinal Tissue and 3D In Vitro Intestinal Organoids. *J. Vis. Exp.* (2017). doi:10.3791/56662
123. Moolenbeek, C. & Ruitenberg, E. The 'Swiss roll': a simple technique for histological studies of the rodent intestine. *Lab. Anim.* 1, 57–59 (1981).
124. Rothenberg ME, Nusse Y, Kalisky T, Lee JJ, Dalerba P, Scheeren F, Lobo N, Kulkarni S, Sim S, Qian D, Beachy PA, Pasricha PJ, Quake SR, and C. M. Identification of a cKit+ Colonic Crypt Base Secretory Cell That Supports Lgr5+ Stem Cells in Mice Michael. 142, 1195–1205 (2012).
125. Paddison, P. J. *et al.* Cloning of short hairpin RNAs for gene knockdown in mammalian

cells. *Nat. Methods* 1, 163–167 (2004).

126. Gibson, D. G. *et al.* Enzymatic assembly of DNA molecules up to several hundred kilobases. *Nat. Methods* 6, 343–345 (2009).
127. Sanger, F., Nicklen, S. & Coulson, R. DNA sequencing with chain-terminating inhibitors. *Proc. Natl. Acad. Sci.* 74, 5463–5467 (1977).
128. Oskarsson, T. & Trumpp, A. The Myc trilogy: Lord of RNA polymerases. *Nat. Cell Biol.* 7, 215–217 (2005).
129. He, T. *et al.* Identification of c-MYC as a Target of the APC Pathway. *Science (80-.).* 281, 1509–1512 (1998).
130. Rowan, A. J. *et al.* APC mutations in sporadic colorectal tumors: A mutational 'hotspot' and interdependence of the 'two hits'. *Proc. Natl. Acad. Sci.* 97, 3352–3357 (2000).
131. Pin, C. *et al.* An individual based computational model of intestinal crypt fission and its application to predicting unrestrictive growth of the intestinal epithelium. *Integr. Biol.* 213–228 (2015). doi:10.1039/c4ib00236a
132. Arnout G. Schepers, Hugo J. Snippert, Daniel E. Stange, Maaike van den Born, Johan H. van Es, Marc van de Wetering, H. C. Lineage Tracing Reveals Lgr5+ Stem Cell Activity in Mouse Intestinal Adenomas. 337, 730–736 (2012).
133. Lee, J. L. & Streuli, C. H. Integrins and epithelial cell polarity. *J. Cell Sci.* 127, 3217–3225 (2014).
134. Bartolini, F. & Gundersen, G. G. Generation of noncentrosomal microtubule arrays. *J. Cell Sci.* 119, 4155–4163 (2006).
135. Thyberg, J. & Moskalewski, S. Microtubules and the organization of the Golgi complex. *Exp. Cell Res.* 159, 1–16 (1985).
136. Farin, H. F., Van Es, J. H. & Clevers, H. Redundant sources of Wnt regulate intestinal stem cells and promote formation of paneth cells. *Gastroenterology* 143, 1518-1529.e7 (2012).
137. Lahar, N. *et al.* Intestinal subepithelial myofibroblasts support in vitro and in vivo growth of human small intestinal epithelium. *PLoS One* 6, 1–9 (2011).
138. Valenta, T. *et al.* Wnt Ligands Secreted by Subepithelial Mesenchymal Cells Are Essential for the Survival of Intestinal Stem Cells and Gut Homeostasis. *Cell Rep.* 15, 911–918 (2016).
139. Morin, P. J. *et al.* Activation of Beta-Catenin – Tcf Signaling in Colon Cancer by

Mutations in Beta-Catenin or APC. 275, (1997).

140. Cadigan, K. M. & Waterman, M. L. TCF/LEFs and Wnt Signaling in the Nucleus. *Cold Spring Harb. Perspect. Biol.* 4, (2012).
141. Van de Wetering, M., Castrop, J., Korinek, V. & Clevers, H. Extensive alternative splicing and dual promoter usage generate Tcf-1 protein isoforms with differential transcription control properties. *Mol. Cell. Biol.* 16, 745–752 (1996).
142. Wilson, M. H., Coates, C. J. & George, A. L. PiggyBac transposon-mediated gene transfer in human cells. *Mol. Ther.* 15, 139–145 (2007).
143. Vasquez, R. J., Howell, B., Yvon, A. M., Wadsworth, P. & Cassimeris, L. Nanomolar concentrations of nocodazole alter microtubule dynamic instability in vivo and in vitro. *Mol. Biol. Cell* 8, 973–985 (1997).
144. Tuveson, D. & Clevers, H. Cancer modeling meets human organoid technology. *Science (80-.).* 364, 952–955 (2019).
145. Perdiz, D., Mackeh, R., Poüs, C. & Baillet, A. The ins and outs of tubulin acetylation: More than just a post-translational modification? *Cell. Signal.* 23, 763–771 (2011).
146. van Bergeijk, P., Hoogenraad, C. C. & Kapitein, L. C. Right Time, Right Place: Probing the Functions of Organelle Positioning. *Trends Cell Biol.* 26, 121–134 (2016).
147. Wang, Y. & Huang, S. Golgi structure formation, function, and post-translational modifications in mammalian cells. *F1000Research* 6, 1–13 (2017).
148. Bouchet, B. P. & Akhmanova, A. Microtubules in 3D cell motility. *J. Cell Sci.* 130, 39–50 (2017).
149. Petrosyan, A. Onco-Golgi: Is Fragmentation a Gate to Cancer Progression? *Biochem. Mol* 1, 165–171 (2015).
150. Kellokumpu, S., Sormunen, R. & Kellokumpu, I. Abnormal glycosylation and altered Golgi structure in colorectal cancer: Dependence on intra-Golgi pH. *FEBS Lett.* 516, 217–224 (2002).
151. Sugioka, K. & Sawa, H. Formation and functions of asymmetric microtubule organization in polarized cells. *Curr. Opin. Cell Biol.* 24, 517–525 (2012).
152. Doxsey, S. Re-evaluating centrosome function. *Nat. Rev. Mol. Cell Biol.* 2, 688–698 (2001).
153. Tang, N. & Marshall, W. F. Centrosome positioning in vertebrate development. *J. Cell Sci.* 125, 4951–4961 (2012).

154. Nigg, E. A. Centrosome aberrations: cause or consequence of cancer progression? *Nat. Rev. Cancer* 2, 1–11 (2002).
155. Pihan, G. A. *et al.* Centrosome defects can account for cellular and genetic changes that characterize prostate cancer progression. *Cancer Res.* 61, 2212–2219 (2001).
156. Pihan, G. A. *et al.* Centrosome defects and genetic instability in malignant tumors. *Cancer Res.* 58, 3974–3985 (1998).
157. Ghadimi, B. M. *et al.* Centrosome amplification and instability occurs exclusively in aneuploid, but not in diploid colorectal cancer cell lines, and correlates with numerical chromosomal aberrations. *Genes Chromosom. Cancer* 27, 183–190 (2000).
158. Basto, R. *et al.* Centrosome Amplification Can Initiate Tumorigenesis in Flies. *Cell* 133, 1032–1042 (2008).
159. Lingle, W. L. & Salisbury, J. L. Altered centrosome structure is associated with abnormal mitoses in human breast tumors. *Am. J. Pathol.* 155, 1941–1951 (1999).
160. Fodde, R. *et al.* Mutations in the APCtumour suppressor gene cause chromosomal instability. *Nat. Cell Biol.* 3, 433–438 (2001).
161. Lengauer, C., Kinzler, K. W. & Vogelstein, B. Genetic instability in colorectal cancers. *Nature* 386, 623–627 (1997).
162. Carroll, T. D. *et al.* Interkinetic nuclear migration and basal tethering facilitates post-mitotic daughter separation in intestinal organoids. *J. Cell Sci.* 130, 3862–3877 (2017).
163. Lechuga, S., Naydenov, N. G., Feygin, A., Jimenez, A. J. & Ivanov, A. I. A vesicle trafficking protein aSNAP regulates Panth cell differentiation in vivo. 486, 951–957 (2017).
164. Cooper, G. *The Cell: A Molecular approach. Microtubule Motors and Movements.* (2000).
165. Ayabe, T. *et al.* Secretion of microbicidal α-defensins by intestinal Paneth cells in response to bacteria. *Nat. Immunol.* 1, 113–118 (2000).
166. Vaishnava, S., Behreddt, C. L., Ismail, A., Eckmann, L. & Hooper, L. V. Paneth cells directly sense gut commensals and maintain homeostasis at the intestinal host-microbial interface. *PNAS* 105, 20858–20863 (2008).
167. Farin, H. F. *et al.* Paneth cell extrusion and release of antimicrobial products is directly controlled by immune cell–derived IFN-γ. *J. Exp. Med.* 211, 1393–1405 (2014).
168. Nishisho, I. *et al.* Mutations of Chromosome 5q21 Genes in FAP and Colorectal Cancer

Patients. *Sci. Reports* 371, 665–670 (1991).

169. Feil, R., Wagner, J., Metzger, D. & Chambon, P. Regulation of Cre Recombinase Activity by Mutated Estrogen Receptor Ligand-Binding Domains. *Biochem. Biophys. Res. Commun.* 237, 752–757 (1997).
170. Sur, I. K. *et al.* Mice Lacking a Myc Enhancer That Includes Human SNP rs6983267 Are Resistant to Intestinal Tumors. *Science (80-.).* 338, 1360–1363 (2012).
171. Dave, K. *et al.* Mice deficient of Myc super-enhancer region reveal differential control mechanism between normal and pathological growth. *Elife* 6, 1–25 (2017).
172. Andreu, P. *et al.* Crypt-restricted proliferation and commitment to the Paneth cell lineage following Apc loss in the mouse intestine. *Development* 132, 1443–1451 (2005).
173. Morin, P. J., Vogelstein, B. & Kinzler, K. W. Apoptosis and APC in colorectal tumorigenesis. *Proc. Natl. Acad. Sci.* 93, 7950–7954 (1996).
174. Faux, M. C. *et al.* Restoration of full-length adenomatous polyposis coli (APC) protein in a colon cancer cell line enhances cell adhesion. *J. Cell Sci.* 117, 427–439 (2004).
175. Bahmanyar, S., Nelson, W. J. & Barth, A. I. M. Role of APC and Its Binding Partners in Regulating Microtubules in Mitosis. *Adv. Exp. Medicicne Biol.* 65–74 (2009).
176. Penman, G. A., Leung, L. & Näthke, I. S. The adenomatous polyposis coli protein (APC) exists in two distinct soluble complexes with different functions. *J. Cell Sci.* 118, 4741–4750 (2005).
177. Jalal, S. *et al.* Actin cytoskeleton self-organization in single epithelial cells and fibroblasts under isotropic confinement. *J. Cell Sci.* 132, 1–14 (2019).
178. Pepperkok, R., Bre, M. H., Davoust, J. & Kreis, T. E. Microtubules are stabilized in confluent epithelial cells but not in fibroblasts. *J. Cell Biol.* 111, 3003–3012 (1990).
179. Lesko, A. C. & Prosperi, J. R. Epithelial Membrane Protein 2 and β1 integrin signaling regulate APC-mediated processes. *Exp. Cell Res.* 350, 190–198 (2017).
180. Kriz, V. & Korinek, V. WNT, RSPO and hippo signalling in the intestine and intestinal stem cells. *Genes (Basel).* 9, 1–18 (2018).
181. Falk, P., Roth, K. A. & Gordon, J. I. Lectins are sensitive tools for defining the differentiation programs of mouse gut epithelial cell lineages. *Am. J. Physiol.* 266, (1994).
182. Salzman, N. H., Ghosh, D., Huttner, K. M., Paterson, Y. & Bevins, C. L. Protection

against enteric salmonellosis in transgenic mice expressing a human intestinal defensin. *Nature* 422, 3–7 (2003).

183. Buske, P. *et al.* On the biomechanics of stem cell niche formation in the gut - modelling growing organoids. *FEBS J.* 279, 3475–3487 (2012).
184. Yu, S. *et al.* Paneth Cell Multipotency Induced by Notch Activation following Injury. *Cell Stem Cell* 23, 46-59.e5 (2018).
185. Schwitalla, S. *et al.* Intestinal tumorigenesis initiated by dedifferentiation and acquisition of stem-cell-like properties. *Cell* 152, 25–38 (2013).
186. Yan, K. S. *et al.* The intestinal stem cell markers Bmi1 and Lgr5 identify two functionally distinct populations. *Proc. Natl. Acad. Sci.* 109, 466–471 (2012).
187. Serra, D. *et al.* Self-organization and symmetry breaking in intestinal organoid development. *Nature* (2019). doi:10.1038/s41586-019-1146-y
188. Riemer, P. *et al.* Oncogenic β-catenin and PIK3CA instruct network states and cancer phenotypes in intestinal organoids. *J. Cell Biol.* 216, 1567–1577 (2017).
189. Levayer, R. & Lecuit, T. Breaking down EMT. *Nat. Cell Biol.* 10, 757–759 (2008).
190. Rusan, N. M. & Peifer, M. Original CIN: Reviewing roles for APC in chromosome instability. *J. Cell Biol.* 181, 719–726 (2008).
191. Rocha, C. *et al.* Tubulin glycylases are required for primary cilia, control of cell proliferation and tumor development in colon. *EMBO J.* 33, 2247–2260 (2014).
192. Higgins, M., Obaidi, I. & McMorrow, T. Primary cilia and their role in cancer. *Oncol. Lett.* 17, 3041–3047 (2019).
193. Näthke, L. H. and I. Changes in cell and tissue organization in cancer of the breast and colon. *Curr. Opin. Cell Biol.* 87–95 (2014). doi:10.1016/j.surg.2006.10.010.Use
194. Hernandez, P. & Tirnauer, J. S. Tumor suppressor interactions with microtubules: Keeping cell polarity and cell division on track. *Dis. Model. Mech.* 3, 304–315 (2010).

Appendix

Plasmid maps as detailed in Table 2.8 and used in this study produced using SnapGene software.

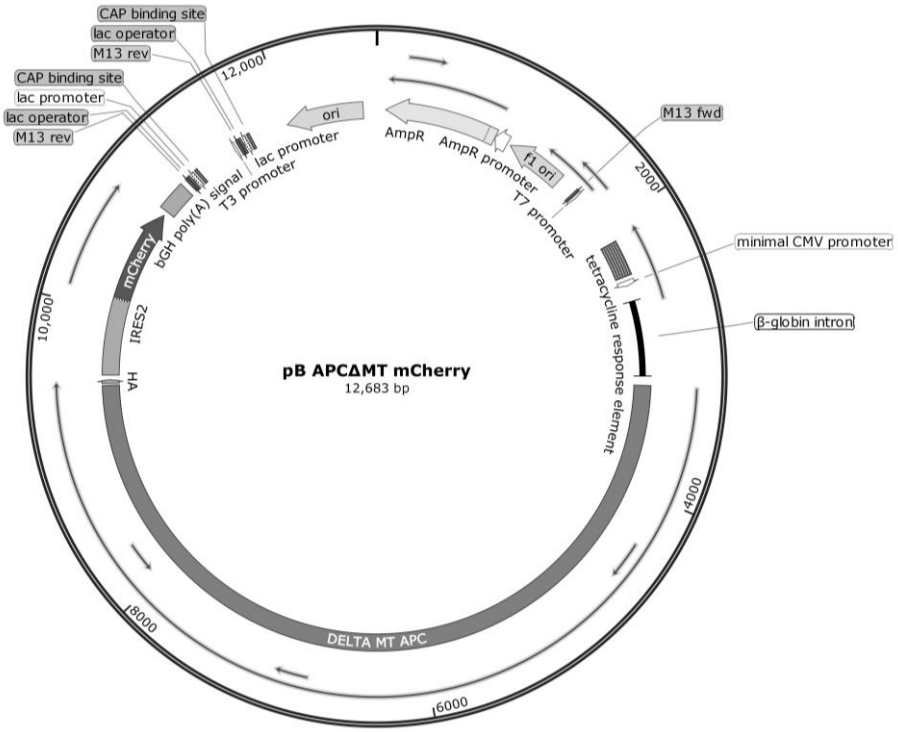

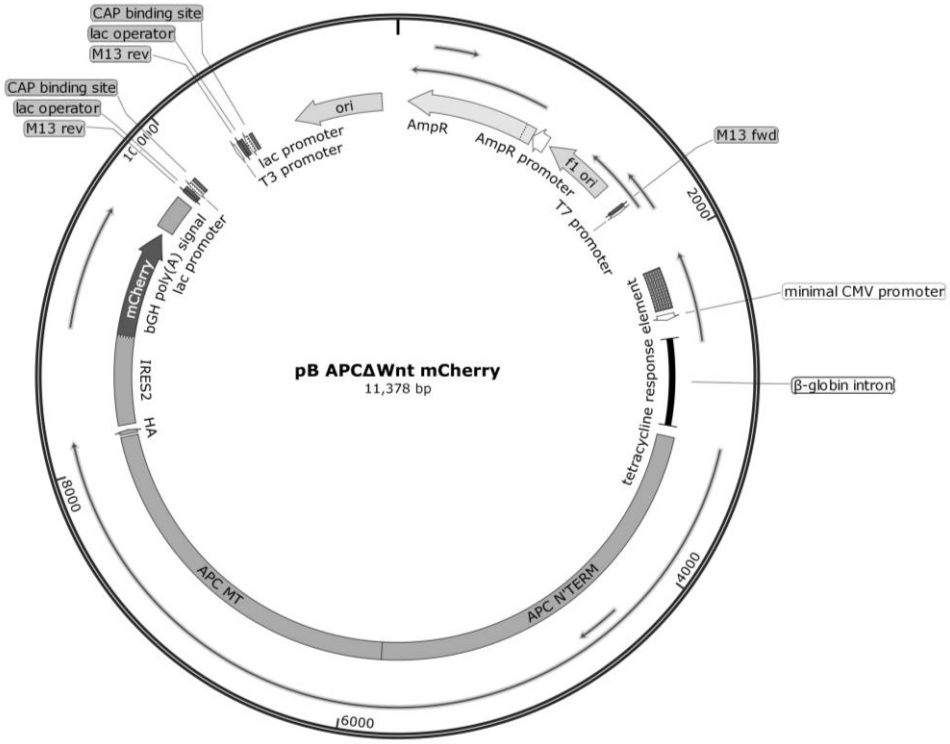

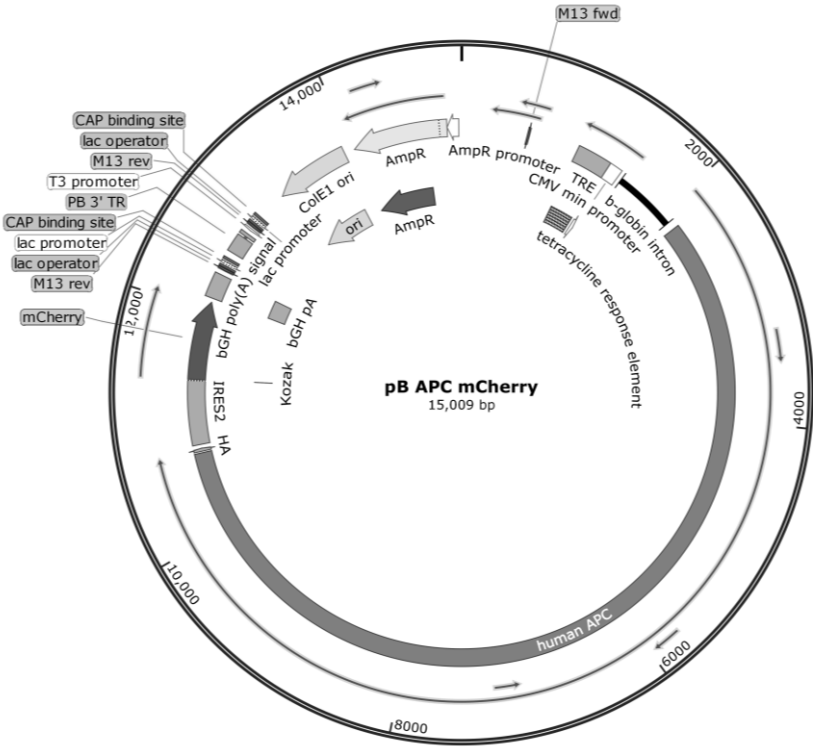
M13 fwd
CAP binding site
lac operator
M13 rev
T3 promoter
PB 3' TR
CAP binding site
lac promoter
lac operator
M13 rev
mCherry
14,000
2000
4000
6000
8000
10,000
12,000
AmpR
AmpR promoter
ColE1 ori
ori
AmpR
TRE
CMV min promoter
b-globin intron
tetracycline response element
lac promoter
bGH poly(A) signal
bGH pA
Kozak
IRES2
HA
human APC
pB APC mCherry
15,009 bp

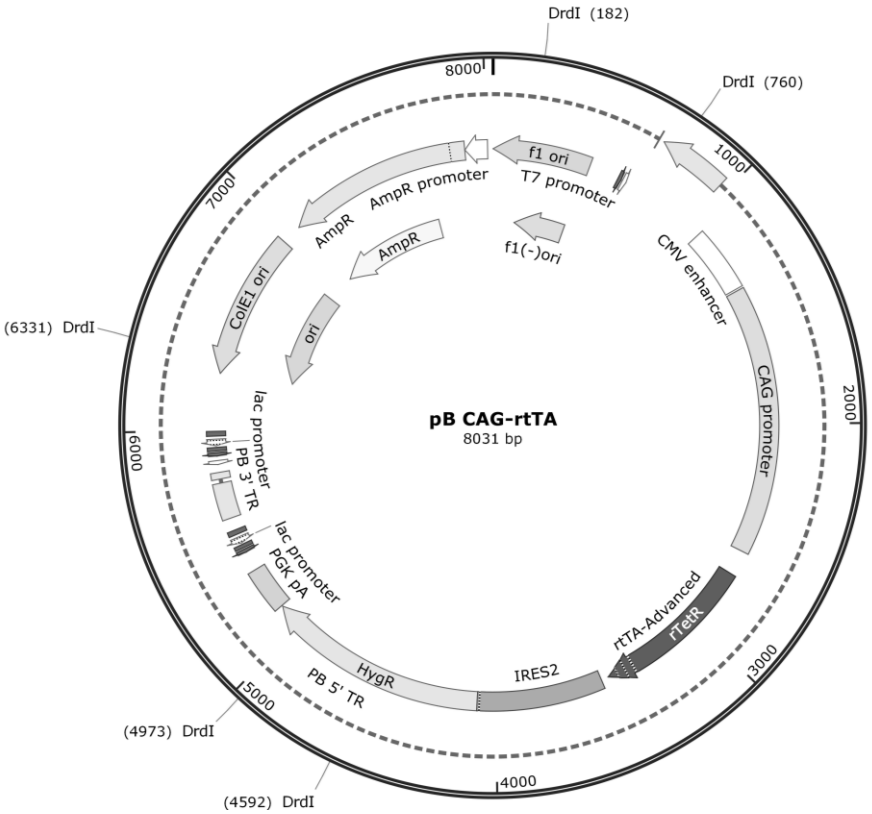
DrdI (182)
DrdI (760)
(6331) DrdI
(4973) DrdI
(4592) DrdI
8000
1000
2000
3000
4000
5000
6000
7000
f1 ori
T7 promoter
AmpR promoter
AmpR
AmpR
f1(-)ori
ColE1 ori
ori
CMV enhancer
CAG promoter
lac promoter
PB 3' TR
lac promoter
PGK pA
rtTA-Advanced
rTetR
HygR
IRES2
PB 5' TR
pB CAG-rtTA
8031 bp


pB shApc mCherry
6840 bp
f1 ori
PB 5' TR
AmpR promoter
AmpR
M13 fwd
T7 promoter
PB 5' TR
1000
f1(-)ori
tetracycline response element
minimal CMV promoter
TRE
CMV min promoter
6000
ColE1 ori
ori
rabbit b-globin intron
2000
lac promoter
T3 promoter
5000
CAP binding site
lac operator
M13 rev
PB 3' TR
T7 promoter
shAPC total
HA
CAP binding site
lac promoter
lac operator
M13 rev
IRES2
4000
mCherry
3000
bGH poly(A) signal

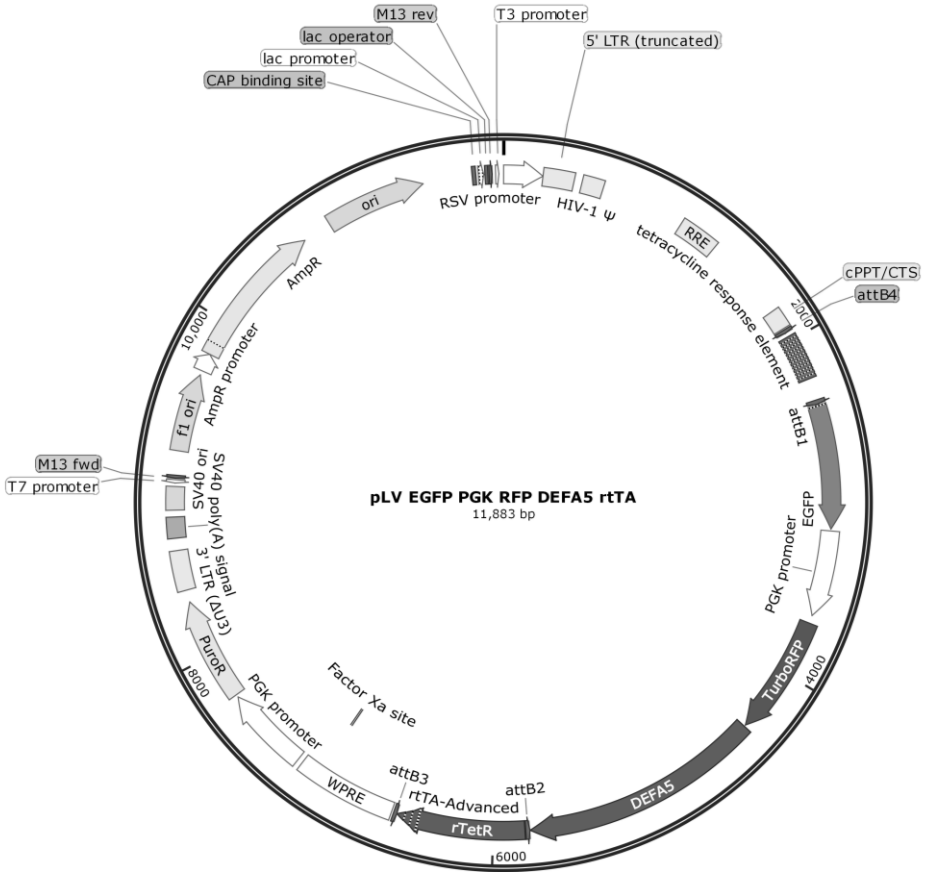
M13 rev
T3 promoter
lac operator
5' LTR (truncated)
lac promoter
CAP binding site
ori
RSV promoter
HIV-1 ψ
RRE
tetracycline response element
cPPT/CTS
attB4
2000
AmpR
10,0000
AmpR promoter
attB1
f1 ori
M13 fwd
T7 promoter
SV40 ori
pLV EGFP PGK RFP DEFA5 rtTA
11,883 bp
EGFP
PGK promoter
SV40 poly(A) signal
3' LTR (ΔU3)
TurboRFP
4000
PuroR
8000
PGK promoter
Factor Xa site
attB3
attB2
WPRE
rtTA-Advanced
DEFA5
rTetR
6000

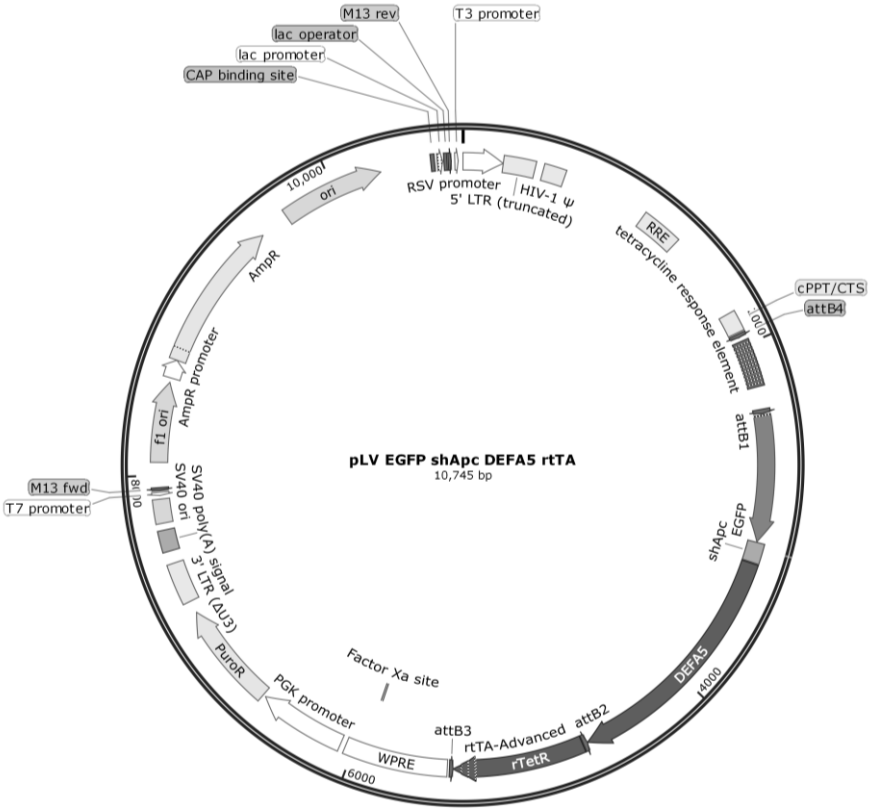
M13 rev
T3 promoter
lac operator
lac promoter
CAP binding site
10,000
ori
RSV promoter
5' LTR (truncated)
HIV-1 ψ
RRE
tetracycline response element
cPPT/CTS
attB4
attB1
shApc
EGFP
DEFA5
4000
attB2
rtTA-Advanced
rTetR
attB3
Factor Xa site
PGK promoter
WPRE
6000
PuroR
3' LTR (ΔU3)
SV40 poly(A) signal
SV40 ori
M13 fwd
T7 promoter
f1 ori
AmpR promoter
AmpR
pLV EGFP shApc DEFA5 rtTA
10,745 bp

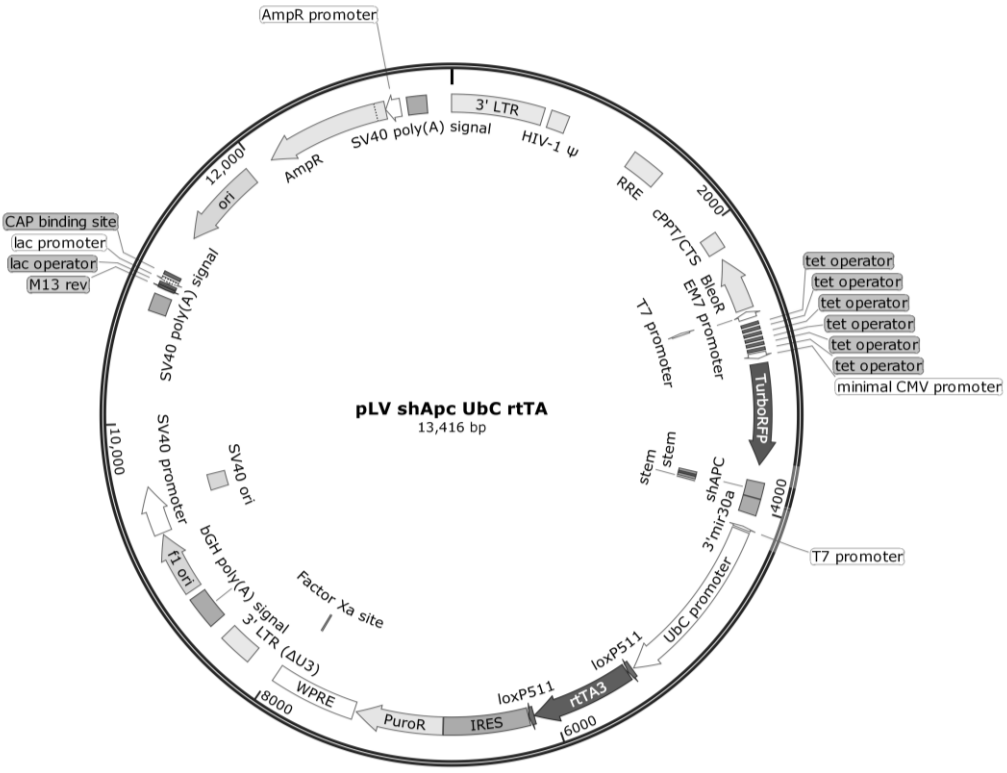
AmpR promoter
3' LTR
SV40 poly(A) signal
HIV-1 ψ
12,000
ori
AmpR
RRE
2000
cPPT/CTS
CAP binding site
lac promoter
lac operator
M13 rev
SV40 poly(A) signal
BleoR
EM7 promoter
T7 promoter
tet operator
tet operator
tet operator
tet operator
tet operator
tet operator
minimal CMV promoter
TurboRFP
pLV shApc UbC rtTA
13,416 bp
10,000
SV40 promoter
SV40 ori
stem
stem
shAPC
3'mir30a
4000
T7 promoter
bGH poly(A) signal
f1 ori
Factor Xa site
3' LTR (ΔU3)
UbC promoter
loxP511
WPRE
loxP511
rtTA3
8000
PuroR
IRES
6000

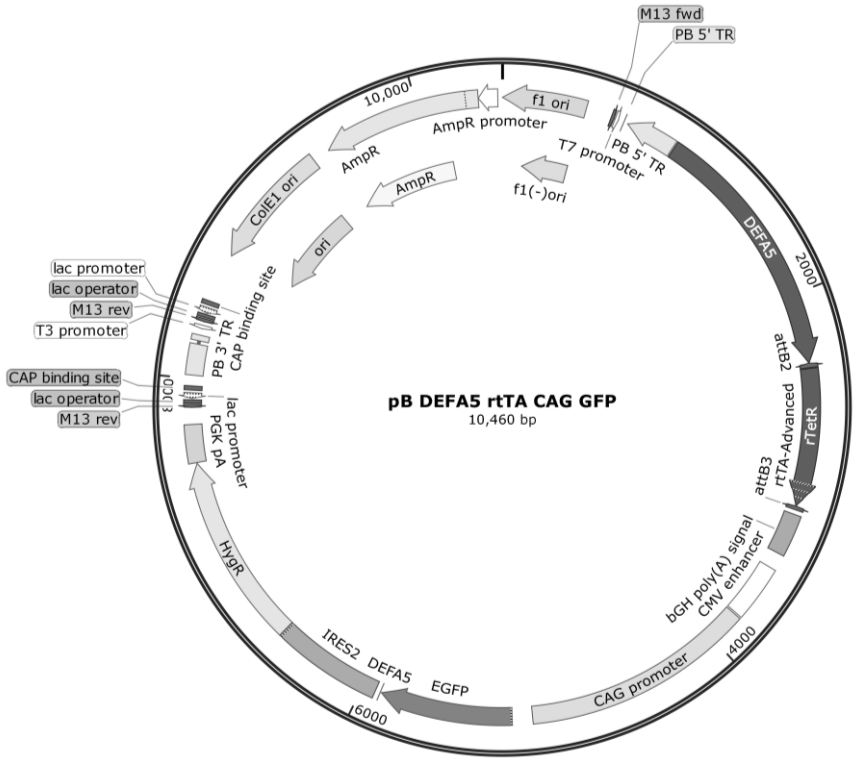
M13 fwd
PB 5' TR
10,000
f1 ori
AmpR promoter
AmpR
T7 promoter
PB 5' TR
f1(-)ori
AmpR
ColE1 ori
ori
DEFA5
2000
attB2
rtTA-Advanced
rTetR
lac promoter
lac operator
M13 rev
T3 promoter
PB 3' TR
CAP binding site
CAP binding site
lac operator
M13 rev
lac promoter
PGK pA
attB3
bGH poly(A) signal
CMV enhancer
HygR
IRES2
DEFA5
EGFP
CAG promoter
4000
6000
pB DEFA5 rtTA CAG GFP
10,460 bp

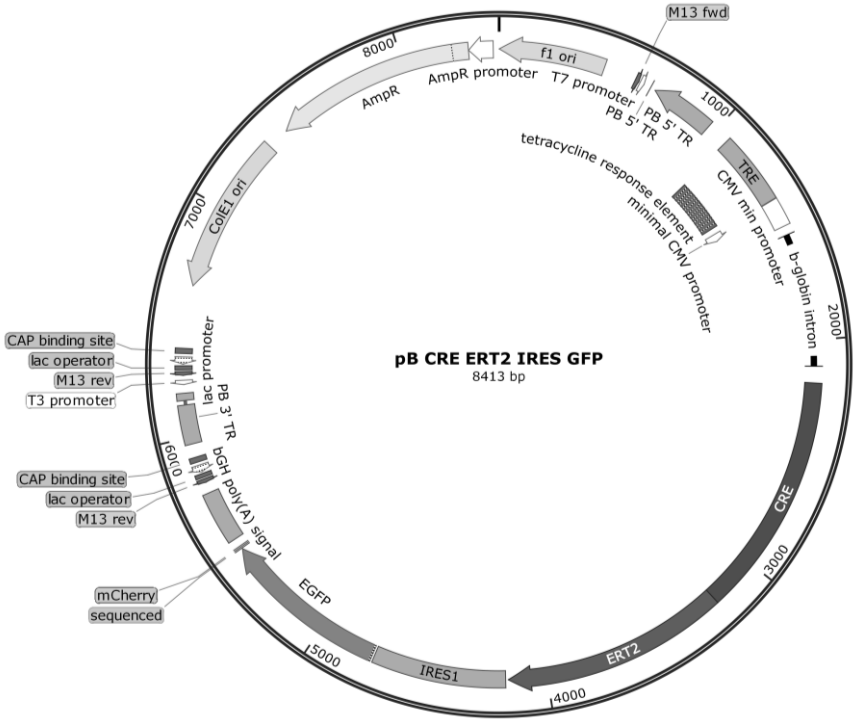
M13 fwd
8000
f1 ori
AmpR promoter
T7 promoter
PB 5' TR
PB 5' TR
1000
AmpR
tetracycline response element
minimal CMV promoter
TRE
CMV min promoter
b-globin intron
2000
7000
ColE1 ori
CAP binding site
lac operator
M13 rev
T3 promoter
lac promoter
PB 3' TR
CRE
3000
6000
CAP binding site
lac operator
M13 rev
bGH poly(A) signal
mCherry
sequenced
EGFP
5000
IRES1
ERT2
4000
pB CRE ERT2 IRES GFP
8413 bp

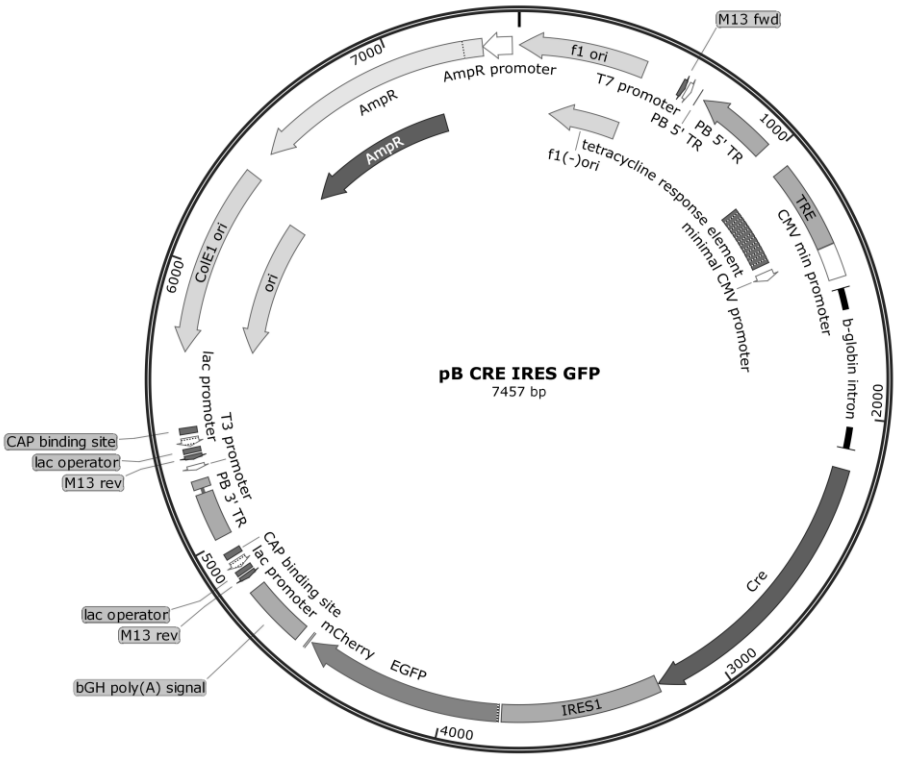
pB CRE IRES GFP
7457 bp
M13 fwd
f1 ori
T7 promoter
PB 5' TR
PB 5' TR
1000
TRE
CMV min promoter
b-globin intron
2000
Cre
3000
IRES1
EGFP
4000
mCherry
CAP binding site
lac promoter
5000
T3 promoter
PB 3' TR
CAP binding site
lac operator
M13 rev
lac operator
M13 rev
bGH poly(A) signal
6000
ColE1 ori
ori
AmpR
AmpR promoter
7000
AmpR
f1(-)ori
tetracycline response element
minimal CMV promoter